The Potential of Half a Million Neurons

Studies with electrocorticography and functional MRI in motor and language areas

Dora Hermes

The studies described in this thesis were performed at the Rudolf Magnus Institute of Neuroscience, Department of Neurology and Neurosurgery, University Medical Center Utrecht, The Netherlands.

Research in this thesis was supported by a VICI grant from the Dutch Technology Foundation STW, applied science division of NWO and the Technology Program of the Ministery of Economic Affairs to Prof. Dr. N. F. Ramsey.

ISBN: 978-90-3935-764-4
Printer by: Proefschriftmaken.nl

The Potential of Half a Million Neurons

Studies with electrocorticography and functional MRI in motor and language areas

De potentiaal van een half miljoen neuronen

Studies met electrocorticografie en functionele MRI in motor en taal gebieden

Proefschrift

ter verkrijging van de graad van doctor
aan de Universiteit Utrecht op gezag van
de rector magnificus, prof.dr. G.J. van der Zwaan,
ingevolge het besluit van het college voor promoties
in het openbaar te verdedigen op
dinsdag 3 april 2012 des middags te 12.45 uur

door

Dora Hermes

geboren op 13 juli 1982
te Nijmegen

Promotor: Prof. Dr. N.F. Ramsey

Contents

Chapter 1

Introduction

Background

Brain function can be viewed from different perspectives. We can zoom in from a global view where the brain is viewed in its entirety to more local perspectives where distinctions are made between hemispheres, lobes, Brodmann areas, cortical columns, cortical layers or individual neurons. Techniques that measure neuronal activity complement each other in terms of spatiotemporal characteristics. Each technique provides a unique view of the brain: from local processing in individual neurons to global brain dynamics. In order to understand brain function, it is necessary to study the neurophysiology at all the different scales. In this thesis we studied neurophysiology at the scale of millimeters, where interactions between local and global brain processes can be investigated.

Local neurophysiology can be measured with needle electrodes inserted into the brain. These electrodes record action potentials from individual neurons and firing rates from small neuronal populations. They can also measure the local field potential (LFP), which reflects the synaptic input from a neuronal population within a radius of ~250 micrometer from the electrode tip [1]. Global neurophysiology can be measured with electroencephalography (EEG) by simply placing electrodes on the scalp. The EEG signal reflects distributed patterns of synaptic activity from neuronal populations in a volume one centimeter and larger (Nunez et al., 2001; Nunez and Srinivasan, 2006). Only studying neurophysiology at the scale of micrometers and at the scale of centimeters is not sufficient to understand brain function: the intermediate scale of millimeters cannot be neglected for several reasons.

First, intermediate scales are important because certain functional units may only be represented at the intermediate scale and the signal recorded at more local scales does not simply extrapolate to larger scales. The firing in a single neuron may not represent the population, like one instrument does not represent the music of an orchestra and one voice may not represent the chanting of a crowd. The motor cortex for example has a somatotopic representation, with different body parts represented in different areas. The detail of these representations was unclear and it was questioned whether within the hand region there are sub-populations that represent different fingers. Local recordings suggest that within the hand area there are no finger-specific spots: single unit recordings have shown that finger specific neurons that only fire during the movement of one finger can be found throughout the whole hand region [2, 3]. Global EEG recordings are spatially not specific enough to distinguish areas within the hand region. When neuronal populations at the millimeter scale were recorded, spots within the motor hand area were found that are specific for different fingers [4]. A neuronal population at the millimeter scale thus seems to be a functional unit for

neural computation with properties that cannot be studied in either individual neurons or global dynamics reflected in the EEG signal alone [5].

Another important reason to study neurophysiology at the scale of millimeters is because functional magnetic resonance imaging (fMRI) has also demonstrated interesting correlates of brain function at this resolution [6, 7]. FMRI is largely responsible for the rapid growth in studies of human brain function, but is an indirect measurement of brain activity that reflects changes in blood flow, blood volume and oxygenation. The coupling between these vascular processes and neuronal population activity is not yet fully understood and to what extend functional correlates found by fMRI research represent neuronal activity is unclear. FMRI can measure the entire human brain noninvasively and is measured in voxels; cubes with a typical diameter of 1-4 mm. At this resolution different finger representations have been found in motor cortex, categorical representations of faces, houses and objects were dissociated in visual areas and areas involved in emotion or cognitive processes such as language, memory and attention could be localized for the first time in large populations of healthy subjects. This multitude of findings confirms that interesting, dissociable brain functions can be investigated at the scale of the fMRI voxel.

Electrocorticography (ECoG) provides a unique opportunity to record neurophysiology at the scale of millimeters in humans. ECoG is generally measured in certain patient populations, such as patients with epilepsy, when electrodes are implanted directly on the brain for clinical purposes. Most ECoG electrodes are spaced with heart to heart distance of 1 centimeter and each electrode has a measurement surface of 2.3 millimeter in diameter. An ECoG electrode of 2.3 millimeter in diameter sits directly on top of a neuronal population of about half a million neurons [8, 9]. About 80% of these neurons are glutamatergic cells and the other 20% are inhibitory GABAergic interneurons [10]. The ECoG signal reflects the aggregate of the electrical potential from these different cells and is unique in its properties. It has a better signal to noise ratio than EEG or magnetoencephalography (MEG). While the advantage of EEG and MEG is that these techniques are noninvasive and measure brain activity with a high temporal resolution, it is difficult to identify the source(s) of these signals. EEG has a spatial resolution of centimeters and while MEG may have a slightly higher spatial resolution of a couple of millimeters neither EEG nor MEG can measure activity from non-synchronous sources [11-15]. ECoG allows these measurements with both good spatial and good temporal fidelity.

This introduction will first give a short overview of the unique properties of the ECoG signal and how it can be decomposed into the frequency domain to reveal different aspects of brain function. Then we will introduce the fMRI signal and the current understanding of the coupling between neuronal activity and the fMRI signal. The introduction will focus on motor

and language areas, but will sometimes diverge to visual cortex, since some processes were first discovered in visual areas.

ECoG and spectral power change

ECoG electrodes are generally implanted to localize critical brain areas in tumor or epilepsy patients and for epilepsy monitoring. To localize motor function neurosurgeons already stimulated ECoG electrodes in the 1930s. By running small electrical currents across two electrodes on primary motor areas, where Betz cells are located that directly project through spinal cord nuclei to the target muscles, a movement could be elicited [16]. Not in all brain areas the stimulation of ECoG electrodes elicits behavior. Language areas such as Broca's and Wernicke's area can be localized by the induction of speech arrest [17].

In the setting of epilepsy monitoring, the ECoG signal is used to localize the seizure focus. Since ECoG electrodes cover a large area of cortex, including healthy tissue, the ECoG signal can also be used to study normal motor and language mechanisms. The ECoG signal reflects the aggregate of activity in the underlying neuronal population. It can be decomposed into the frequency domain to reveal different aspects of neuronal activity. The powerspectrum of the ECoG signal follows a power law with on top of that oscillations in different frequency bands [18]. Changes in the power in different bands correlate with brain function. As such, these reflect different processes and a rough distinction can be made between global low frequency processes and local high frequency processes.

Low frequencies

Synchronous low frequency rhythms in the brain can occur over large areas of cortex and are easily measured with EEG. The first human brain rhythm was revealed by EEG recordings in 1930 [19]. In electrodes on occipital areas oscillations were noted around a 10 Hz frequency: the occipital alpha rhythm. The amplitude of the alpha rhythm increased when people closed their eyes, and visual input was reduced.

After the initial discovery of the alpha rhythm, EEG research showed that Rolandic cortex displayed a different rhythm. Sensorimotor areas show oscillations between 10 and 20 Hz that are suppressed during movement [20, 21]. These rhythms are now known as mu, beta or sensorimotor rhythms. ECoG studies investigated the spatial specificity of these sensorimotor rhythms. They showed that the power decrease during movement is distributed around pre and postcentral gyri and is somatotopically specific for hand, mouth and foot areas [22, 23]. The power decrease in sensorimotor rhythms is too distributed however, to make distinctions on a smaller scale such as that of the finger [4].

In language areas, much less is known about dominant low frequency rhythms, probably because these are not synchronous over large areas of cortex and can, therefore, not be easily assessed with EEG. In 1981 ECoG research showed a flattening of the ECoG signal during object naming [24], which was later demonstrated to be a decrease in alpha amplitude (7-12Hz) [25]. A more recent study noted changes in several low frequency rhythms across different language areas while listening to words during a linguistic target detection task [26]. They suggested that the theta rhythm might play an important role in language processing.

Cortical low frequency rhythms have been hypothesized to be generated by thalamocortical interactions [27-29], but this view has also been debated [11]. It is important to better understand the role and mechanisms of these low frequency rhythms because they can be markers of neurological diseases [30]. The low frequency rhythm in motor cortex for example, shows specific abnormalities in patients with motor diseases such as Parkinson's disease [31], dystonia [32] or tremor [33].

High frequencies

In addition to measuring low frequencies, intracranial recordings allow easy measurement of high frequencies of over 60 Hz. In contrast with distributed low frequency decreases, high frequencies show more localized increases in power during movement. In motor cortex, this high frequency power increase does not only show a somatotopic specificity for hand, tongue and foot areas, but also distinguishes individual digits [4]. High frequency changes in motor areas show an accurate timing with respect to movement: high frequency power increases 50-100 msec before the onset of movement and can be used to accurately decode the timecourse of individual finger movements [34].

Similar as in motor cortex, language areas such as Wernicke's and Broca's area show local increases in high frequency power during language processing [35]. These increases in high frequency power are locked in time to the onset of speech perception, processing and production [26, 36-39]. High frequency changes from Wernicke's area have even be used to decode different spoken words [40].

During brain function the high frequency range can show both power changes in frequency specific gamma oscillations and broadband changes. In visual cortex, the gamma rhythm has been extensively investigated (for reviews see [41, 42]) and has been suggested to be generated by synchronous interneuron activity [43]. In motor cortex however, ECoG research showed that high frequency increases during movement are not specific for a gamma frequency [18], but show a broadband change in power that can be measured in all frequencies of over 60Hz. Simultaneous recordings of LFPs and neuronal spiking activity have recently shown that this broadband change is indeed a different phenomenon from the

gamma rhythm and is linked to population firing rate [44, 45]. Broadband high frequency power increases thus reflect local neuronal processing in the population underneath an electrode.

Since the distinction between gamma rhythms and broadband activity has only recently been made, previous work often refers to broadband activity as high gamma, which may be confused with the frequency specific gamma rhythm. In the studies in this thesis we will use the term high frequency band (HFB) if no clear gamma rhythm is noted and high frequencies most likely reflect broadband activity. When referring to other research in the introduction and discussion of this thesis, the term 'high frequencies' will be used if studies did not specifically look at gamma rhythms and their figures do not show clear evidence for gamma rhythms.

Low and high frequency activity are not strictly separated phenomena. Several studies have shown that the phase of low frequency oscillations can be coupled to high frequencies [46-50]. This coupling suggests that high frequencies may be facilitated by low frequency rhythms. Since ECoG can measure both low frequency rhythms and local high frequencies, it provides an eminent opportunity to investigate their relationship.

Neurophysiological correlates of fMRI

Functional MRI can measure the hemodynamic correlates of brain function. Brain function requires oxygen, which is supplied by blood flow throughout the brain. When oxygen is extracted from the blood, oxyhemoglobin changes into deoxyhemoglobin. In the initial discovery of fMRI in 1990 Ogawa et al., noted that deoxyhemoglobin is paramagnetic and thus creates a magnetic susceptibility artifact that can be picked up in an MRI scanner [51]. Since oxyhemoglobin does not have this effect, the relative concentration of deoxyhemoglobin can be measured with fMRI.

When neuronal activity results in oxygen use, the fMRI signal decreases. However, the use of oxygen is not the major contributor to the fMRI signal, since neuronal activity also results in the release of vasoactive substances independent of the metabolic demand and blood flow rapidly exceeds the flow necessary to meet the demand for oxygen, resulting in a positive fMRI signal [8, 52-55]. The fMRI signal is thus influenced by blood oxygenation, blood flow and blood volume, and is also called the blood oxygen level dependent (BOLD) response. The BOLD response is quite slow and peaks about 6 seconds after neuronal activity.

It is only partially understood what neuronal activity drives the BOLD response. Two different lines of research show that synaptic activity, rather than neuronal firing, is a better predictor of the BOLD response. First, synaptic activity regulates the vascular response rather than spiking output [56]. Second, it has been shown that the local field potential (LFP),

which reflects synaptic activity, simply correlates better with the BOLD signal than firing rate [57, 58].

The following model (simplified here) has been proposed for how synaptic glutamatergic signaling results in the BOLD response [59]. This complex cascade starts with the release of glutamate from a presynaptic neuron. Glutamate acts on the post-synaptic neuron leading to depolarization of the membrane, opening of the voltage sensitive Ca^{2+} channels and Ca^{2+} influx. Increases in intracellular calcium in turn result in the activation of enzymes that trigger vasodilators and an increase in blood flow. Glutamate in the synaptic cleft simultaneously acts on astrocytes surrounding the synapse [60]. This results in elevation of Ca^{2+} in astrocytes, which also results in vasodilation through the activation of enzymes and by indirectly acting on smooth muscle cells. Glutamatergic neurons comprise the majority of the cerebral cortex, so their share in the BOLD response will be most significant, but little is known about how inhibitory GABA-ergic signaling is coupled to the BOLD signal [10, 52].

Since synaptic activity is a better predictor of the BOLD signal than firing rate, spectral power changes, which mainly reflect synaptic activity, should show a good correspondence in terms of correlation and localization with the BOLD signal. Multiple studies that recorded LFPs have indeed shown that high frequency and gamma power changes are significant correlates of the BOLD signal as primate and cat studies have shown in visual cortex [57, 61] and human intracranial recordings have shown in auditory cortex [62]. Several studies have also shown that this correlation is only partial (for a review see [63]). For example, in visual cortex of awake primates it has been noted that perceptual suppression resulted in a BOLD increase, while in the LFP no associated changes in high frequency power were measured [64]. Another primate study showed increases in blood flow in visual cortex during anticipation, but found no concurrent change in the LFP or firing rate [65]. Human MEG and fMRI data also found that there are gamma changes specific to the spatial frequency of a stimulus, while these are not noted in the BOLD signal [66]. In terms of the location of activity, MEG studies in humans have shown that gamma changes in visual cortex co-localize well with BOLD changes [67]. Human intracranial studies showed that BOLD changes co-localize relatively well with high frequency power changes measured with needle electrodes in temporal cortex [68, 69] and with high frequency power changes measured with ECoG in dorsolateral prefrontal cortex [70]. However, in these intracranial recording studies a number of fMRI sites were found where BOLD activity did not correlated with high frequency activity.

Low frequency power changes as measured with EEG and MEG have also been compared with the BOLD signal [67, 71-73]. These studies found that decreases in power in occipital alpha oscillations and decreases in power in sensorimotor rhythms both correlate with BOLD signal increases. Again, when only these low frequencies are considered, BOLD

change and neurophysiology do not always match. For example, mismatches in the location of low frequency and BOLD activity have been found (for a review see [74]). Also, EEG work showed that while increases in BOLD matched decreases in low frequency power during movement in contralateral motor areas, suppression of the BOLD signal in ipsilateral motor cortex did not correspond to low frequency power increase [75].

While these studies show that low and high frequency power changes both correlate with BOLD change, they indicate that neither process can fully explain the BOLD signal. The relation between these two processes and their independent relation with the BOLD signal thus remains unclear. In order to understand the full neurophysiological correlates of fMRI both processes need to be considered and independently related with the BOLD signal.

Clinical setting

The studies described in this thesis were performed at the department of neurology and neurosurgery and have various clinical applications. Some of this research fits within the framework of brain computer interfacing (BCI). In BCI a signal from the brain is used to control a computer device in order to help paralyzed patients communicate. One of the ongoing discussions in this field is which brain signal is best suited to control a computer device [70, 76-78]. Due to the ECoG signal quality and the fact that it is relatively less invasive compared to needle electrodes, it has been proposed that neuronal population activity as measured with ECoG would be a good option to drive a brain computer interface. In theory, an electrode could be placed on a motor, motor imagery, language or working memory area and the signal from this electrode is then used to drive a cursor on a computer screen. It is not a trivial question which part of the ECoG signal is optimal for BCI and what the optimal brain area for such an electrode would be. These questions were kept in mind throughout this project and will be addressed in the discussion.

Outline of the thesis

Brain dynamics with different levels of detail reveal distinct mechanisms in the brain. FMRI has revealed multiple interesting neuronal correlates of behavior at the scale of millimeters and ECoG provides the unique opportunity to better understand the neurophysiology at a comparable scale. In this thesis, we will study basic properties of the ECoG signal: different processes will be derived from the electric potential and their link to the fMRI signal will be studied.

At the start of this series of studies, there was no method available to accurately localize the ECoG electrodes on the brain of an individual subject using a CT scan with the

electrodes and the anatomical MRI of this patient. In chapter 2 I will describe a method we developed to localize the ECoG electrodes and how we validated this method.

As noted above, several studies have reported dissociations between fMRI and electrophysiology, especially when these are measured with different resolutions. In chapter 3, we describe such an apparent dissociation between fMRI and the signal measured with EEG. We used ECoG to solve the mismatch between fMRI and scalp EEG.

To further investigate to what extent ECoG could explain the fMRI signal, we conducted the study described in chapter 4. Power changes during hand movement in different low frequency bands and a high frequency band were extracted from the ECoG signal. The spatial variability in fMRI and ECoG was then used to better understand how the fMRI signal correlates with these spectral power changes.

In chapter 5, we further explored the interaction between neurophysiological processes reflected in low and high frequencies in the ECoG during repeated movement. Previous research has shown that beta oscillations in motor cortex may inhibit sensorimotor processing. Beta power is continuously decreased during fast repeated movement, indicating that motor areas are continuously released from inhibition. The effect of this state on the local neuronal activity in motor and sensory areas is investigated with high resolution ECoG arrays.

In chapter 6, we studied the neurophysiology of language areas. Language can only be studied in humans and ECoG provides a unique opportunity to investigate neuronal population activity in frontal and temporal language areas. In the setting of verb generation, we explored the role of low frequencies in these areas by studying the interactions with the high frequencies that reflect local neuronal activity. We linked these low frequency and high frequency processes to the fMRI signal measured in the same subjects.

In chapter 7 we summarize the findings of these different studies. Furthermore, we discuss what these findings can tell us about neuronal population physiology and the fMRI signal. Limitations of these studies will be discussed and suggestions for future directions will be given.

References

1. Katzner, S.*, et al.* Local origin of field potentials in visual cortex. *Neuron* **61**, 35-41 (2009).
2. Schieber, M.H. Constraints on somatotopic organization in the primary motor cortex. *J Neurophysiol* **86**, 2125-2143 (2001).
3. Schieber, M.H. & Hibbard, L.S. How somatotopic is the motor cortex hand area? *Science* **261**, 489-492 (1993).
4. Miller, K.J., Zanos, S., Fetz, E.E., den Nijs, M. & Ojemann, J.G. Decoupling the cortical power spectrum reveals real-time representation of individual finger movements in humans. *J Neurosci* **29**, 3132-3137 (2009).
5. Freeman, W.J. Mesoscopic neurodynamics: from neuron to brain. *Journal of physiology, Paris* **94**, 303-322 (2000).
6. Sanchez-Panchuelo, R.M., Francis, S., Bowtell, R. & Schluppeck, D. Mapping human somatosensory cortex in individual subjects with 7T functional MRI. *J Neurophysiol* **103**, 2544-2556 (2010).
7. Formisano, E.*, et al.* Mirror-symmetric tonotopic maps in human primary auditory cortex. *Neuron* **40**, 859-869 (2003).
8. Logothetis, N.K. What we can do and what we cannot do with fMRI. *Nature* **453**, 869-878 (2008).
9. Rockel, A.J., Hiorns, R.W. & Powell, T.P. The basic uniformity in structure of the neocortex. *Brain* **103**, 221-244 (1980).
10. Buzsaki, G., Kaila, K. & Raichle, M. Inhibition and brain work. *Neuron* **56**, 771-783 (2007).
11. Nunez, P.L., Wingeier, B.M. & Silberstein, R.B. Spatial-temporal structures of human alpha rhythms: theory, microcurrent sources, multiscale measurements, and global binding of local networks. *Human brain mapping* **13**, 125-164 (2001).
12. Ahlfors, S.P.*, et al.* Cancellation of EEG and MEG signals generated by extended and distributed sources. *Human brain mapping* **31**, 140-149 (2010).
13. Dale, A.M. & Halgren, E. Spatiotemporal mapping of brain activity by integration of multiple imaging modalities. *Current opinion in neurobiology* **11**, 202-208 (2001).
14. Pfurtscheller, G. & Cooper, R. Frequency dependence of the transmission of the EEG from cortex to scalp. *Electroencephalogr Clin Neurophysiol* **38**, 93-96 (1975).
15. Hamalainen, M., Hari, R., Ilmoniemi, R.J., Knuutila, J. & Lounasmaa, O.V. Magnetoencephalography - theory, instrumentation, and applications to noninvasive studies of the working human brain. *Reviews of Modern Physics* **65**, 413 (1993).
16. Penfield, W. & Boldrey, E. Somatic motor and sensory representation in the cerebral cortex of man as studied by electrical stimulation. *Brain* **60**, 389-443 (1938).
17. Ojemann, G.A. & Whitaker, H.A. Language localization and variability. *Brain and language* **6**, 239-260 (1978).
18. Miller, K.J., Sorensen, L.B., Ojemann, J.G. & denNijs, M. Power-Law Scaling in the Brain Surface Electric Potential. *PLoS Comput Biol* **5**, e1000609 (2009).
19. Berger, H. Electroencephalogram of humans. *J. Psychol. Neurol.* **40**, 160-179 (1930).
20. Jasper, H.H. & Andrews, H.L. Electro-encephalography. III. Normal differentiation of occipital and precentral regions in man. *Archives of Neurology and Psychiatry* **39**, 96-115 (1938).
21. Chatrian, G.E., Petersen, M.C. & Lazarte, J.A. The Blocking of the Rolandic Wicket Rhythm and Some Central Changes Related to Movement. *Electroencephalogr. Clin. Neurophysiol.* **11**, 497-510 (1959).
22. Crone, N.E.*, et al.* Functional mapping of human sensorimotor cortex with electrocorticographic spectral analysis. I. Alpha and beta event-related desynchronization. *Brain* **121 (Pt 12)**, 2271-2299 (1998).
23. Miller, K.J.*, et al.* Spectral changes in cortical surface potentials during motor movement. *J Neurosci* **27**, 2424-2432 (2007).
24. Fried, I., Ojemann, G.A. & Fetz, E.E. Language-related potentials specific to human language cortex. *Science* **212**, 353-356 (1981).
25. Ojemann, G.A., Fried, I. & Lettich, E. Electrocorticographic (ECoG) correlates of language. I. Desynchronization in temporal language cortex during object naming. *Electroencephalogr Clin Neurophysiol* **73**, 453-463 (1989).
26. Canolty, R.T.*, et al.* Spatiotemporal dynamics of word processing in the human brain. *Frontiers in neuroscience* **1**, 185-196 (2007).

27. Llinas, R.R. & Steriade, M. Bursting of thalamic neurons and states of vigilance. *J Neurophysiol* **95**, 3297-3308 (2006).
28. Steriade, M., McCormick, D.A. & Sejnowski, T.J. Thalamocortical oscillations in the sleeping and aroused brain. *Science* **262**, 679-685 (1993).
29. Pfurtscheller, G. & Lopes da Silva, F.H. Event-related EEG/MEG synchronization and desynchronization: basic principles. *Clin Neurophysiol* **110**, 1842-1857 (1999).
30. Uhlhaas, P.J. & Singer, W. Neural synchrony in brain disorders: relevance for cognitive dysfunctions and pathophysiology. *Neuron* **52**, 155-168 (2006).
31. Lim, V.K., Hamm, J.P., Byblow, W.D. & Kirk, I.J. Decreased desychronisation during self-paced movements in frequency bands involving sensorimotor integration and motor functioning in Parkinson's disease. *Brain research bulletin* **71**, 245-251 (2006).
32. Hummel, F., Andres, F., Altenmuller, E., Dichgans, J. & Gerloff, C. Inhibitory control of acquired motor programmes in the human brain. *Brain* **125**, 404-420 (2002).
33. Schnitzler, A., Timmermann, L. & Gross, J. Physiological and pathological oscillatory networks in the human motor system. *Journal of Physiology-Paris* **99**, 3-7 (2006).
34. Kubanek, J., Miller, K.J., Ojemann, J.G., Wolpaw, J.R. & Schalk, G. Decoding flexion of individual fingers using electrocorticographic signals in humans. *Journal of neural engineering* **6**, 066001 (2009).
35. Sinai, A*., et al.* Electrocorticographic high gamma activity versus electrical cortical stimulation mapping of naming. *Brain* **128**, 1556-1570 (2005).
36. Miller, K.J., Abel, T.J., Hebb, A.O. & Ojemann, J.G. Rapid online language mapping with electrocorticography. *J Neurosurg Pediatr* **7**, 482-490 (2011).
37. Edwards, E*., et al.* Spatiotemporal imaging of cortical activation during verb generation and picture naming. *NeuroImage* **50**, 291-301 (2010).
38. Pei, X*., et al.* Spatiotemporal dynamics of electrocorticographic high gamma activity during overt and covert word repetition. *NeuroImage* **54**, 2960-2972 (2011).
39. Towle, V.L*., et al.* ECoG gamma activity during a language task: differentiating expressive and receptive speech areas. *Brain* **131**, 2013-2027 (2008).
40. Kellis, S*., et al.* Decoding spoken words using local field potentials recorded from the cortical surface. *Journal of neural engineering* **7**, 056007 (2010).
41. Singer, W. Neuronal synchrony: a versatile code for the definition of relations? *Neuron* **24**, 49-65, 111-125 (1999).
42. Fries, P. Neuronal gamma-band synchronization as a fundamental process in cortical computation. *Annual review of neuroscience* **32**, 209-224 (2009).
43. Cardin, J.A*., et al.* Driving fast-spiking cells induces gamma rhythm and controls sensory responses. *Nature* **459**, 663-667 (2009).
44. Manning, J.R., Jacobs, J., Fried, I. & Kahana, M.J. Broadband shifts in LFP power spectra are correlated with single-neuron spiking in humans. *Journal of Neuroscience* **29**, 13613–13620 (2009).
45. Ray, S. & Maunsell, J.H. Different origins of gamma rhythm and high-gamma activity in macaque visual cortex. *PLoS biology* **9**, e1000610 (2011).
46. Osipova, D., Hermes, D. & Jensen, O. Gamma power is phase-locked to posterior alpha activity. *PloS one* **3**, e3990 (2008).
47. Canolty, R.T*., et al.* High gamma power is phase-locked to theta oscillations in human neocortex. *Science* **313**, 1626-1628 (2006).
48. Miller, K.J*., et al.* Dynamic modulation of local population activity by rhythm phase in human occipital cortex during a visual search task. *Frontiers in human neuroscience* **4**, 197 (2010).
49. Lisman, J. & Buzsaki, G. A neural coding scheme formed by the combined function of gamma and theta oscillations. *Schizophrenia bulletin* **34**, 974-980 (2008).
50. Voytek, B*., et al.* Shifts in gamma phase-amplitude coupling frequency from theta to alpha over posterior cortex during visual tasks. *Frontiers in human neuroscience* **4**, 191 (2010).
51. Ogawa, S. & Lee, T.M. Magnetic resonance imaging of blood vessels at high fields: in vivo and in vitro measurements and image simulation. *Magn Reson Med* **16**, 9-18 (1990).
52. Riera, J.J. & Sumiyoshi, A. Brain oscillations: ideal scenery to understand the neurovascular coupling. *Current opinion in neurology* **23**, 374-381 (2010).
53. Lindauer, U*., et al.* Neurovascular coupling in rat brain operates independent of hemoglobin deoxygenation. *J Cereb Blood Flow Metab* **30**, 757-768 (2010).
54. Fox, P.T. & Raichle, M.E. Focal physiological uncoupling of cerebral blood flow and oxidative metabolism during somatosensory stimulation in human subjects. *Proceedings of the National Academy of Sciences of the United States of America* **83**, 1140-1144 (1986).

55. Fox, P.T., Raichle, M.E., Mintun, M.A. & Dence, C. Nonoxidative glucose consumption during focal physiologic neural activity. *Science* **241**, 462-464 (1988).
56. Attwell, D. & Iadecola, C. The neural basis of functional brain imaging signals. *Trends in neurosciences* **25**, 621-625 (2002).
57. Logothetis, N.K., Pauls, J., Augath, M., Trinath, T. & Oeltermann, A. Neurophysiological investigation of the basis of the fMRI signal. *Nature* **412**, 150-157 (2001).
58. Viswanathan, A. & Freeman, R.D. Neurometabolic coupling in cerebral cortex reflects synaptic more than spiking activity. *Nature neuroscience* **10**, 1308-1312 (2007).
59. Lauritzen, M. Reading vascular changes in brain imaging: is dendritic calcium the key? *Nature reviews* **6**, 77-85 (2005).
60. Petzold, G.C. & Murthy, V.N. Role of astrocytes in neurovascular coupling. *Neuron* **71**, 782-797 (2011).
61. Niessing, J.*, et al.* Hemodynamic signals correlate tightly with synchronized gamma oscillations. *Science* **309**, 948-951 (2005).
62. Mukamel, R.*, et al.* Coupling between neuronal firing, field potentials, and FMRI in human auditory cortex. *Science* **309**, 951-954 (2005).
63. Ekstrom, A. How and when the fMRI BOLD signal relates to underlying neural activity: the danger in dissociation. *Brain research reviews* **62**, 233-244 (2009).
64. Maier, A.*, et al.* Divergence of fMRI and neural signals in V1 during perceptual suppression in the awake monkey. *Nature neuroscience* **11**, 1193-1200 (2008).
65. Sirotin, Y.B. & Das, A. Anticipatory haemodynamic signals in sensory cortex not predicted by local neuronal activity. *Nature* **457**, 475-479 (2009).
66. Muthukumaraswamy, S.D. & Singh, K.D. Functional decoupling of BOLD and gamma-band amplitudes in human primary visual cortex. *Human brain mapping* **30**, 2000-2007 (2009).
67. Brookes, M.J.*, et al.* GLM-beamformer method demonstrates stationary field, alpha ERD and gamma ERS co-localisation with fMRI BOLD response in visual cortex. *NeuroImage* **26**, 302-308 (2005).
68. Lachaux, J.P.*, et al.* Relationship between task-related gamma oscillations and BOLD signal: new insights from combined fMRI and intracranial EEG. *Human brain mapping* **28**, 1368-1375 (2007).
69. Ojemann, G.A.*, et al.* Neuronal correlates of functional magnetic resonance imaging in human temporal cortex. *Brain* **133**, 46-59 (2010).
70. Vansteensel, M.J.*, et al.* Brain-computer interfacing based on cognitive control. *Annals of neurology* **67**, 809-816 (2010).
71. Ritter, P., Moosmann, M. & Villringer, A. Rolandic alpha and beta EEG rhythms' strengths are inversely related to fMRI-BOLD signal in primary somatosensory and motor cortex. *Human brain mapping* **30**, 1168-1187 (2009).
72. Winterer, G.*, et al.* Complex relationship between BOLD signal and synchronization/desynchronization of human brain MEG oscillations. *Human brain mapping* **28**, 805-816 (2007).
73. Scheeringa, R.*, et al.* Trial-by-trial coupling between EEG and BOLD identifies networks related to alpha and theta EEG power increases during working memory maintenance. *NeuroImage* **44**, 1224-1238 (2009).
74. Rosa, M.J., Daunizeau, J. & Friston, K.J. EEG-fMRI integration: a critical review of biophysical modeling and data analysis approaches. *Journal of integrative neuroscience* **9**, 453-476 (2010).
75. Yuan, H., Perdoni, C., Yang, L. & He, B. Differential electrophysiological coupling for positive and negative BOLD responses during unilateral hand movements. *J Neurosci* **31**, 9585-9593 (2011).
76. Leuthardt, E.C., Schalk, G., Moran, D. & Ojemann, J.G. The emerging world of motor neuroprosthetics: a neurosurgical perspective. *Neurosurgery* **59**, 1-14; discussion 11-14 (2006).
77. Wolpaw, J.R., Birbaumer, N., McFarland, D.J., Pfurtscheller, G. & Vaughan, T.M. Brain-computer interfaces for communication and control. *Clin Neurophysiol* **113**, 767-791 (2002).
78. Schalk, G.*, et al.* Two-dimensional movement control using electrocorticographic signals in humans. *Journal of neural engineering* **5**, 75-84 (2008).

Chapter 2

Automated electrocorticographic electrode localization on individually rendered brain surfaces

Dora Hermes[1], Kai J. Miller[2], Herke Jan Noordmans[3], Mariska J. Vansteensel[1], Nick F. Ramsey[1]

[1] Rudolf Magnus Institute of Neuroscience, University Medical Center Utrecht, Department of Neurology and Neurosurgery, section Brainfunction and Plasticity, Utrecht, The Netherlands
[2] Neurobiology and Behavior, University of Washington, Seattle, WA, United States
[3]Department of Medical Technology and Clinical Physics, University Medical Center Utrecht, Utrecht, The Netherlands

Journal of Neuroscience Methods (2010) 185: 293–298

Abstract

Brain surface electrocorticographic (ECoG) recordings can investigate human brain electrophysiology at the cortical surface with exceptionally high signal to noise ratio and spatio-temporal resolution. To be able to use the high spatial resolution of ECoG for accurate brain function mapping and neurophysiology studies, the exact location of the ECoG electrodes on the brain surface should be known. Several issues complicate robust localization: surgical photographs of the electrode array made after implantation are often incomplete because the grids may be moved underneath the skull, beyond the exposed area. Computed tomography (CT) scans made after implantation will clearly localize electrodes, but the effects of surgical intervention may cause the exposed brain to move away from the skull and assume an unpredictable shape (the so-called brain shift). First, we present a method based on a preoperative magnetic resonance imaging (MRI) co-registered with a post-implantation CT scan to localize the electrodes and that automatically corrects for the brain shift by projecting the electrodes to the surface of the cortex. The calculated electrode positions are visualized on the individual subjects brain surface rendering. Second, the method was validated by comparison with surgical photographs, finding a median difference between photographic and calculated electrode centers-of-mass of only 2.6mm, across 6 subjects. Third, to illustrate its utility we demonstrate how functional MRI and ECoG findings in the same subject may be directly compared in a simple motor movement experiment even when electrodes are not visible in the craniotomy.

Introduction

One of the latest additions to the cognitive neuroscience toolbox is electrocorticography (ECoG), where detailed information about the regional and functional organization of the brain is obtained from patients who are implanted with cortical electrodes for diagnostic purposes. Human ECoG is unique in the detail of electrical signal properties (e.g. spatial [1] and temporal [2] resolution), and is growingly applied to cognitive paradigms in the service of cognitive neuroscience. Although patients, typically suffering from epilepsy, exhibit abnormal activity in some brain regions, most of the electrodes cover healthy brain tissue, allowing for extrapolation of findings in cognitive experiments to the normal population.

ECoG recordings measure the electrical potential from the brain surface, using exposed metal electrodes. ECoG recordings are used to functionally identify different brain areas such as motor [3-6], language [7-9], auditory [10], and visual cortex [11], or, for example, to study spontaneous neuronal activity [12] and neurophysiology [13]. The analyses of ECoG electrode signals are done on individual patients and above all are highly specific to the brain tissue from which signal is sampled [14]. Electrodes are typically 2.3 mm in diameter and measure virtually no signal from immediately adjacent neural tissue. A major problem faced in ECoG research is to identify exactly where these electrodes are located. Rough estimations are, given the size of electrodes, insufficient for application of ECoG to neuroscientific questions regarding the regional and functional organization of the brain.

Several issues complicate accurate localization of these electrodes. First, matching photographs made of the grid after implantation to an MRI scan [15], is not sufficient, since neurosurgeons try to minimize the size of the craniotomy and will usually slide electrodes under the skull, away from the exposed area. Second, computed tomography (CT) scans, made after implantation, can localize electrode positions (Noordmans et al., 2001), but the shape of the brain surface is generally changed by the surgical procedure. Leakage of CSF after opening of the dura, the thickness of the implanted material, and the general reaction to surgical intervention, may all cause the exposed brain to move away from the skull and assume an unpredictable shape. This brain shift may cause a significant mismatch that can be more than 1 cm between the CT scan and a magnetic resonance image (MRI) scan obtained preoperatively [16, 17]. Third, post-implantation structural MRI scans would offer a solution to this problem [18, 19], but the clinical safety guidelines of many institutions prohibit post-implant MRI scans for the risk of electrode induction heating [20].

Apart from the few studies using post-implant MRI scans, all papers on ECoG that we are aware of use either a match of MRI rendering to photos, hence ignoring the electrodes positioned under the skull and out of view of a camera, or ignore the shift after matching CT to MRI. Several studies projected electrode locations to a standardized brain in Talairach

coordinates using a method based upon X-rays [21], but this method suffers from the fact that identified electrode locations cannot be linked to subject-specific gyral anatomy, which can vary greatly from person to person. Dalal et al., (2008) approached the problem using operative photos to visually localize the ECoG electrodes on a reconstructed cortex from a preoperative MRI, and combined this with X-rays to include electrodes not visible in the craniotomy. Their manual registration procedure, however, takes quite long, even with experience, and it has not been established whether their method is reproducible across experimenters, or whether it might also work to localize subtemporal or interhemispheric electrodes (where no part of the array is revealed by the craniotomy, making extrapolation less reliable).

Here we present a new method that uses a preoperative MRI co-registered with a post-implantation CT scan to localize the electrodes, and then automatically corrects for the brain shift by projecting the electrodes to the surface of the cortex. It consists of a MATLAB (The Mathworks, Inc., Natick, MA, USA) based package used in combination with SPM5 software (http://www.fil.ion.ucl.ac.uk/spm/). To validate the accuracy of the projection, the auto-registered electrode locations are compared with operative photographs in six patients. For one additional patient we illustrate the usefulness of this method, by showing that electrodes outside the craniotomy can now be included in, for instance, investigation of the relationship between fMRI activation and ECoG.

Materials and methods

Patients

Seven patients were implanted with platinum electrodes (AdTech, Racine, WI, USA) for epilepsy monitoring. Electrodes had a diameter of 2.3 mm exposed (4.0 mm overall) and an inter-electrode distance of 1 cm center-to-center. All patients gave written informed consent, and the study was approved by the ethical committee of the University Medical Centre Utrecht, in accordance with the Declaration of Helsinki 2004.

Technique

Before implantation, structural MRI scans were made on a 1.5T (patients 2, 3, 6 and 7) or 3T (patients 1 and 4-5) scanner (Philips Achieva, Best, The Netherlands). Voxel size for the patients were 0.6 mm x 0.6 mm x 0.6 mm, 0.9 mm x 0.9 mm x 1.2 mm or 1 mm x 1 mm x 1 mm (see supplement for details). One day after surgical ECoG electrode array placement, a high resolution 3D CT scan was made to locate the electrodes (Philips Tomoscan SR7000, voxel size 0.5 mm x 0.5 mm x 1 mm).

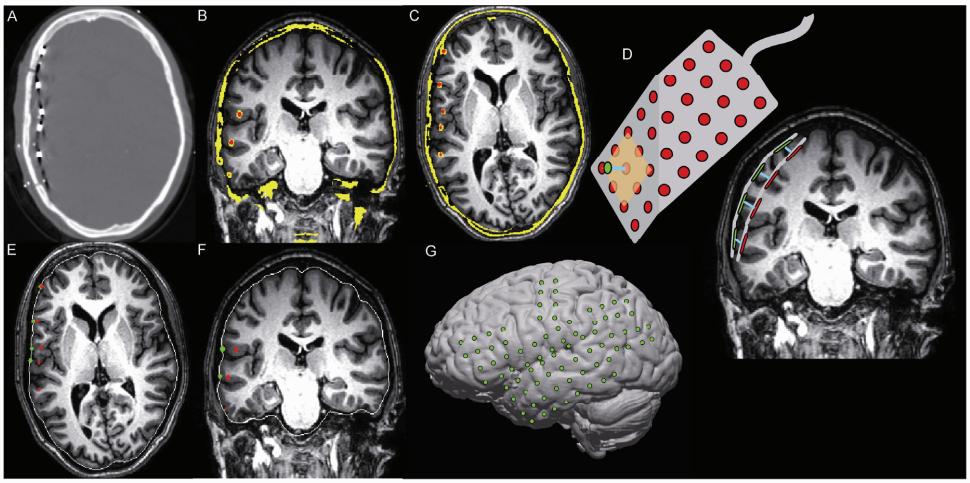

Figure 1. Projection method. (**A**) One slice of the CT scan. (**B** and **C**) Thresholded CT (yellow) with detected electrodes (red) overlaid on an MRI, the brain shift, with electrodes shifted beneath the pre-implantation surface. (**D**) Schematic representation of the projection method. Electrodes are located under the cortical surface (red), are projected to the cortical surface in the direction of the norm of the grid (blue lines), resulting in locations on the cortical surface (green). (**E** and **F**) Example for patient 1, original electrode positions (red), cortical surface (white) and projected electrodes (green). (**G**) Rendering of the cortex with projected electrodes.

First the CT was coregistered and re-sliced to the MRI coordinate frame, using a normalized mutual information routine in the SPM5 analysis environment (Fig. 1A-C) [22]. Mutual information based coregistration has been developed to coregister images from multiple modalities and previous studies have shown that mutual information performs well for the coregistration of CT and MR images [23-26] Approximate locations of desired electrodes were identified manually on the CT by selecting high intensity clusters. Then these clusters were automatically masked by way of thresholding (watershed) and the center of mass of each cluster was assumed to be the location of an electrode. Each electrode was projected from the location found on the CT to the cortical surface of the co-registered MRI scan (Fig. 1D) using the following procedure: the MRI was segmented into grey and white matter compartments using unified segmentation in SPM5 [27]. These compartments were combined into one image, and the resulting volume was then smoothed and thresholded (see supplemental material Table S1), yielding a smoothed cortical surface to which shifted electrodes could be automatically projected (Fig. 1E-F). Each electrode was then projected to the point on the surface in the direction of the local norm vector of the electrode grid (Fig. 1D). The local norm vector was the vector perpendicular to the plane defined by a principal component analysis of a matrix A, where matrix A contains the coordinates on the electrode and its nearest neighbors. For grids consisting of two rows, the electrode of interest and its

three nearest neighbors were used to calculate the local norm vector. For grids consisting of single rows it is impossible to calculate a unique norm vector and these are projected to the closest point on the cortical surface.

Validation

To estimate the accuracy of the projection method, the projected electrodes were visualized on a 3D rendering of the cortical surface (Fig. 1D, 2C), and compared to photos taken during implantation (preoperative photo) and explantation (postoperative photo) of the electrodes for patients 1-6 (no postoperative photos were available for patient number six, and for this patient only the preoperative photo was used for verification of the projection). We used MATLAB and Adobe Photoshop (Adobe Systems, Inc, San Jose, CA, USA) to match the photo to the rendering with computed electrode locations. While on the rendering of the brain the sulci were clearly visible, on the operative photos only blood vessels were clearly visible as landmarks of cortical anatomy. Therefore a reference photo of the brain without electrodes (taken immediately before implantation, Fig. 2B) was used on which both blood vessels and sulci could be marked (Fig. 2D and E respectively). Sulci on the rendering of the brain with the projected electrodes were matched to sulci on the reference photo (Fig. 2F and H) and blood vessels on the pre- and postoperative photos were matched to blood vessels on the reference photo (Fig. 2A and G). Fig. 2F shows how affine and non-affine transformations were used to visually match these photos and that relative positions between sulci and electrode locations were preserved. With affine transformations (rotations, translations and resizing) the rendering and photo with electrodes were roughly matched to sulci and vasculature of the reference photo. After only affine transformations, mainly edges were not accurately registered to the reference photo as shown in the bottom panel in fig. 2F. Warping (in Adobe Photoshop CS3) was subsequently applied only at the edges of the rendering or photo to accurately coregister these to the reference photo (blind to the electrode locations which were repositioned together with the warping). Supplementary Fig. S1 shows the matched photos for all subjects. Electrodes on these matched pictures were overlaid and center to center distances between electrodes on operative photos and projected electrodes were calculated (Fig. 2I). On each picture a reference pair of adjacent electrodes (with a known center-to-center distance of 1 cm) was used to determine the scale.

Application example

To illustrate the usefulness of this method, fMRI with ECoG results of a motor task were overlaid in patient 7. In the motor task the patient moved the thumb during four (fMRI) or five (ECoG) 30 second blocks of movement (thumb flexion/extension at the rate of 2Hz) alternated with five or six 30 second blocks of rest respectively.

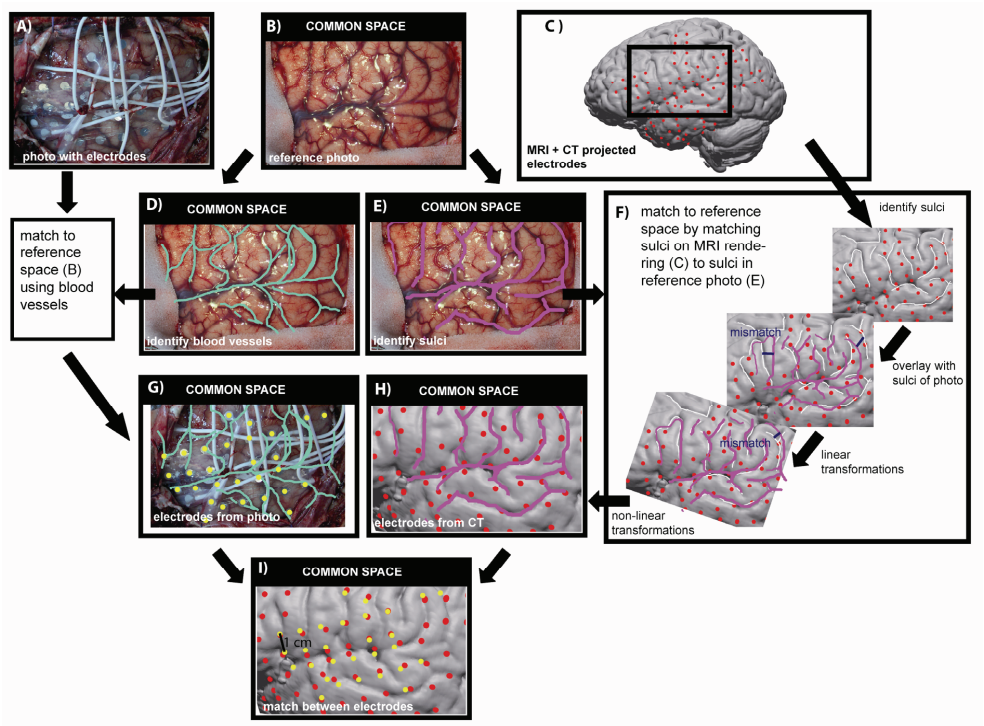

Figure 2. Validation of the projection method. In a reference intra-operative photo (**B**) blood vessels (cyan, in **D**) and sulci (pink, in **E**) were marked. On the rendered surface (MRI) with projected electrodes (**C**) sulci were identified (white) and matched to the sulci on the photo (pink) (**F**). Both linear and non-linear transformations were required to obtain a good match between sulci. In blue the initial mismatch, and mismatch after linear transformation is marked. Note that these transformations do not affect relative positions between electrodes (red) and sulci (white) on the rendering. The same procedure was performed to match blood vessels on the reference photo (**D**) to blood vessels on the operative photo with electrodes (**A**). After registering all photos into common space, the rendering of the brain was visualized with projected electrodes (red) and electrodes from the operative photo (yellow) (**H**). Within a grid, spacing between electrodes was 1 cm.

Before surgery fMRI scans were acquired on a 3T scanner with a 3D PRESTO scan [28, 29]. In one run 340 volumes were acquired with the following parameters: TR/TE 22.5/32.4 ms, flip angle 10 degrees, FOV = 256 mm x 224 mm x 160 mm, acquisition voxel size 4 mm isotropic). Using SPM5 functional images were realigned and coregistered with the anatomical image. A general linear model, including a regressor for motor activation (block design) and realignment parameters to control for movement artifacts, was estimated. The regression coefficient map for the motor task was converted to a statistical map with t-values for assessment of the regions involved in thumb movement, results are reported at $t>3.11$ ($p<0.001$, uncorrected).

The same task was performed by the patient during ECoG recordings. ECoG data were acquired with a 128 channel recording system (SD-128, Micromed, Treviso, Italy) with a sampling rate of 512 Hz, and were band-pass filtered (0.15 – 134.4 Hz). Signals were re-referenced to the common

average of all intracranial electrodes and two second epochs were extracted from movement and rest blocks (respectively 70 and 85 epochs). For each of these epochs, the power spectral density was calculated every 1 Hz by Welch's method [30] with 250 ms windows, overlap of 125 ms and a Hamming window to attenuate edge effects. After normalizing (by element-wise division) the power spectra of each epoch with respect to the mean power over all epochs at each frequency, the log of the normalized power was averaged from 75 to 95 Hz. A t-test was performed on the average log normalized power for each electrode over movement versus rest epochs to assess which electrodes showed significant increases in power during movement. Results are reported at $p<0.05$, Bonferroni corrected for multiple comparisons over electrodes.

Results

Technique

Electrodes were projected to the surface of the brain in the direction orthogonal to the local surface of the shifted cortex (Fig. 1). Supplemental Fig. S2 shows for one subject that a lateral projection would have led to substantially different results. For each patient, the projection procedure, including up to 128 electrodes, took less than 2 hours (including preprocessing of MR and CT scans, for any of three users).

Validation

Distances between electrodes on the photo and the projection are shown in Fig. 3 for patient 1-6 (postoperative photos for patient 1-5, preoperative for patient 6, supplemental Fig. S1). The median distance between the projected electrodes and electrodes on the photo was 2.6 mm (less than 3.4 mm for 75% of the electrodes, less than 5.6 mm for all electrodes). The same results were obtained when preoperative photos were used (median distance to preoperative photo = 2.4 mm, range 0–6.8 mm) and the distance of the projected electrodes to electrodes on the pre- and postoperative photo did not differ (nonparametric Wilcoxon rank sum test, $p=0.92$).

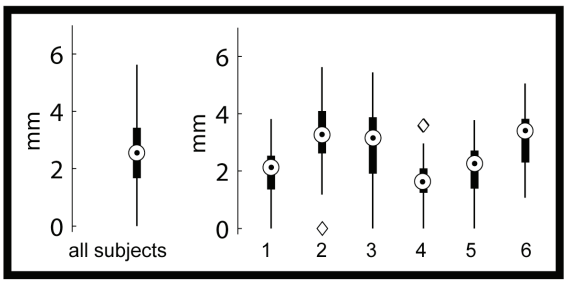

Figure 3. Validation results. Box-plots of the distance between projected electrodes and electrodes on the operative photo with all subjects included and for each subject individually. Circles indicate the median distance, thick bars 50% of the distribution, thin bars indicate the maximum and minimum distance, outliers are indicated by diamonds (points larger than $q_3+1.5(q_3–q_1)$ or smaller than $q_1–1.5(q_3–q_1)$ with q_1 and q_3 the 25th and 75th percentile respectively).

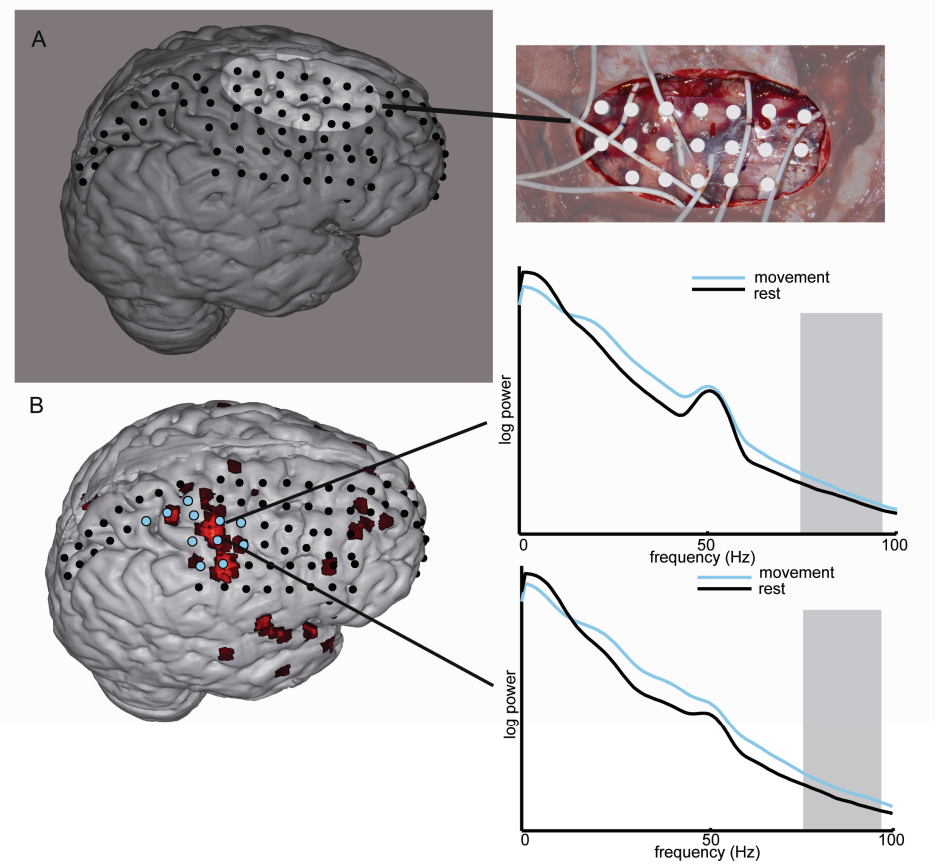

Figure 4. Illustration of the technique in practice. (**A**) Craniotomy indicated on the rendering of the cortical surface with electrode positions and photo. (**B**) Rendering of the cortical surface with in red fMRI regions that were significantly activated by left thumb movement compared to rest ($t_{(325)}$>3.11, p<0.001 uncorrected). In cyan: electrodes with significant increases in power in the high frequency bands (75-95 Hz) during movement compared to rest (p<0.05 Bonferroni corrected for total number of electrodes). For two electrodes that showed a significant difference, power spectra averaged over movement (cyan) and rest (black) epochs are shown. At 50 Hz a line noise (ambient contamination) peak is visible.

Application example

Fig. 4A shows the craniotomy of patient 7 where only 19 out of 104 ECoG electrodes were visible. Electrodes that showed significant power differences (p<0.05 Bonferroni corrected) in high frequencies (75-95 Hz) during thumb movement compared to rest were located outside the craniotomy on the pre- and postcentral gyri (Fig. 4B). All electrodes were located in or near areas that showed significant differences in BOLD activation ($t_{(325)}$>3.11, p<0.001 uncorrected) during the same motor task.

Discussion

The identification of the exact location of the electrodes is an important issue in ECoG research. This study first presents a method to localize ECoG electrodes on an individual, preoperative MRI scan.

The MRI was co-registered with a CT scan made after implantation of the ECoG electrodes. The CT was then used to localize the ECoG electrodes and these electrodes were automatically projected on the cortical surface of the MRI. Second, to validate the method, a comparison between projected electrode locations and operative photos in six patients showed that this method localized electrodes to a 2.6 mm median accuracy, a value that is in the order of the electrode diameter (2.3 mm). Third, to illustrate the utility of the method we show a match between fMRI and ECoG data from a motor task for one patient with electrodes on the sensorimotor areas outside the craniotomy. Electrodes were projected to the surface of the brain, correcting for a brain shift that can be on the order of 1 cm or more [16, 17]. To enable an automatic procedure, it was assumed that electrodes have to be projected orthogonal to the local surface of the shifted cortex and that this transformation would be a good approximation of the brain shift. Other corrections for the brain shift, such as a simple lateral projection, would have led to substantially different results. An orthogonal projection is a simple transformation that proves to be robust and the validation with photos shows that its results are reliable across subjects. Similar precision to this study was reported by Dalal et al (2008) who presented a semi-automated method in which X-rays and operative photos are used to visually localize electrodes on a preoperative MRI. Visually matching electrode positions is, however, much more time consuming and depends heavily on the expertise of the experimenter. Our method is independent of human expertise and most importantly, it does not rely on photos and therefore yields reliable results in electrodes positioned under the skull away from the opening.

A critical step in our study is the accuracy of the coregistration of CT and MRI scans. For coregistration of CT and MRI scans mutual information was applied, because many previous studies have shown that it yields very accurate matching results [23-26], see also [31] for a survey of these studies. Although for the purpose of the present study a high resolution MRI scan was obtained for high detail of surface rendering, lower resolution MRI scans (which may be the standard in many clinical settings) can be expected to yield the same results in terms of accuracy of matching (see also West et al., 1999). The fact that mutual information based co-registration uses all voxels in the images and it does not assume a specific functional relationship between tissue intensities across modalites ensures a reliable global match between two images of different modalities [32].

The accuracy of the projection method was validated using photos of the brain taken during implantation and explantation of the grids. Operative photos can be used as a gold standard of electrode positions, but others have reported that there can be a difference in electrode positions between pre and postoperative photos [15]. Electrodes can be shifted during closure of the dura after implantation as well as during opening before explantation. However, the distance between the projected electrodes and electrodes on pre- or postoperative photos did not differ.

To illustrate a potential benefit of the method, an example is shown where the relationship between fMRI and ECoG may be investigated even if electrodes are outside the craniotomy. In such cases, photographs would be of no use for invisible electrodes, limiting investigation to visible cortex. Given our estimate of projection accuracy based on the present study, and the reasonable assumption that the correction method yields equal results for visible and non-visible electrodes, the example illustrates an added value of the technique.

There are several other advantages in using this technique, one of which is that it is fully automated. It is readily implemented, since it only requires MATLAB and SPM5. As long as the surface of a volume can be estimated, electrodes can be projected in the direction of the norm vector of the grid to the closest point on the surface. When one hemisphere is removed from the MRI, interhemispheric electrodes can be localized and the same can be done for subtemporal electrodes after segmentation and removal of the cerebellum. Coregistration with other medical images such as angiograms is also possible, allowing one to see whether an electrode is located on a blood vessel. When projecting the electrodes to an individual MRI scan, the electrode coordinates are specific for the subjects' brain volume, and when normalizing this to MNI or Talairach space, coordinates in these standard spaces can easily be extracted. Only a high resolution pre-implantation MRI and a high resolution post-implantation CT scan are required and the software is available upon request from the authors.

In conclusion, this method enables localization of ECoG electrodes on individually rendered cortical surfaces. It enables rapid and accurate localization of ECoG measures to brain anatomy. ECoG measures can now be seamlessly integrated with findings from other experimental modalities, such as fMRI, constituting a powerful tool for exploration of neural physiology in humans.

Acknowledgements

The authors thank Peter Gosselaar and Peter van Rijen for implantation of the grids, Frans Leijten and Cyrille Ferrier for their help in acquiring the data and Josien Pluim for her advice on image coregistration. This research is supported by the Dutch Technology Foundation STW, applied science division of NWO and the Technology Program of the Ministery of Economic Affairs, and the University of Utrecht, grant UGT7685. We appreciate the enthusiastic participation of the patient's and staff at UMC hospital in Utrecht.

References

1. Cooper, R., Winter, A.L., Crow, H.J. & Walter, W.G. Comparison of subcortical, cortical and scalp activity using chronically indwelling electrodes in man. *Electroencephalography and Clinical Neurophysiology* **18**, 217-228 (1965).
2. Miller, K.J., Zanos, S., Fetz, E.E., den Nijs, M. & Ojemann, J.G. Decoupling the cortical power spectrum reveals real-time representation of individual finger movements in humans. *J Neurosci* **29**, 3132-3137 (2009).
3. Crone, N.E.*, et al.* Functional mapping of human sensorimotor cortex with electrocorticographic spectral analysis. I. Alpha and beta event-related desynchronization. *Brain* **121**, 2271-2299 (1998).
4. Crone, N.E., Miglioretti, D.L., Gordon, B. & Lesser, R.P. Functional mapping of human sensorimotor cortex with electrocorticographic spectral analysis. II. Event-related synchronization in the gamma band. *Brain* **121**, 2301-2315 (1998).
5. Pfurtscheller, G., Graimann, B., Huggins, J.E., Levine, S.P. & Schuh, L.A. Spatiotemporal patterns of beta desynchronization and gamma synchronization in corticographic data during self-paced movement. *Clin Neurophysiol* **114**, 1226-1236 (2003).
6. Miller, K.J.*, et al.* Spectral changes in cortical surface potentials during motor movement. *J Neurosci* **27**, 2424-2432 (2007).
7. Crone, N.E., Boatman, D., Gordon, B. & Hao, L. Induced electrocorticographic gamma activity during auditory perception. Brazier Award-winning article, 2001. *Clin Neurophysiol* **112**, 565-582 (2001).
8. Crone, N.E.*, et al.* Electrocorticographic gamma activity during word production in spoken and sign language. *Neurology* **57**, 2045-2053 (2001).
9. Sinai, A.*, et al.* Electrocorticographic high gamma activity versus electrical cortical stimulation mapping of naming. *Brain* **128**, 1556 (2005).
10. Edwards, E., Soltani, M., Deouell, L.Y., Berger, M.S. & Knight, R.T. High gamma activity in response to deviant auditory stimuli recorded directly from human cortex. *Journal of neurophysiology* **94**, 4269-4280 (2005).
11. Yoshor, D., Bosking, W.H., Ghose, G.M. & Maunsell, J.H. Receptive fields in human visual cortex mapped with surface electrodes. *Cereb Cortex* **17**, 2293-2302 (2007).
12. Nir, Y.*, et al.* Interhemispheric correlations of slow spontaneous neuronal fluctuations revealed in human sensory cortex. *Nature Neurosci* **11**, 1100-1108 (2008).
13. Canolty, R.T.*, et al.* High gamma power is phase-locked to theta oscillations in human neocortex. *Science* **313**, 1626-1628 (2006).
14. Ball, T., Schulze-Bonhage, A., Aertsen, A. & Mehring, C. Differential representation of arm movement direction in relation to cortical anatomy and function. *Journal of neural engineering* **6**, 016006 (2009).
15. Wellmer, J.*, et al.* Digital photography and 3D MRI-based multimodal imaging for individualized planning of resective neocortical epilepsy surgery. *Epilepsia* **43**, 1543-1550 (2002).
16. Dalal, S.S.*, et al.* Localization of neurosurgically implanted electrodes via photograph-MRI-radiograph coregistration. *Journal of neuroscience methods* **174**, 106-115 (2008).
17. Hill, D.L.*, et al.* Sources of error in comparing functional magnetic resonance imaging and invasive electrophysiological recordings. *Journal of neurosurgery* **93**, 214-223 (2000).
18. Schulze-Bonhage, A.H.*, et al.* Visualization of subdural strip and grid electrodes using curvilinear reformatting of 3D MR imaging data sets. *Ajnr* **23**, 400-403 (2002).
19. Studholme, C., Novotny, E., Zubal, I.G. & Duncan, J.S. Estimating tissue deformation between functional images induced by intracranial electrode implantation using anatomical MRI. *NeuroImage* **13**, 561-576 (2001).
20. Bhavaraju, N.C., Nagaraddi, V., Chetlapalli, S.R. & Osorio, I. Electrical and thermal behavior of non-ferrous noble metal electrodes exposed to MRI fields. *Magnetic resonance imaging* **20**, 351-357 (2002).
21. Miller, K.J.*, et al.* Cortical electrode localization from X-rays and simple mapping for electrocorticographic research: The "Location on Cortex" (LOC) package for MATLAB. *Journal of neuroscience methods* **162**, 303-308 (2007).
22. Wells, W.M., 3rd, Viola, P., Atsumi, H., Nakajima, S. & Kikinis, R. Multi-modal volume registration by maximization of mutual information. *Medical image analysis* **1**, 35-51 (1996).
23. Studholme, C., Hill, D.L. & Hawkes, D.J. Automated 3-D registration of MR and CT images of the head. *Medical image analysis* **1**, 163-175 (1996).

24. Hill, D.L., Batchelor, P.G., Holden, M. & Hawkes, D.J. Medical image registration. *Physics in medicine and biology* **46**, R1-45 (2001).
25. Maes, F., Collignon, A., Vandermeulen, D., Marchal, G. & Suetens, P. Multimodality image registration by maximization of mutual information. *IEEE transactions on medical imaging* **16**, 187-198 (1997).
26. West, J.*, et al.* Retrospective intermodality registration techniques for images of the head: surface-based versus volume-based. *IEEE transactions on medical imaging* **18**, 144-150 (1999).
27. Ashburner, J. & Friston, K.J. Unified segmentation. *NeuroImage* **26**, 839-851 (2005).
28. Neggers, S.F., Hermans, E.J. & Ramsey, N.F. Enhanced sensitivity with fast three-dimensional blood-oxygen-level-dependent functional MRI: comparison of SENSE-PRESTO and 2D-EPI at 3 T. *NMR in biomedicine* **21**, 663-676 (2008).
29. Ramsey, N.F.*, et al.* Phase navigator correction in 3D fMRI improves detection of brain activation: quantitative assessment with a graded motor activation procedure. *NeuroImage* **8**, 240-248 (1998).
30. Welch, P. The use of fast Fourier transform for the estimation of power spectra: A method based on time averaging over short, modified periodograms. *IEEE Trans. Audio Electroacoustics* **15**, 70-73 (1967).
31. Pluim, J.P., Maintz, J.B. & Viergever, M.A. Mutual-information-based registration of medical images: a survey. *IEEE transactions on medical imaging* **22**, 986-1004 (2003).
32. Roche, A., Malandain, G. & Udupa, J.K. Unifying maximum likelihood approaches in medical image registration. *Int J Imag Syst Tech* **11**, 71-80 (2000).

Chapter 2 supplementary material

Table S1. MRI scan parameters and preprocessing parameters for each subject. Scan parameters include matrix size, voxel size, repetition time (TR), echo time (TE), and degrees of flip angle. Preprocessing parameters include the smoothing kernel of the gray and white matter compartments in mm full width half max (FWHM) and cutoff threshold to define the cortical surface. The amount of smoothing and threshold were dependent on the type and quality of the structural scan.

Subject	Scanner	Matrix Size	Voxel Size (mm)	TR (ms)	TE (ms)	Flip angle	Smoothing kernel (mm FWHM)	Threshold
1	3T	260x322x267	0.6x0.6x0.6	7.7	3.8	8	6	0.1
2	1.5T	256x256x100	0.9x0.9x1.2	30	13	30	16	0.3
3	1.5T	256x256x104	0.9x0.9x1.2	30	13	30	6	0.1
4	3T	288x288x175	1x1x1	8.4	3.8	8	10	0.05
5	3T	288x288x175	1x1x1	8.4	3.8	8	10	0.1
6	1.5T	256x256x100	0.9x0.9x1.2	30	4.6	30	6	0.1
7	3T	288x288x175	1x1x1	8.4	3.8	8	16	0.25

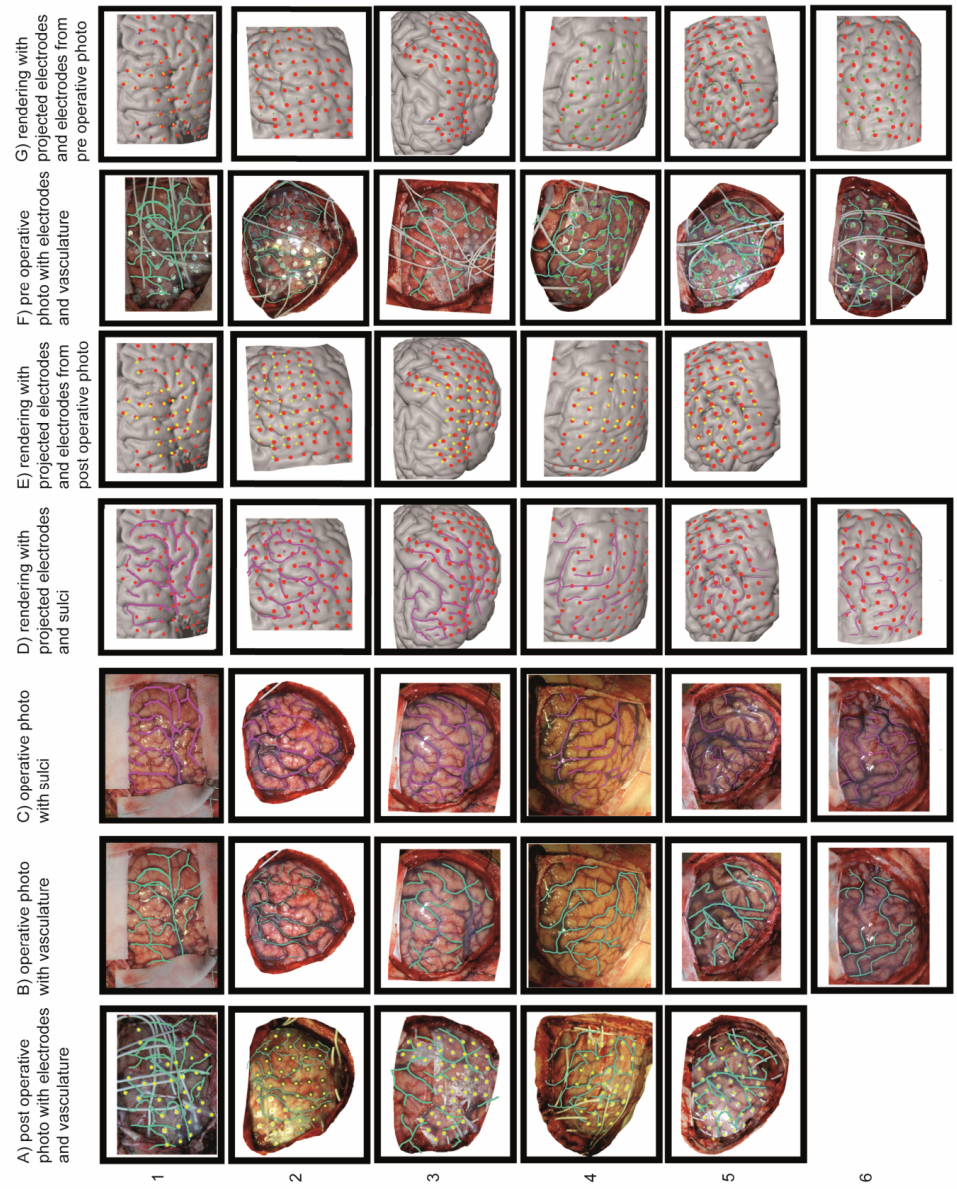

Figure S1. Figures used to verify projection method for all subjects (rows). Columns: postoperative photo with electrodes (yellow) and vasculature (cyan), reference photo of the brain with vasculature (cyan), reference photo with sulci (pink), rendering with projected electrodes (red) and sulci (pink), rendering with projected electrodes (red) and electrodes from postoperative photo (yellow), preoperative photo with electrodes and vasculature (cyan), rendering with projected electrodes (red) and electrodes from preoperative photo (colors). For patient six, no postoperative photos were available.

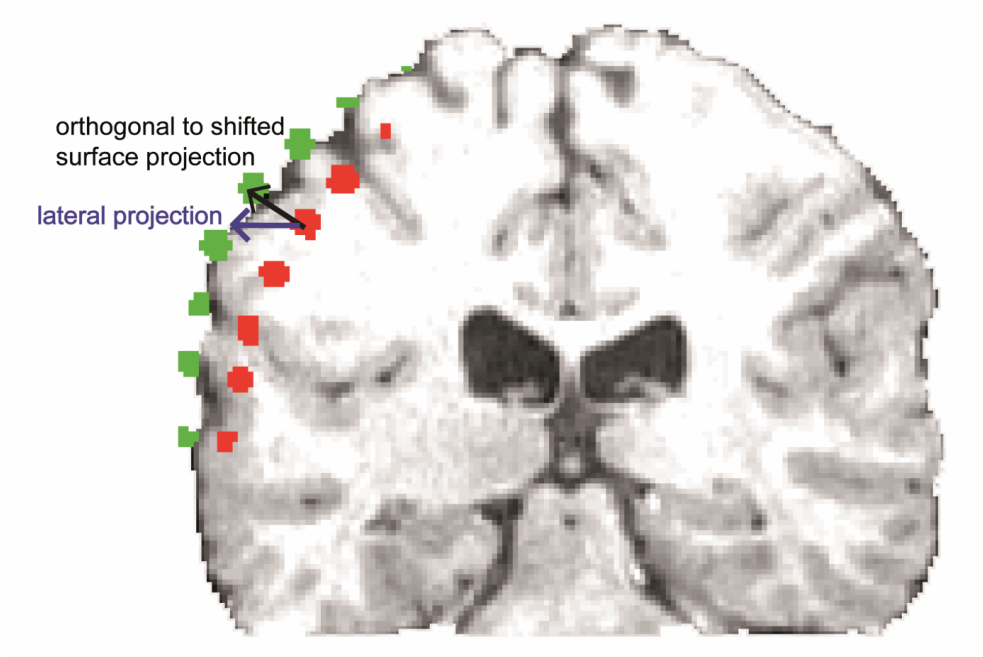

Figure S2. Electrodes were projected to the surface of the brain in the direction orthogonal to the local surface of the shifted cortex (green to red positions, indicated by black arrow). A lateral projection (blue arrow) would have lead to substantially different results.

Chapter 3

fMRI based identification of brain areas involved in motor imagery for implantable BCIs

D. Hermes[1], M.J. Vansteensel[1], A.M. Albers[1], M.G. Bleichner[1], M.R. Benedictus[1], C. Mendez Orellana[1,2], E.J. Aarnoutse[1], N.F. Ramsey[1]

[1] Rudolf Magnus Institute of Neuroscience, University Medical Center Utrecht, Department of Neurology and Neurosurgery, section Brain Function and Plasticity, Utrecht, The Netherlands

[2] Department of Neurology, Erasmus MC, University Medical Center, Rotterdam, The Netherlands

Journal of Neural Engineering (2011) 8, 2.

Abstract

For the development of minimally invasive brain computer interfaces (BCIs) it is important to accurately localize the area of implantation. Using fMRI, we investigated which brain areas are involved in motor imagery. Twelve healthy subjects performed a motor execution and imagery task during separate fMRI and EEG measurements. fMRI results showed that during imagery premotor and parietal areas were most robustly activated in individual subjects, but surprisingly, no activation was found in the primary motor cortex. EEG results showed spectral power decreases in contralateral sensorimotor rhythms (8-24Hz) during both movement and imagery. To further verify the involvement of the motor imagery areas found with fMRI, one epilepsy patient performed the same task during both fMRI and ECoG recordings. Significant ECoG low (8-24Hz) and high (65-95Hz) frequency power changes were observed selectively on premotor cortex and these co-localized with fMRI. During a subsequent BCI task, excellent performance (91%) was obtained based on ECoG power changes from the localized premotor area. These results indicate that other areas than the primary motor area may be more reliably activated during motor imagery. Specifically, the premotor cortex may be a better area to implant an invasive BCI.

Introduction

Implantable brain computer interfaces (BCIs) require a stable, reliable signal from an area that can easily be localized before implanting a device [1]. Motor imagery is one of the most used strategies to control a non-invasive BCI and this study investigates whether we can localize a brain area that is specifically and reliably activated during motor imagery.

BCI studies recording multiunits from several areas in the macaque have shown that in addition to primary motor cortex (M1), premotor cortex (PMc) and supplementary motor areas (SMA) have signals that would perform just as well to control a BCI [2]. In humans, functional magnetic resonance imaging (fMRI) allows us to measure the whole brain non-invasively with high spatial resolution and to investigate which areas are activated during motor imagery. Previous fMRI studies have shown that group analyses reveal largely consistent PMc, SMA and dorsal parietal cortex activation during motor imagery [3-11]. In contrast, highly variable results in M1 activation during motor imagery have been observed, for reviews see [9, 11]. Most of these studies have been performed on a group level, but implanting a BCI in a patient requires localization in an individual subject. As the areas active during motor imagery can differ between subjects with different motor imagery ability [10] and activity patterns can change with practice [12, 13], it is important to know which of these motor imagery areas can be identified on a single subject basis. We have previously shown that fMRI can accurately localize function-specific regions in individuals [1, 14]. Here we investigate which brain areas are most robustly activated during motor imagery as it is used in a BCI setup.

We recorded fMRI and EEG separately in 12 subjects and found that in fMRI premotor areas were robustly activated during imagery in every individual subject. ECoG recordings in one patient showed that on these premotor areas spectral power changes co-localized with preoperative fMRI results in the same subject. Furthermore, using the signal from this premotor area during BCI resulted in very good performance (91%).

Methods

Subjects

Twelve healthy right handed BCI naïve participants (age range 19-25 years, 6 females) and one patient (age 17, female) scheduled for the implantation of ECoG arrays (AdTech, Racine, WI, USA) for epilepsy monitoring gave written informed consent to participate in this study. This study was approved by the ethical committee of the University Medical Center Utrecht, in accordance with the Declaration of Helsinki 2008.

Task

All subjects performed a motor execution and imagery task. The task consisted of an instruction ('move', 'imagine' or 'rest', presented for 1.3 s) followed by a block of 15.7 seconds during which a square flashed every 600 ms interleaved by a fixation cross. Subjects were instructed to respectively execute or kinesthetically imagine tapping an alternating finger of the right hand to the thumb at the rhythm of the square or think of nothing in particular during the rest condition. The patient performed the same task but with the left hand.

fMRI measurement

Scans were acquired on a Philips 3T Achieva. During the motor imagery task 871 fMRI PRESTO scans [15] were acquired (FA = 10 degrees, FOV = 224x256x160 mm, voxel size 4x4x4 mm, TE/TR= 33/23 ms, time per whole-brain volume 0.6 s). Functional scans were realigned and coregistered to an anatomical scan (FA = 8 degrees, FOV = 288x288x175, voxel size 1x1x1 mm, TE/TR = 3.8/8.4 ms). Data from the healthy subjects were normalized to MNI space using a unified segmentation procedure [16] and smoothed with an 8 mm full width half max to allow group comparisons. EMG was measured over the right hand extensor digitorum communis and abductor pollicis brevis with four scanner compatible surface electrodes (MR Physiology Logging, Philips Medical Systems Nederland B.V., Eindhoven, Netherlands). The EMG data were analyzed similar as described in [17]. First, the EMG signal was notch filtered at 45 and 90 Hz to remove fMRI artifacts, and high pass filtered at 10 Hz to remove movement artifacts. To regain low frequency components, the signal was rectified. Data were then bandpass filtered between 2 and 130 Hz and the power was calculated. Outliers larger than 2 times the standard deviation were removed. The EMG power was averaged between the 2 recorded channels and convolved with a hemodynamic response function. This regressor was standardized by dividing by the standard deviation and was used as a regressor for the GLM in the fMRI analysis. The GLM also contained a regressor for motor imagery blocks and a separate regressor for the instruction. Parameter estimates of movement (EMG) and imagery blocks were tested for significance with a t-test. Group analysis for significance of movement and imagery activity across subjects are reported at $p<0.001$ uncorrected, cluster size larger than 10 voxels.

EEG and ECoG measurement

EEG and ECoG data were acquired with a 128 channel recording system (Micromed, Treviso, Italy) with 512 Hz sampling rate and 0.15–134.4 Hz band-pass filter. In the patient, arrays of ECoG electrodes were implanted subdurally for the localization of the epileptic seizure focus (for planning of surgical removal). These platinum electrodes had an inter

electrode spacing of 0.5 or 1 cm and an exposed surface of 2.3 mm in diameter. Electrodes were localized from a CT scan and were projected to the cortical surface [18]. EMG signal was measured from the right hand extensor digitorum communis and abductor pollicis brevis to control for EMG during motor imagery.

Signals were re-referenced to the common average of all EEG/ECoG electrodes and two-second epochs were extracted from movement, imagery and rest blocks. Electrodes and epochs that showed eye blink, muscle (EEG) or epileptic (ECoG) artifacts were rejected. For each epoch, the power spectral density was calculated in steps of 1 Hz by Welch's method [19] with 1 s windows and a Hamming window to attenuate edge effects. Spectral power changes for movement and imagery compared to rest periods were then calculated. Power spectra of each epoch were normalized (by element-wise division) with respect to the mean power over all epochs at each frequency and were log-transformed. The log normalized power was then averaged for 8-24 Hz (EEG and ECoG) and for 65-95 Hz (ECoG). T-tests indicated whether differences between rest and (imagined) movement periods were significant, and results are reported at $p<0.05$, Bonferroni corrected for the number of electrodes. For visualization purposes and to quantify the difference in power between movement and rest and motor imagery and rest the r^2 was calculated [20]. The r^2 indicates the percentage of variance explained by different task conditions (movement versus rest and motor imagery versus rest).

BCI control

BCI2000 with the Sigfried module was used for the BCI task [21] in the patient. The ECoG activity from 65-95 Hz from the electrode closest to the area found in fMRI was used to control a cursor in a standard 2-target one-dimensional BCI task in which the cursor moves from left to right (in 2.3 sec) to hit a target on the upper or lower right part of the screen [1]. The patient controlled the y-position of the cursor by imagining the same finger tapping as in the motor imagery task or relaxing during 6 sessions of each 4 minutes (174 trials).

Results

fMRI results

Healthy subjects group image analysis showed that during executed movement there was significant activity in the left M1, bilateral PMc, SMA, primary sensory areas, dorsal parietal cortex, cerebellum and basal ganglia, the left thalamus and right inferior temporal cortex. A part of this network was also activated during imagined movement: during motor imagery there was significant activity in the left PMc, bilateral SMA, dorsal parietal cortex, basal ganglia and cerebellum. Surprisingly, no activity in M1 during motor imagery was found.

As individual subject analyses are more relevant for BCIs and group analyses could hide effects in individual subjects, we also calculated the significantly activated voxels ($t>3.0$, $p<0.001$ uncorrected) for each individual. We superimposed these individual maps, as shown in Fig. 1A. The number of subjects in which a specific area was activated is shown in color. This figure shows a clear absence of activity during imagery in M1 and an overlap for all 12 subjects in the PMc and for almost all subjects in the dorsal parietal area (max 10).

To more specifically test whether there was no significant activity in M1 during motor imagery, we defined M1 from the average anatomical scan by manual segmentation. Within the segmented M1, shown in Fig. 1B, the number of significant voxels during imagery did not differ from zero (3 voxels on average, $t=1.91$, $p=0.08$). During movement there was significant activation in M1 across all subjects (49 voxels on average, $t=29.11$, $p<0.001$). Also, the fMRI signal change in M1 during imagery did not differ from zero ($t=-1.35$, $p=0.20$), whereas during movement there was significant signal increase in M1 ($t=11.47$, $p<0.001$).

EEG results

Fig. 1C shows that in EEG there were significant decreases in power (8-24 Hz) during both movement and imagery compared to rest on contralateral electrodes. In 10 of 12 individual subjects this decrease was significant ($p<0.05$ Bonferroni corrected for multiple comparisons) in contralateral electrodes around sensorimotor cortex (C3, CP3, CCP3, CCP5). The other two subjects showed a power decrease during imagery in these electrodes, but this did not survive multiple comparison correction. These spectral power decreases in contralateral sensorimotor rhythms are similar to those classically seen in other EEG based BCI studies and this suggests that the motor imagery strategy used by the subjects could be used similarly to control an EEG based BCI.

ECoG results and BCI performance

The ECoG data showed significant changes in power in low (8-24 Hz) and high frequencies (65-95 Hz) during motor execution and imagery. Fig. 1D shows that during motor imagery high frequency power increases were localized specifically on the premotor area that showed significant fMRI activation. Electrical stimulation of these electrodes elicited no hand movement. Spectral power decreases in low frequencies were a bit more distributed around this area. Fig. 1D shows that neither low nor high frequency changes were observed on M1.

The cursor in the BCI task was controlled by high frequency power changes from 65-95 Hz from the electrode on the premotor area that was found to be robustly activated by fMRI (indicated in Fig. 1D). On average, the patient performed the BCI task with 91% correct (while 50% is chance level).

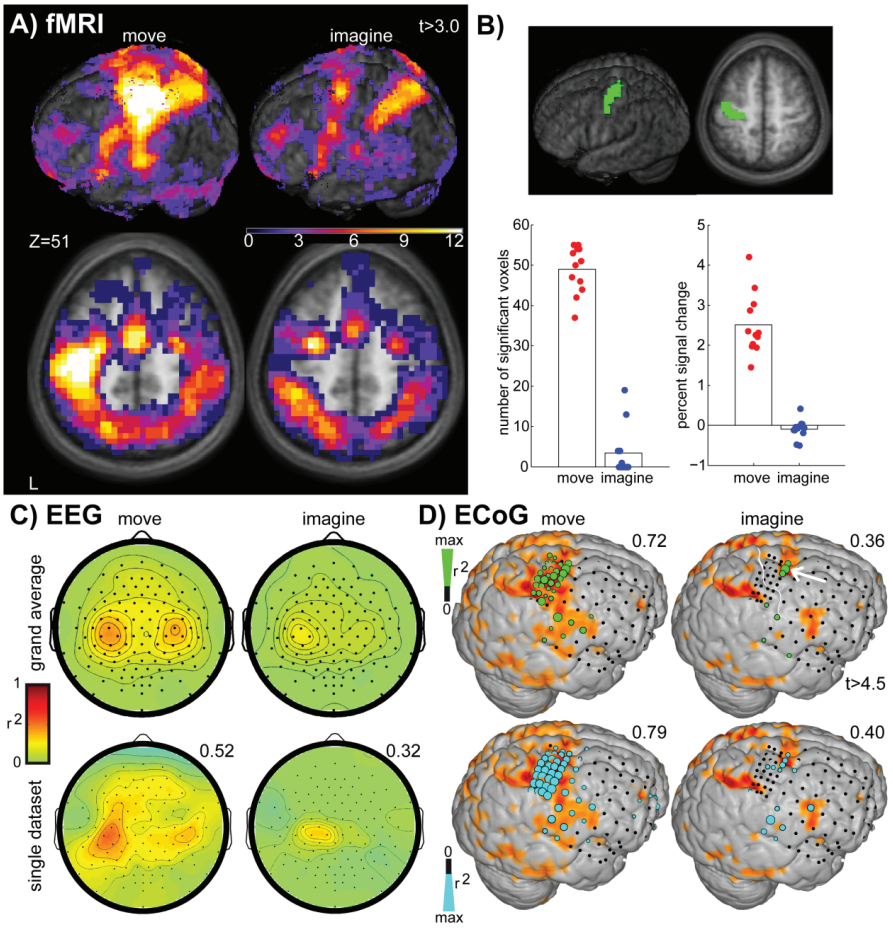

Figure 1. fMRI, EEG and ECoG results. (A) Significant fMRI activity (t>3.0) was calculated for each individual during movement (left panel) and imagery (right panel) compared to rest. These maps are displayed superimposed, and the colorscale indicates the number of subjects that showed significant activation in a region. Results are displayed on the average normalized anatomical scan of all 12 subjects. (B) The primary motor cortex was manually delineated on the average anatomical scan. Within this region the number of significant voxels during movement (red) and imagery (blue) were calculated (left bar graph). We also calculated the percent signal change during movement (red) and imagery (blue), displayed in the right bar graph. (C) The EEG data in the top panel show the grand average r^2 across all 12 subjects during movement (left panel) and imagery (right panel), the color scale ranges from 0 to 1. In the lower panel a representative subject is shown, maximum r^2 values are denoted in the top right. (D) The ECoG data overlaid on the fMRI BOLD increases during movement (left panel) and imagery (right panel) compared to rest (orange, t>4.5, $p_{FWE\ corrected}<0.05$) on the surface rendering of the individual patient. ECoG spectral power increases during movement and imagery in high (65-95 Hz) frequencies are displayed in green in the top panel, decreases in low (8-24 Hz) frequencies are shown in cyan in the bottom panel. For significant electrodes, the size indicates the size of the r^2, which is scaled to the maximum r^2 denoted in the top right. An arrow in the top right panel indicates the electrode used for BCI control and a white line indicates the central sulcus.

Discussion

This study investigated which brain areas were robustly activated during motor imagery and could be localized as a target for an invasive BCI. The fMRI results showed that during motor imagery there was robust activation of the dorsal premotor cortex (PMc) across individual subjects. This activity co-localized with spectral power increase in high frequencies and decrease in low frequency sensorimotor rhythms as measured with ECoG during the same task. The signal from this premotor area was then used to control a BCI, and yielded very good performance (91%).

Previous BCI studies have generally focused on signals from M1 [22-24] . However, signals from other regions may be just as suitable to control a BCI [2]. While several fMRI studies have indicated that M1 may be activated during motor imagery, there is also a large amount of literature that suggests the opposite, for reviews see [9, 11]. In our study we found no evidence for M1 activity during motor imagery. We did find activity in the PMc and previous studies have shown that the dorsal PMc is important for generating the motor plan, before the signal for movement execution is generated in M1 [25, 26]. The fMRI changes in the PMc co-localized well with ECoG signal change in high frequencies, indicating that the signal we measure with fMRI is related to high frequency power change, as has also been shown in other studies [27-29]. Since the spectral power changes in high frequencies from this area yielded very good BCI performance, the results strongly suggest that fMRI localization of PMc for motor imagery is reliable enough for subsequent electrode positioning for a BCI implant.

In addition to the PMc, the dorsal parietal area was activated across almost all subjects during fMRI. Previous studies on motor imagery have suggested that this area is involved in sensorimotor mapping [26] or movement simulation [30] and patients with lesions in this area have impaired motor imagery capabilities [31]. Research in non-human primates has shown that signals from this area can be used to decode intended movement direction and are suitable to control a BCI [32], but since ECoG electrodes did not cover this area, we were unable to further explore the suitability of this area for ECoG motor imagery based BCI control.

There are several possible explanations for the difference between this study and other BCI studies that do find M1 activation during motor imagery. For one, not many studies have corrected for (subtle) movements during imagery. In the present study movement was eliminated from imagery fMRI maps by including EMG in the analysis directly. Secondly, M1 activity may be stronger when feedback is given as compared to activity during a localizer task [24]. Previous studies have indeed shown that attention can modulate signal changes during movement in M1 [33]. Third, motor imagery may differ from attempted movement:

tetraplegic patients have successfully generated activity in M1 by *attempting* movement [34]. Whereas M1 may thus be suitable for BCI control, our fMRI results suggest that other areas, such as the dorsal premotor cortex, are more robust in their activation pattern and easy to localize in an individual subject. While ECoG results could only be collected in one patient, they confirmed the fMRI results and signals from PMd resulted in successful BCI performance. Further ECoG studies are required to determine the generalizability of our findings across patients.

While fMRI indicated no activity of M1 during motor imagery, the EEG data showed spectral power decreases in sensorimotor rhythms that peaked around contralateral sensorimotor areas. Considering the ECoG data which showed low frequency spectral power change in PMc co-localized on the areas found by fMRI and also other studies that reported good co-localization between fMRI and low frequency power decrease [35, 36], it is unlikely that we measured signals from different areas with EEG and fMRI. The fact that parietal and premotor areas, specifically dorsal PMc, are adjacent to the central sulcus, and that the EEG signal exhibits an inherently lower spatial resolution than fMRI, may contribute to the apparent focus over primary sensorimotor areas that we saw on the scalp in this study. More complex EEG analysis methods or a different reference strategy such as a Laplacian, which is more sensitive to local changes [37], or infinite reference [38] may be able to test this notion by teasing apart the signal from these different areas. We chose here for a simple analysis and common average reference, to show that our motor imagery task elicited EEG results that are comparable to those of other BCI studies.

In conclusion, this study suggests that for implanting an invasive BCI, the premotor cortex may be a more suitable target than the primary motor cortex. Furthermore, the match between the fMRI and ECoG data further confirms the reliability of PRESTO fMRI for preoperative localization of areas suitable for BCI implants [1].

Acknowledgements

The authors thank Geertjan Huiskamp, Herke Jan Noordmans, Cyrille Ferrier and Frans Leijten for their help in collecting the data, Peter Gosselaar and Peter van Rijen for implanting the electrodes and the staff of the clinical neurophysiology department for their time. This research is supported by the Dutch Technology Foundation STW, applied science division of NWO and the Technology Program of the Ministery of Economic Affairs, and the University of Utrecht, grant UGT7685, and by the Braingain Smartmix Consortium.

References

1. Vansteensel, M.J., *et al.* Brain-computer interfacing based on cognitive control. *Annals of neurology* **67**, 809-816 (2010).
2. Carmena, J.M., *et al.* Learning to control a brain-machine interface for reaching and grasping by primates. *PLoS biology* **1**, E42 (2003).
3. Decety, J., *et al.* Mapping motor representations with positron emission tomography. *Nature* **371**, 600-602 (1994).
4. Porro, C.A., *et al.* Primary motor and sensory cortex activation during motor performance and motor imagery: a functional magnetic resonance imaging study. *J Neurosci* **16**, 7688-7698 (1996).
5. Deiber, M.P., *et al.* Cerebral processes related to visuomotor imagery and generation of simple finger movements studied with positron emission tomography. *NeuroImage* **7**, 73-85 (1998).
6. Gerardin, E., *et al.* Partially overlapping neural networks for real and imagined hand movements. *Cereb Cortex* **10**, 1093-1104 (2000).
7. Naito, E., *et al.* Internally simulated movement sensations during motor imagery activate cortical motor areas and the cerebellum. *J Neurosci* **22**, 3683-3691 (2002).
8. Ehrsson, H.H., Geyer, S. & Naito, E. Imagery of voluntary movement of fingers, toes, and tongue activates corresponding body-part-specific motor representations. *Journal of neurophysiology* **90**, 3304-3316 (2003).
9. de Lange, F.P., Roelofs, K. & Toni, I. Motor imagery: a window into the mechanisms and alterations of the motor system. *Cortex; a journal devoted to the study of the nervous system and behavior* **44**, 494-506 (2008).
10. Guillot, A., *et al.* Functional neuroanatomical networks associated with expertise in motor imagery. *NeuroImage* **41**, 1471-1483 (2008).
11. Munzert, J., Lorey, B. & Zentgraf, K. Cognitive motor processes: the role of motor imagery in the study of motor representations. *Brain research reviews* **60**, 306-326 (2009).
12. Lacourse, M.G., Orr, E.L., Cramer, S.C. & Cohen, M.J. Brain activation during execution and motor imagery of novel and skilled sequential hand movements. *NeuroImage* **27**, 505-519 (2005).
13. Lafleur, M.F., *et al.* Motor learning produces parallel dynamic functional changes during the execution and imagination of sequential foot movements. *NeuroImage* **16**, 142-157 (2002).
14. Rutten, G.J., Ramsey, N.F., van Rijen, P.C., Noordmans, H.J. & van Veelen, C.W. Development of a functional magnetic resonance imaging protocol for intraoperative localization of critical temporoparietal language areas. *Annals of neurology* **51**, 350-360 (2002).
15. Neggers, S.F., Hermans, E.J. & Ramsey, N.F. Enhanced sensitivity with fast three-dimensional blood-oxygen-level-dependent functional MRI: comparison of SENSE-PRESTO and 2D-EPI at 3 T. *NMR in biomedicine* **21**, 663-676 (2008).
16. Ashburner, J. & Friston, K.J. Unified segmentation. *NeuroImage* **26**, 839-851 (2005).
17. van Rootselaar, A.F., *et al.* Simultaneous EMG-functional MRI recordings can directly relate hyperkinetic movements to brain activity. *Human brain mapping* **29**, 1430-1441 (2008).
18. Hermes, D., Miller, K.J., Noordmans, H.J., Vansteensel, M.J. & Ramsey, N.F. Automated electrocorticographic electrode localization on individually rendered brain surfaces. *Journal of neuroscience methods* **185**, 293-298 (2010).
19. Welch, P. The use of fast Fourier transform for the estimation of power spectra: A method based on time averaging over short, modified periodograms. *IEEE Trans. Audio Electroacoustics* **15**, 70-73 (1967).
20. Sheikh, H., McFarland, D.J., Sarnacki, W.A. & Wolpaw, J.R. Electroencephalographic(EEG)-based communication: EEG control versus system performance in humans. *Neuroscience letters* **345**, 89-92 (2003).
21. Schalk, G., Brunner, P., Gerhardt, L.A., Bischof, H. & Wolpaw, J.R. Brain-computer interfaces (BCIs): detection instead of classification. *Journal of neuroscience methods* **167**, 51-62 (2008).
22. Hochberg, L.R., *et al.* Neuronal ensemble control of prosthetic devices by a human with tetraplegia. *Nature* **442**, 164-171 (2006).
23. Velliste, M., Perel, S., Spalding, M.C., Whitford, A.S. & Schwartz, A.B. Cortical control of a prosthetic arm for self-feeding. *Nature* **453**, 1098-1101 (2008).
24. Miller, K.J., *et al.* Cortical activity during motor execution, motor imagery, and imagery-based online feedback. *Proceedings of the National Academy of Sciences of the United States of America* **107**, 4430-4435 (2010).
25. de Lange, F.P., Helmich, R.C. & Toni, I. Posture influences motor imagery: an fMRI study. *NeuroImage* **33**, 609-617 (2006).
26. de Lange, F.P., Hagoort, P. & Toni, I. Neural topography and content of movement representations. *Journal of cognitive neuroscience* **17**, 97-112 (2005).

27. Logothetis, N.K., Pauls, J., Augath, M., Trinath, T. & Oeltermann, A. Neurophysiological investigation of the basis of the fMRI signal. *Nature* **412**, 150-157 (2001).
28. Niessing, J.*, et al.* Hemodynamic signals correlate tightly with synchronized gamma oscillations. *Science* **309**, 948-951 (2005).
29. Lachaux, J.P.*, et al.* Relationship between task-related gamma oscillations and BOLD signal: new insights from combined fMRI and intracranial EEG. *Human brain mapping* **28**, 1368-1375 (2007).
30. Johnson, S.H.*, et al.* Selective activation of a parietofrontal circuit during implicitly imagined prehension. *NeuroImage* **17**, 1693-1704 (2002).
31. Sirigu, A.*, et al.* The mental representation of hand movements after parietal cortex damage. *Science* **273**, 1564-1568 (1996).
32. Shenoy, K.V.*, et al.* Neural prosthetic control signals from plan activity. *Neuroreport* **14**, 591-596 (2003).
33. Johansen-Berg, H. & Matthews, P.M. Attention to movement modulates activity in sensori-motor areas, including primary motor cortex. *Experimental brain research. Experimentelle Hirnforschung* **142**, 13-24 (2002).
34. Shoham, S., Halgren, E., Maynard, E.M. & Normann, R.A. Motor-cortical activity in tetraplegics. *Nature* **413**, 793 (2001).
35. Ritter, P., Moosmann, M. & Villringer, A. Rolandic alpha and beta EEG rhythms' strengths are inversely related to fMRI-BOLD signal in primary somatosensory and motor cortex. *Human brain mapping* **30**, 1168-1187 (2009).
36. Brookes, M.J.*, et al.* GLM-beamformer method demonstrates stationary field, alpha ERD and gamma ERS co-localisation with fMRI BOLD response in visual cortex. *NeuroImage* **26**, 302-308 (2005).
37. McFarland, D.J., McCane, L.M., David, S.V. & Wolpaw, J.R. Spatial filter selection for EEG-based communication. *Electroencephalography and clinical neurophysiology* **103**, 386-394 (1997).
38. Yao, D.*, et al.* A comparative study of different references for EEG spectral mapping: the issue of the neutral reference and the use of the infinity reference. *Physiological measurement* **26**, 173-184 (2005).

Chapter 4

Neurophysiologic correlates of fMRI in human motor cortex

D. Hermes[1], K.J. Miller[2], M.J. Vansteensel[1], E.J. Aarnoutse[1], F.S.S. Leijten[1], N.F. Ramsey[1]

[1] Rudolf Magnus Institute of Neuroscience, University Medical Center Utrecht, Department of Neurology and Neurosurgery, section Brain Function and Plasticity, Utrecht, The Netherlands

[2] Neurobiology and Behavior, University of Washington, Seattle, WA, United States

Human Brain Mapping (2011, Jun 20) [Epub ahead of print]

Abstract

The neurophysiological underpinnings of functional magnetic resonance imaging (fMRI) are not well understood. In order to understand the relationship between the fMRI blood oxygen level dependent (BOLD) signal and neurophysiology across large areas of cortex, we compared task related BOLD change during simple finger movement to brain surface electric potentials measured on a similar spatial scale using electrocorticography (ECoG). We found that spectral power increases in high frequencies, which have been related to local neuronal activity, co-localized with spatially focal BOLD peaks on primary sensorimotor areas. Independent of high frequencies, decreases in low frequency rhythms, thought to reflect an aspect of cortical-subcortical interaction, co-localized with weaker BOLD signal increase. A regression analysis showed that there was a direct parametric relation between the amplitude of the task induced BOLD change on primary sensorimotor areas and high frequency change. Low frequency change explained an additional, different part of the BOLD variance. Together, these spectral power changes explained a significant 36% of the spatial variance in the BOLD signal change (R^2=0.36). These results suggest that BOLD signal change is largely induced by two separate neurophysiological mechanisms, one being spatially focal neuronal processing and the other spatially distributed low frequency rhythms.

Introduction

Functional magnetic resonance imaging (fMRI) is a widely used tool to investigate human brain function. In both clinical and research settings, statistical maps of the blood oxygen level dependent (BOLD) change that fMRI measures are used to localize function to specific brain regions in individual subjects. How these maps of fMRI activation represent underlying neuronal processing remains unclear [1, 2].

Previous studies investigating the relationship between BOLD signal change and neurophysiology have adopted the strategy of selecting a small patch of cortex in a functionally-relevant area, and then tracking both BOLD signal change and electrophysiological change over time [3-5]. These studies have shown that in one area of cortex BOLD change is best related to high frequency power changes in the local field potential. Although these studies provide compelling evidence for a relationship, they describe only part of the picture relating BOLD change to neuronal physiology. First, BOLD signal change may be present in the absence of electrophysiological change [6]. Previous studies, which pre-selected functional patches of cortex, may be biased to capture only a particular aspect of the BOLD-neurophysiology relationship, while missing others. Second, since the shape of the heamodynamic response function differs across areas of cortex [7], different cortical regions may exhibit different relationships between population-scale neurophysiology and metabolic demand reflected in the BOLD signal. Third, individual subject behaviorally-induced BOLD activity maps typically display large BOLD signal changes in primary areas known to be related to that behavior, as well as more variable, weaker, signal changes in surrounding and other regions [8, 9]. Since previous studies focused on the BOLD peaks, it is unclear whether the BOLD change in these surrounding areas has a neurophysiological correlate. Fourth, BOLD changes correlate with synaptic processing reflected in local field potentials (LFPs) [1, 2] and in addition to high frequency power changes in the LFP behavior is also associated with power changes in low frequency oscillations in the LFP [10, 11]. High frequency power change thus may not reflect the complete neurophysiology related to BOLD change.

We examined the relationship between BOLD and neurophysiology without selecting a region based on activation. If the modalities are indeed closely tied, one should find changes in both modalities in some regions, and absence of both in other regions. In addition to the presence or absence of behavior-associated change, the magnitude of change should also be correlated between modalities. This requires measuring at multiple patches of cortex. Electrocorticographic (ECoG) recordings allow for electrophysiological measurements sampled at multiple points across large areas of cortical surface. Previous ECoG studies have investigated the spatial distribution of spectral power changes. They have shown that

broadband power increases, revealed at high frequencies, are typically local, on areas primarily involved in the task [12, 13]. Power decreases in low frequency sensorimotor rhythms are distributed over larger areas of cortex [14, 15]. These spectral changes are associated with different processes: broadband power change is associated with local neuronal processing [16, 17] whereas low frequency oscillations reflect an aspect of subcortical-cortical interaction [18-21].

To examine the relationship between these different types of physiology and the BOLD signal, eight patients performed a simple finger movement task first during fMRI, and repeated this task during ECoG recordings after implantation of electrode arrays for clinical purposes. For each patient, about 70 ECoG electrodes were placed in rectilinear arrays covering almost half of one hemisphere at a time. This provided us with the opportunity to measure neuronal populations over distributed cortical sites. Individual electrodes were spaced at a centimeter distance from one another and each electrode sampled from a cortical surface of several millimeters, which translates to the volume of a typical fMRI voxel. Maps of electrocortical activity could thus be compared to surface renderings of fMRI activity maps across the full range of behavior-associated activation. We found that the magnitude of focal BOLD change in primary sensorimotor areas was parametrically related to the change in high frequency power. Spectral change in low frequency sensorimotor rhythms explained additional variance of BOLD change in a more distributed fashion.

Materials and Methods

Participants and procedure

Eight patients (3 females, supplementary Table 1) scheduled for the implantation of ECoG arrays (AdTech, Racine, WI, USA) for epilepsy monitoring gave written informed consent to participate in this study. The study was approved by the ethical committee of the University Medical Center Utrecht, in accordance with the Declaration of Helsinki 2004. During a preoperative fMRI session and during ECoG recordings these patients performed the same hand movement task that consisted of 30 second movement blocks (visually cued thumb/finger flexion at the rate of 2Hz) alternated with 30 second blocks of rest (Fig. 1) for 4.5-5.5 minutes.

Magnetic Resonance Measurement

Preoperatively, fMRI scans were acquired on a Philips ACS-NT 1.5T or Achieva 3T scanner with a PRESTO [22, 23] sequence (1.5T: 340 scans, TR/TE 24.02/37 ms, flip angle 9.5 degrees, FOV = 256x96x192 mm, acquisition voxel size 4 mm isotropic, 3T: 442 scans TR/TE 22.5/33.2 ms, flip angle 10 degrees, FOV = 256x224x160 mm, acquisition voxel size 4 mm

isotropic). Functional images were realigned and coregistered using normalized mutual information [24] with an anatomical scan using SPM5 (http://www.fil.ion.ucl.ac.uk/spm/). The anatomical image was segmented in gray and white matter with unified segmentation [25].

fMRI analysis

Statistical analyses were performed on a single subject basis and therefore no smoothing was applied. A GLM was estimated with one regressor for hand movement activation (a 30s box car for movement blocks convolved with a standard hemodynamic response function, see Fig. S1), data were corrected for low frequency drifts by a 128s high pass filter and corrected for serial correlations with a first order AR model.

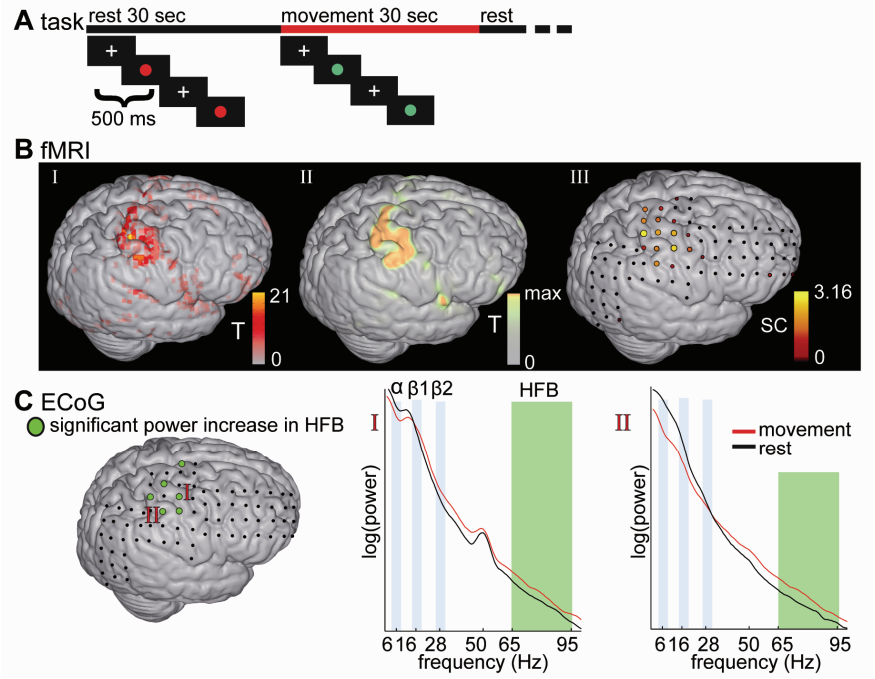

Figure 1. Experimental setting. ***(A)*** Participants performed a blocked motor task with 30 second periods of rest (when a red cue was presented at 2 Hz) interleaved with 30 second periods of thumb/finger movement (when a green cue was presented at 2 Hz). ***(B)*** Representative image of the pre-implantation fMRI results showing a statistical t-map of BOLD change during movement compared to rest. fMRI results were rendered on the cortical surface with a search depth of up to 8 mm below the cortical surface and are clearly visible on pre and post central gyri. For visualization, these maps were smoothed as shown in the middle panel. On the right panel, the estimated percentage of BOLD signal change per electrode is shown. ***(C)***, From the ECoG, electric potential power spectra were calculated for each electrode. Power spectra are shown for two electrodes on pre and post central gyri that showed significant increases during movement in the high frequency band (HFB) from 65-95 Hz. During movement there were power decreases in low frequency bands (α, β1 and β2) and a broadband increase in the HFB. At 50 Hz the ambient "line" noise peak is visible. On the rendering, electrodes in green showed significant ($p<0.05$, Bonferroni corrected over electrodes) HFB increases.

Electrocorticographic measurement

Arrays of ECoG electrodes were implanted subdurally for localization of seizure focus during the course of treatment for epilepsy. These platinum electrodes had an inter electrode spacing of 1 cm and a measurement surface of 2.3 mm in diameter. Electrodes were localized from a CT and projected to the cortical surface of each patient [26]. ECoG data were acquired with a 128 channel recording system (Micromed, Treviso, Italy) with 512 Hz sampling rate and 0.15–134.4 Hz band-pass filter.

ECoG analysis

Signals were re-referenced to the common average of all intracranial electrodes and two second epochs were extracted from movement and rest blocks. Electrodes and epochs that showed large epileptic artifacts were rejected (on average two electrodes per patient were rejected prior to common average referencing). Electrodes in grids that were mostly on frontal, parietal and occipital lobes were selected for further analysis (Supplemental Fig. S2) resulting in 67 (range 47-81) electrodes on average per subject. For each epoch, the power spectral density was calculated every 1 Hz by Welch's method [27] with 200 ms windows and a Hamming window to attenuate edge effects.

Since the center frequency for α and β bands can differ between subjects, subject-specific α and β bands were defined as the peaks in the power spectrum from the rest period as follows (see also supplemental Fig. S2). A power law ($constant \cdot f^{X}$) was fit to the power spectrum from the rest period for each electrode and the power was normalized (by element-wise division at each frequency) with respect to this power law [17]. Peaks in the normalized power spectrum, i.e. where the first derivative was 0, were detected for each electrode. These peaks were convolved with a small Gaussian and the average over these peaks was calculated. The center frequency (f) for each low frequency rhythm was defined as the largest peak of the average Gaussians with α: $f \leq 13$ Hz, β1: $13 < f \leq 24$ Hz and β2: $24 < f < 30$ Hz. Low frequency rhythms were detected in classic sensorimotor α and β1 bands ($\alpha \leq 13$ Hz, $13 < \beta1 \leq 24$ Hz) and a β2 rhythm ($24 < \beta2 < 30$ Hz) was found in 7 out of 8 subjects (β2 rhythms have previously been shown in layer V of somatosensory cortex [28]).

Spectral power changes for movement compared to rest periods in low frequency bands and in a high frequency band (HFB, 65-95Hz) were then calculated. The power spectra of each epoch were normalized (by element-wise division) with respect to the mean power over all epochs at each frequency and the log was taken. The log normalized power was then averaged for α, β1 and β2 bands (center frequency f +/- 2Hz) and for HFB from 65-95 Hz. A t-test was performed to test whether differences between rest and movement periods were significant, and results are reported at $p<0.05$, Bonferroni corrected for the number of electrodes. The signal change from rest to movement periods was calculated by

the difference in log normalized power between movement and rest blocks and divided by the standard deviation across all epochs to control for possible differences in variance between different frequency bands (supplemental Fig. S1).

Spatial alignment of ECoG and fMRI

For each ECoG electrode, the magnitude of the BOLD signal change for movement compared to rest was estimated by taking the parameter estimates from the GLM and correcting these for the amplitude of the regressor, which results in the percentage of BOLD signal change with respect to the global mean. To correct for the 1 cm spacing in between electrodes, the estimated percentage of BOLD signal change was averaged across gray matter voxels in an 8mm radius of an electrode (Fig. 1B, right panel, supplemental Fig. S1). This way the fMRI data directly underneath the surface of the grids were optimally matched to the electrodes. Functional MRI results are displayed on the rendered cortical surface as t-maps, which were generated by testing the GLM hand movement parameters estimates for statistical significance. Fig. 1B (left panel) shows an example of these fMRI t-maps rendered on the cortical surface. For visualization of the overlap between fMRI and ECoG the fMRI t-maps were smoothed with cosine kernel of 6 mm radius (Fig. 1B, middle panel).

fMRI versus ECoG

It was tested whether the magnitude of the BOLD signal change correlated spatially with the magnitude of the spectral power change in HFB. For each electrode, the BOLD signal change and spectral power change were calculated as described above. For each subject, a linear regression model ($Y = X\beta + \varepsilon$) was fitted, where Y is a vector with the percentage of BOLD signal change for each electrode and X the design matrix containing a regressor with spectral power changes in HFB for each electrode and an intercept. This model was tested for significance in each individual subject by an F-test. To test whether across subjects there was a significant correlation between BOLD and spectral change, it was tested whether the regression coefficients (β) differed significantly from 0 by a t-test. As an indication of the overlap between BOLD and ECoG, we calculated the percentage of BOLD variance that the model explained (R^2).

To check whether the correlation would not be due to the fact that both BOLD changes and high frequency power changes both peak in the hand sensorimotor area, we looked more specifically at the correlation between HFB and BOLD change within this area. Electrodes over the primary sensorimotor hand area were selected by manual delineation of the hand region on pre and post central gyri. The anterior and posterior borders consisted of the pre- and post-central sulci; ventral and dorsal borders were drawn where clinical stimulation data indicated the start of mouth and leg areas. This resulted in on average 11

electrodes per subject, range 4-27 electrodes. The regression analysis was then re-applied to this subset of electrodes.

To test whether low frequency bands explained additional variance in the BOLD signal change independently of HFB change the explained variance was calculated (R^2) and adjusted for the number of regressors $R^2_{adjusted}=1-(n-1)/(n-k-1)*(1-R^2)$. In a stepwise regression procedure, regressors for low frequency power changes were each added to the model and it was tested whether across subjects there was a significant increase in the explained variance ($\Delta R^2_{adjusted}$) by a permutation test (factorial 8 iterations).

Results

fMRI, ECoG, and basic overlap

Fig. 2 illustrates the fMRI and ECoG results for three subjects (Fig. 2A) and across subjects (Fig. 2B) (all individual results are shown in supplemental Fig. S3). Functional MRI results showed that with movement, sensorimotor areas on precentral and postcentral gyri showed BOLD signal increases across all subjects. On a subject-by-subject basis, there are small-and-variable outlying BOLD signal increases that are very heterogeneous across subjects. The ECoG results showed that with movement, there was a significant ($p<0.05$, Bonferroni corrected) power increase in the HFB. These power increases were spatially focal and mostly confined to primary sensorimotor hand areas, as identified by electrocortical stimulation (on average 90% of significant HFB increases were located on a site where electrocortical stimulation between this electrode and one other site elicited hand movement). The power in the low frequency ranges ($\alpha \leq 13$Hz, $13 < \beta1 \leq 24$, and $24 < \beta2 <30$ Hz bands that were defined from the peaks in the power spectrum during rest), decreased significantly with movement, but over larger spatial areas. These areas included, but were less confined to, primary sensorimotor areas (on average 71%, 81% and 77% of significant decreases in respectively α, β1, and β2 bands were located on a site where electrocortical stimulation elicited hand movement).

Fig. 2A shows that fMRI activity spatially overlaps with significant power increases in HFB and power decreases in lower frequencies (α, β1, β2 bands, shown for all individual subjects in S3). As shown in Fig. 3, the BOLD increase was significantly larger underneath electrodes with significant HFB power increases as compared to sites underneath electrodes with no significant spectral power changes (paired t-test, $p<0.05$). Surprisingly, the BOLD change underneath electrodes with α and β1 power decreases was also significantly larger compared to electrodes with no significant spectral power changes, even after excluding electrodes with significant HFB increases ($p<0.05$, by paired t-tests). Sites underneath electrodes with a power decrease in the β2 band showed only a trend in BOLD increase

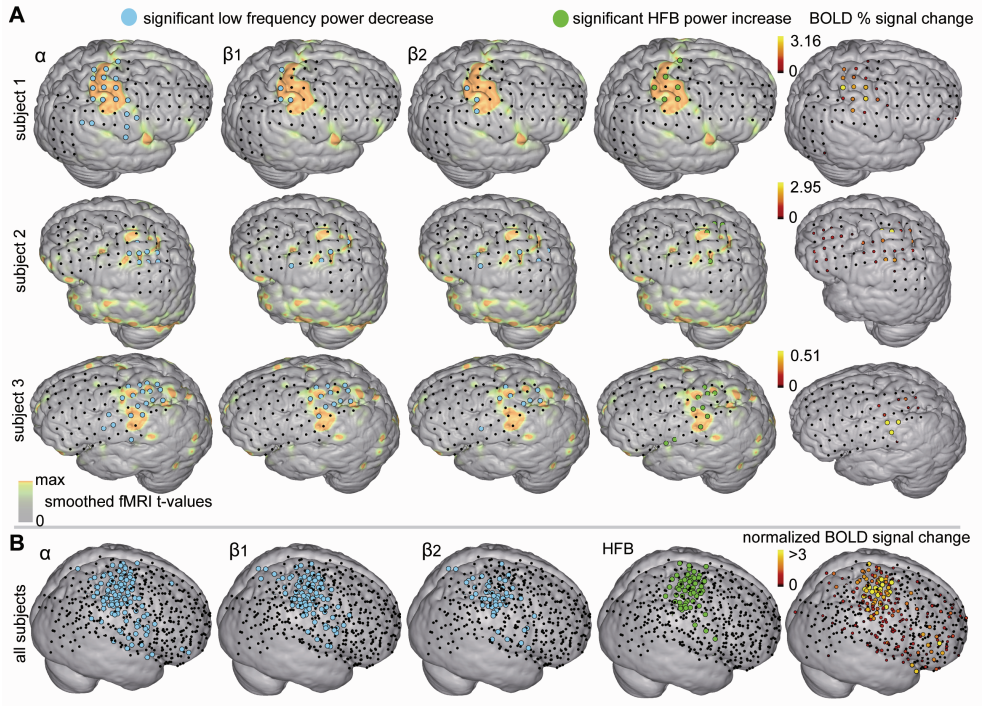

Figure 2. Visualization of overlap between brain-surface fMRI results and electric potential change in different frequency bands**.** ***(A)*** For three representative subjects: rendering with smoothed fMRI results mapped on the surface (the t-values for movement versus rest scaled to the maximum, smoothed with 6 mm cosine kernel for display). Green denotes significant ($p<0.05$, Bonferroni corrected) increase in power in HFB, and cyan significant ($p<0.05$, Bonferroni corrected) decrease in power in low frequency bands. The panels on the right show the estimated percentage of BOLD signal change per electrode. ***(B)*** Group results: for visualization, electrode coordinates were projected to right hemisphere MNI coordinates and displayed on the normalized averaged gray matter across all subjects. Note that power decreases in low frequencies are spatially more distributed than HFB power increases. On the far right the BOLD change for all electrodes is depicted (only for visualization, the estimated percentage of BOLD signal change is normalized with respect to the standard deviation of each subject to eliminate large inter individual differences in the amplitude of the BOLD change and better visualize the overall distribution).

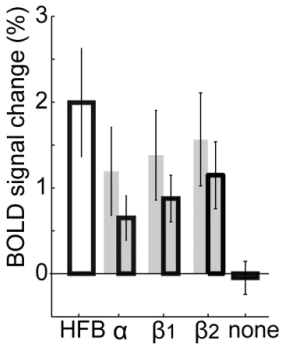

Figure 3. Estimated percentage of BOLD signal change underneath electrodes with significant HFB increases (white), for electrodes with no significant spectral power change (black) and for low frequency power decreases before (gray) and after (gray with black box) controlling for overlap with HFB by exclusion of electrodes with significant HFB increases.

(paired t-test, p=0.06). The BOLD signal change was largest underneath electrodes with HFB power increases (p<0.05, by paired t-tests).

fMRI versus ECoG: correlation between BOLD and HFB

In order to test whether the amplitude of BOLD signal change over different areas of cortex corresponds to different levels of neuronal change, a multiple regression analysis was used to predict the BOLD signal change by spectral power change. For each electrode i, the percentage of BOLD signal change (y_i) and spectral power change in HFB ($x_i = [x_{HFBi}]$) was calculated and entered in the regression model ($Y = XB+\varepsilon$) for each subject individually, see Fig. 4A for an example of the relation between predicted BOLD and BOLD change across electrodes for subject 1. An F-test showed that this regression model was significant in seven of eight subjects (see supplemental Table S3 for individual results). Regression coefficients were significantly positive across subjects (t=2.80, p<0.05, Fig. 4A), indicating that across areas of cortex BOLD change correlated positively with HFB change. On average 23% of the BOLD change was explained by the HFB change.

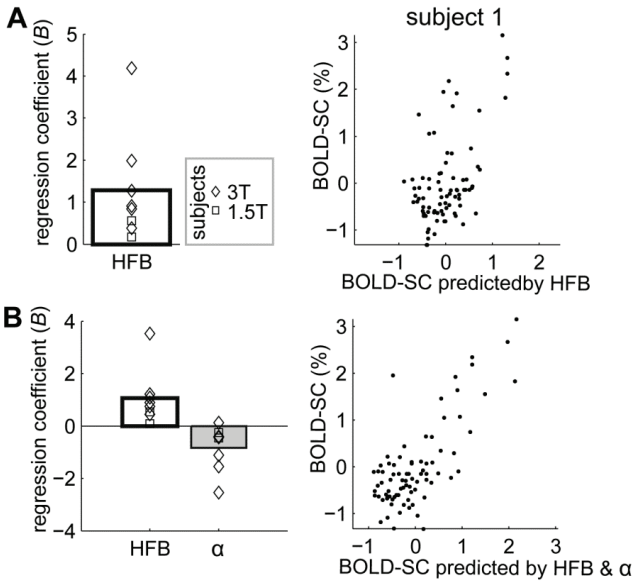

Figure 4. Relationship between BOLD signal change and spectral power change. ***(A)*** Regression coefficients (*B*) from the regression model $Y = XB+\varepsilon$ where $X = [X_{HFB}]$ for each subject show that power change in HFB correlated positively with BOLD signal change. For one subject, the relation between the BOLD change predicted by the model and the actual BOLD change is shown. ***(B)*** Regression coefficients (*B*) from the model $Y = XB+\varepsilon$ where $X = [X_{HFB}\ X_{\alpha}]$ show that power change in HFB correlated positively with BOLD signal change, while spectral changes in the α band correlated negatively. For one subjects the relation between the BOLD change predicted by the model and the actual BOLD change is shown. Note the better fit compared to *(A)* where the model only includes X_{HFB}

To check whether this correlation was not due to the fact that both BOLD change and high frequency power change both peak in the hand sensorimotor area, we looked more specifically at the correlation between HFB and BOLD change within this area. If the amplitude of the BOLD change is a direct reflection of the magnitude of change in underlying neuronal activity, we expect that also within this area there is a tight correlation between the amplitudes of the two modalities. We thus restricted the analysis to the anatomically defined hand region on pre and post central gyri (Fig. 5A). A regression analysis restricted to these electrodes showed that the magnitude of local BOLD signal change was indeed parametrically related to power increases in HFB during the motor movement task (Fig. 5C). Fig. 5B shows that regression coefficients for HFB were significantly larger than zero across subjects ($t=4.21$, $p<0.01$), indicating that there is a positive correlation between HFB and BOLD signal change. The HFB explained on average 46% of the variance in the BOLD signal change ($R^2=0.46$). For individual analyses this regression model was significant in four of the eight subjects and one subject showed a trend (see also supplemental table S3 for statistics in all individual subjects). In the other three subjects (S3, S6 and S8) the maximum estimated BOLD signal change was smaller than in the other five (Fig. 5C). Two of these differed from all others in that they were scanned at a lower magnetic field strength (1.5T), which can result in a smaller magnitude of BOLD signal change [1, 29]. In addition, subjects S6 and S8 had limited electrode coverage of pre and postcentral gyri (4 electrodes), reducing statistical power of the regression model.

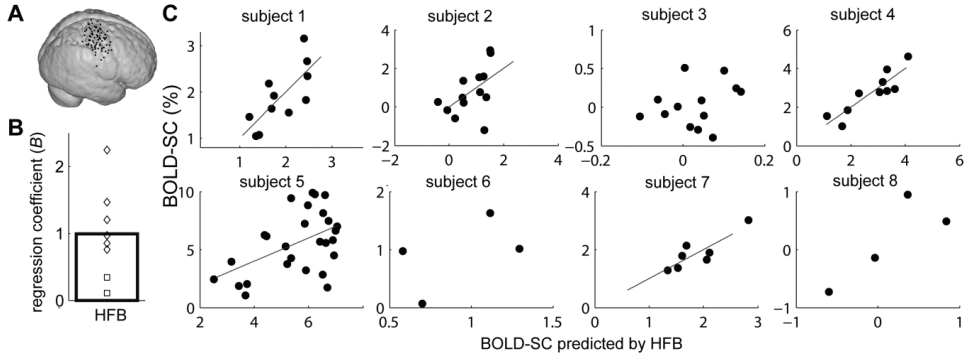

Figure 5. Relationship between BOLD signal change and spectral power change restricted to hand sensorimotor areas. ***(A)*** The rendering displays the spatial distribution of electrodes restricted to primary sensorimotor hand areas across all subjects. ***(B)*** Regression coefficients (*B*) from the regression model $Y = XB+\varepsilon$ where $X = [X_{HFB}]$ for electrodes show that local BOLD signal change correlated positively with power change in HFB. ***(C)*** For all subjects the relation between the BOLD change predicted by the model and the actual BOLD change is shown. Note that the maximum BOLD signal change was larger in subjects 1, 2, 4, 5, and 7 (y axis). Specifically in these cases the correlation between BOLD signal change and HFB power changes was significant or showed a trend and a fitted regression line is shown. Subjects 3 and 6 were scanned on the 1.5T scanner, while all others were scanned on the 3T scanner.

fMRI versus ECoG: do low frequency rhythms explain additional variance in BOLD?

In order to test whether low frequency rhythms explained additional variance in BOLD change, we added these to the regression model of all electrodes (thus fitting the model $Y = XB+\varepsilon$, where $X = [X_{HFB}\ X_{\alpha}]$, $X = [X_{HFB}\ X_{\beta1}]$ or $X = [X_{HFB}\ X_{\beta2}]$). Adding spectral changes in the α band significantly increased the explained variance in the BOLD signal change by 13% (ΔR^2=0.13, $p<0.05$ by permutation test), and for the β1 band there was a marginal trend (ΔR^2=0.12, p=0.06). The β2 band was not significant (ΔR^2=0.10, p=0.12) and will not be considered in further analyses. Fig. 4B shows for subject 1 that the BOLD change predicted by a model including α and HFB change results in a better fit between the predicted and actual BOLD change compared to a model with only HFB (Fig. 4A). Regression coefficients (*B*) indicated that spectral power changes in the α band were significantly negatively correlated with BOLD change (t=-2.71, $p<0.05$), for the β1 band there was a negative trend (t=-2.23, p=0.06), while HFB change correlated positively in both cases. Both high and low frequency power changes thus correlate with BOLD signal change and explain different parts of the variance in BOLD signal change. Together, HFB and α or HFB and β1 explained on average a total of 36% of BOLD variance.

To get an idea of how spectral power changes in α and β1 rhythms influence BOLD changes, we further investigated in which brain areas they explained most variance in the BOLD signal change. It is possible that if there are large power changes in these low frequency rhythms, there is a peak in BOLD on a primary sensorimotor area, similar to HFB change. We therefore restricted the analysis again analysis to the anatomically defined hand region on pre and post central gyri and added the low frequency bands to the regression model of HFB and BOLD. A stepwise regression showed that adding low frequency bands to this model *did not* significantly increase the explained variance in *local* BOLD signal change across subjects (α: p=0.79, β1: p=0.24 by a permutation test). In other words, in primary sensorimotor areas, the α and β1 rhythms do not add information in predicting movement-related changes in BOLD signal change as compared to using the HFB alone.

Discussion

We conducted a study comparing spatial maps of fMRI BOLD signal changes to spectral power changes in the measured ECoG potential. Both modalities were carefully co-registered to allow for direct comparison [26]. A simple motor task was employed and the two modalities were compared in terms of cortical surface distribution and magnitude of signal change. High frequency power increases correlated with focal BOLD peaks on primary sensorimotor areas. We found that low frequency power decreases explain a different part of the BOLD signal change. The results indicate that 36% of the total variance in the BOLD

signal change (both magnitude and distribution) could be explained by a combination of low (<30 Hz) and high (65-95 Hz) frequency ECoG changes.

We found that high frequency power increases correlated with focal BOLD peaks on primary sensorimotor areas (Fig. 4B, S4). Increases in HFB change were focused on primary sensorimotor electrodes during movement (Figs. 1,2,5), consistent with previous studies [12, 13, 15, 30]. This high frequency spectral power change has been shown to correlate directly with firing rate [16, 17, 31], and has been demonstrated to reflect broad-spectral change across all frequencies [13, 15]. Previous studies examined the relationship between spectral power change and BOLD change within a specific region (<500 µm [32]) [3-5, 11]. We extend this relationship found at the neuronal population volumes sampled by micro-electrodes to a widespread network of movement-related regions on the cortical surface. By comparing ECoG and fMRI BOLD signal change during performance of the same task at the same functionally-relevant cortical sites, we demonstrate a direct correlation between the magnitudes of fMRI BOLD and electrophysiologic change. This supports the hypothesis that the amplitude of the BOLD change is a direct reflection of the magnitude of change in underlying neuronal activity.

Interestingly, in addition to high frequency power increases, a significant 13% of BOLD signal change was explained by power decreases in low frequency rhythms. The additional variance in BOLD explained by low frequencies was not restricted to primary areas, suggesting that low frequencies are related to more distributed BOLD changes. Consistent with previous studies [14, 15], low frequency power decreases were spatially more distributed than high frequency power increases. Understanding how different processes reflected in the LFP are integrated in fMRI activation maps is essential to link fMRI findings to both noninvasive EEG and MEG experiments that measure neuronal signals over larger areas of cortex and invasive studies in non human primates that extract neuronal signals from small areas of cortex. EEG and MEG studies suggested that these low frequency rhythms correlate with BOLD changes [33-35]. However, since EEG and MEG intrinsically average over larger volumes of brain tissue, they cannot resolve local neuronal activity with a spatial precision comparable to that of fMRI [36]. While these EEG and MEG studies could show a general co-localization of BOLD and spectral changes, we demonstrate that across areas there is a parametric relationship between BOLD and spectral power change in both low and high frequencies. This parametric relationship suggests a specific coupling between the neurophysiological mechanisms underlying these spectral changes and vascular changes. A general co-localization between fMRI activity and high frequency power change has also been shown by large-scale penetrating electrodes and microelectrodes [37, 38], but they also showed that multiple fMRI sites did not show any high frequency power changes. Using a parametric analysis and investigating the full spectral scale of behavior associated changes we were able to show that low frequency changes explain a different part of the

BOLD signal change. This may indicate that low frequency power changes explain part of these fMRI sites unexplained by high frequency change. It seems likely that the relationship also applies to other brain functions such as language where the spatial distribution of high and low frequency change is local and distributed in a similar manner [39], but this requires confirmation with similar studies on other tasks.

Low frequency sensorimotor rhythms have been associated with reciprocal thalamic and basal ganglia projections to cortex [18-21]. Assuming that these low frequency rhythms reflect inhibition of a cortical region [40], the decrease in power that we measure in α and β1 may reflect a disinhibition or preparation of cortical structures. Lesions and stimulation of specific nuclei in the basal ganglia have indeed been shown to alter metabolism in cortical projection sites [41, 42]. Single subject fMRI activation maps typically consist of focal peaks with a high contrast to noise ratio, surrounded by a more distributed and variable pattern of weaker BOLD signal increase [8, 9]. Our results suggest that these spatially distributed BOLD signal increases may be induced by the neuronal mechanisms underlying the ongoing α and β brain rhythms, while the peaks in BOLD signal change are induced by local neuronal activity.

A complicating factor in the interpretation of fMRI activation maps is that hemodynamic changes occur not only in the capillary bed, but also in the arterial and venous blood vessels that feed and drain those beds, respectively. These changes are known as inflow [43] and draining vein [44] artifacts respectively, and cannot easily be distinguished from BOLD effects originating from the capillary bed. In order to minimize these artifacts in the current study, we used an fMRI acquisition technique that minimizes contribution of larger vessels: 3D PRESTO [22]. Inflow effects are eliminated by acquiring data in whole brain, which enables excitation of the whole brain simultaneously [45]. Draining vein effects are reduced by the use of crusher gradients which cause a rapid dephasing of signal in larger vessels, effectively eliminating those from the fMRI images [46].

Of the variance in BOLD signal change, we could explain 36% on average. The unexplained variance could in part be due to the above-mentioned non-neuronal artifacts. In addition, measuring ECoG and fMRI at different times may have introduced some variability in task performance, and subsequently in brain activity. A simple motor task leaves limited leeway for this, but test-retest fMRI motor studies typically report 40% overlap of activity patterns in individual subjects [47], supporting this notion. Other aspects might contribute to the unexplained variance, such as task related hemodynamic changes that are not reflected by neuronal changes [6], neuronal changes that are not reflected by hemodynamic change and non-linear relations between the two [2] or physiological noise in fMRI, which might affect magnitude of signal change [48]. When considering these possible confounds, the finding that a significant 36% of variance in BOLD signal change could be explained by spectral power

changes in ECoG and the fact that the parametric relation between these two is visible on the level of the individual subject (Figs. 4, 5), indicate that a large part of the fMRI signal changes is related to the measured neurophysiological changes.

In conclusion, by measuring neuronal population activity using ECoG, our study demonstrates that BOLD signal change is largely induced by two separate neurophysiological mechanisms, being spatially focal neuronal processing and spatially more distributed low frequency-driven modulation of cortex. Because of the robust, parametric relationship between the magnitudes of fMRI activity and high frequency power increases within primary sensorimotor cortex, we conclude that BOLD peaks in primary sensorimotor cortex primarily reflect local neuronal processing.

Acknowledgements

The authors thank Erika van Hell, Martin Bleichner, Geertjan Huiskamp, Herke Jan Noordmans, Peter Bos, and Cyrille Ferrier for their help in collecting the data, Ole Jensen, Natalia Petridou and Peter Bandettini for their helpful advice, Peter Gosselaar and Peter van Rijen for implanting the electrodes and the patients and staff of the clinical neurophysiology department for their time and effort. This research is supported by the Dutch Technology Foundation STW, applied science division of NWO and the Technology Program of the Ministery of Economic Affairs, and the University of Utrecht, grant UGT7685.

References

1. Logothetis, N.K. What we can do and what we cannot do with fMRI. *Nature* **453**, 869-878 (2008).
2. Lauritzen, M. Reading vascular changes in brain imaging: is dendritic calcium the key? *Nature reviews* **6**, 77-85 (2005).
3. Logothetis, N.K., Pauls, J., Augath, M., Trinath, T. & Oeltermann, A. Neurophysiological investigation of the basis of the fMRI signal. *Nature* **412**, 150-157 (2001).
4. Niessing, J.*, et al.* Hemodynamic signals correlate tightly with synchronized gamma oscillations. *Science* **309**, 948-951 (2005).
5. Mukamel, R.*, et al.* Coupling between neuronal firing, field potentials, and FMRI in human auditory cortex. *Science* **309**, 951-954 (2005).
6. Sirotin, Y.B. & Das, A. Anticipatory haemodynamic signals in sensory cortex not predicted by local neuronal activity. *Nature* **457**, 475-479 (2009).
7. Miezin, F.M., Maccotta, L., Ollinger, J.M., Petersen, S.E. & Buckner, R.L. Characterizing the hemodynamic response: effects of presentation rate, sampling procedure, and the possibility of ordering brain activity based on relative timing. *NeuroImage* **11**, 735-759 (2000).
8. Rombouts, S.A.*, et al.* Test-retest analysis with functional MR of the activated area in the human visual cortex. *Ajnr* **18**, 1317-1322 (1997).
9. Saad, Z.S., Ropella, K.M., DeYoe, E.A. & Bandettini, P.A. The spatial extent of the BOLD response. *NeuroImage* **19**, 132-144 (2003).
10. Murthy, V.N. & Fetz, E.E. Oscillatory activity in sensorimotor cortex of awake monkeys: synchronization of local field potentials and relation to behavior. *J Neurophysiol* **76**, 3949-3967 (1996).
11. Maier, A.*, et al.* Divergence of fMRI and neural signals in V1 during perceptual suppression in the awake monkey. *Nature neuroscience* **11**, 1193-1200 (2008).
12. Crone, N.E., Miglioretti, D.L., Gordon, B. & Lesser, R.P. Functional mapping of human sensorimotor cortex with electrocorticographic spectral analysis. II. Event-related synchronization in the gamma band. *Brain* **121 (Pt 12)**, 2301-2315 (1998).
13. Miller, K.J., Zanos, S., Fetz, E.E., den Nijs, M. & Ojemann, J.G. Decoupling the cortical power spectrum reveals real-time representation of individual finger movements in humans. *J Neurosci* **29**, 3132-3137 (2009).
14. Crone, N.E.*, et al.* Functional mapping of human sensorimotor cortex with electrocorticographic spectral analysis. I. Alpha and beta event-related desynchronization. *Brain* **121 (Pt 12)**, 2271-2299 (1998).
15. Miller, K.J.*, et al.* Spectral changes in cortical surface potentials during motor movement. *J Neurosci* **27**, 2424-2432 (2007).
16. Manning, J.R., Jacobs, J., Fried, I. & Kahana, M.J. Broadband shifts in LFP power spectra are correlated with single-neuron spiking in humans. *Journal of Neuroscience* **29**, 13613–13620 (2009).
17. Miller, K.J., Sorensen, L.B., Ojemann, J.G. & denNijs, M. Power-Law Scaling in the Brain Surface Electric Potential. *PLoS Comput Biol* **5**, e1000609 (2009).
18. Pfurtscheller, G. & Lopes da Silva, F.H. Event-related EEG/MEG synchronization and desynchronization: basic principles. *Clin Neurophysiol* **110**, 1842-1857 (1999).
19. Brown, P. Oscillatory nature of human basal ganglia activity: relationship to the pathophysiology of Parkinson's disease. *Movement disorders* **18**, 357-363 (2003).
20. Feige, B.*, et al.* Cortical and subcortical correlates of electroencephalographic alpha rhythm modulation. *J Neurophysiol* **93**, 2864-2872 (2005).
21. Schnitzler, A., Timmermann, L. & Gross, J. Physiological and pathological oscillatory networks in the human motor system. *Journal of Physiology-Paris* **99**, 3-7 (2006).
22. Neggers, S.F., Hermans, E.J. & Ramsey, N.F. Enhanced sensitivity with fast three-dimensional blood-oxygen-level-dependent functional MRI: comparison of SENSE-PRESTO and 2D-EPI at 3 T. *NMR in biomedicine* **21**, 663-676 (2008).
23. Ramsey, N.F.*, et al.* Phase navigator correction in 3D fMRI improves detection of brain activation: quantitative assessment with a graded motor activation procedure. *NeuroImage* **8**, 240-248 (1998).
24. Maes, F., Collignon, A., Vandermeulen, D., Marchal, G. & Suetens, P. Multimodality image registration by maximization of mutual information. *IEEE transactions on medical imaging* **16**, 187-198 (1997).
25. Ashburner, J. & Friston, K.J. Unified segmentation. *NeuroImage* **26**, 839-851 (2005).
26. Hermes, D., Miller, K.J., Noordmans, H.J., Vansteensel, M.J. & Ramsey, N.F. Automated electrocorticographic electrode localization on individually rendered brain surfaces. *Journal of neuroscience methods* **185**, 293-298 (2010).

27. Welch, P. The use of fast Fourier transform for the estimation of power spectra: A method based on time averaging over short, modified periodograms. *IEEE Trans. Audio Electroacoustics* **15**, 70-73 (1967).
28. Roopun, A.K.*, et al.* A beta2-frequency (20-30 Hz) oscillation in nonsynaptic networks of somatosensory cortex. *Proceedings of the National Academy of Sciences of the United States of America* **103**, 15646-15650 (2006).
29. Ogawa, S., Menon, R.S., Kim, S.G. & Ugurbil, K. On the characteristics of functional magnetic resonance imaging of the brain. *Annual review of biophysics and biomolecular structure* **27**, 447-474 (1998).
30. Leuthardt, E.C.*, et al.* Electrocorticographic frequency alteration mapping: a clinical technique for mapping the motor cortex. *Neurosurgery* **60**, 260-270; discussion 270-261 (2007).
31. Whittingstall, K. & Logothetis, N.K. Frequency-band coupling in surface EEG reflects spiking activity in monkey visual cortex. *Neuron* **64**, 281-289 (2009).
32. Katzner, S.*, et al.* Local origin of field potentials in visual cortex. *Neuron* **61**, 35-41 (2009).
33. Brookes, M.J.*, et al.* GLM-beamformer method demonstrates stationary field, alpha ERD and gamma ERS co-localisation with fMRI BOLD response in visual cortex. *NeuroImage* **26**, 302-308 (2005).
34. Winterer, G.*, et al.* Complex relationship between BOLD signal and synchronization/desynchronization of human brain MEG oscillations. *Human brain mapping* **28**, 805-816 (2007).
35. Ritter, P., Moosmann, M. & Villringer, A. Rolandic alpha and beta EEG rhythms' strengths are inversely related to fMRI-BOLD signal in primary somatosensory and motor cortex. *Human brain mapping* **30**, 1168-1187 (2009).
36. Ahlfors, S.P.*, et al.* Cancellation of EEG and MEG signals generated by extended and distributed sources. *Human brain mapping* **31**, 140-149 (2010).
37. Lachaux, J.P.*, et al.* Relationship between task-related gamma oscillations and BOLD signal: new insights from combined fMRI and intracranial EEG. *Human brain mapping* **28**, 1368-1375 (2007).
38. Ojemann, G.A.*, et al.* Neuronal correlates of functional magnetic resonance imaging in human temporal cortex. *Brain* **133**, 46-59 (2010).
39. Edwards, E.*, et al.* Comparison of time-frequency responses and the event-related potential to auditory speech stimuli in human cortex. *J Neurophysiol* **102**, 377-386 (2009).
40. Mazaheri, A., Nieuwenhuis, I.L.C., van Dijk, H. & Jensen, O. Prestimulus alpha and mu activity predicts failure to inhibit motor responses. *Human brain mapping* **30**, 1791-1800 (2009).
41. Asanuma, K.*, et al.* Network modulation in the treatment of Parkinson's disease. *Brain* **129**, 2667-2678 (2006).
42. Eidelberg, D.*, et al.* Regional metabolic correlates of surgical outcome following unilateral pallidotomy for Parkinson's disease. *Annals of neurology* **39**, 450-459 (1996).
43. Gao, J.H., Holland, S.K. & Gore, J.C. Nuclear magnetic resonance signal from flowing nuclei in rapid imaging using gradient echoes. *Medical physics* **15**, 809-814 (1988).
44. Turner, R. How much cortex can a vein drain? Downstream dilution of activation-related cerebral blood oxygenation changes. *NeuroImage* **16**, 1062-1067 (2002).
45. Duyn, J.H.*, et al.* 3-dimensional functional imaging of human brain using echo-shifted FLASH MRI. *Magn Reson Med* **32**, 150-155 (1994).
46. Duyn, J.H., Yang, Y., Frank, J.A., Mattay, V.S. & Hou, L. Functional magnetic resonance neuroimaging data acquisition techniques. *NeuroImage* **4**, S76-83 (1996).
47. Raemaekers, M.*, et al.* Test-retest reliability of fMRI activation during prosaccades and antisaccades. *NeuroImage* **36**, 532-542 (2007).
48. Birn, R.M., Diamond, J.B., Smith, M.A. & Bandettini, P.A. Separating respiratory-variation-related fluctuations from neuronal-activity-related fluctuations in fMRI. *NeuroImage* **31**, 1536-1548 (2006).

Chapter 4 supplementary material

Table S1. Subject information

Subject	Age	Sex	Handedness	Movement	Grid location	Scanner
	years	Female/Male	Left/Right		Left/Right	
1	23	M	R	left thumb	R	3 T
2	49	M	R	right thumb	L	3 T
3	18	M	R	right thumb	L	1.5 T
4	13	M	R	right fingers	L	3 T
5	17	F	R	left thumb	R	3 T
6	27	F	R	right thumb	L	1.5 T
7	26	M	R	right thumb	L	3 T
8	33	F	R	right thumb	L	3 T

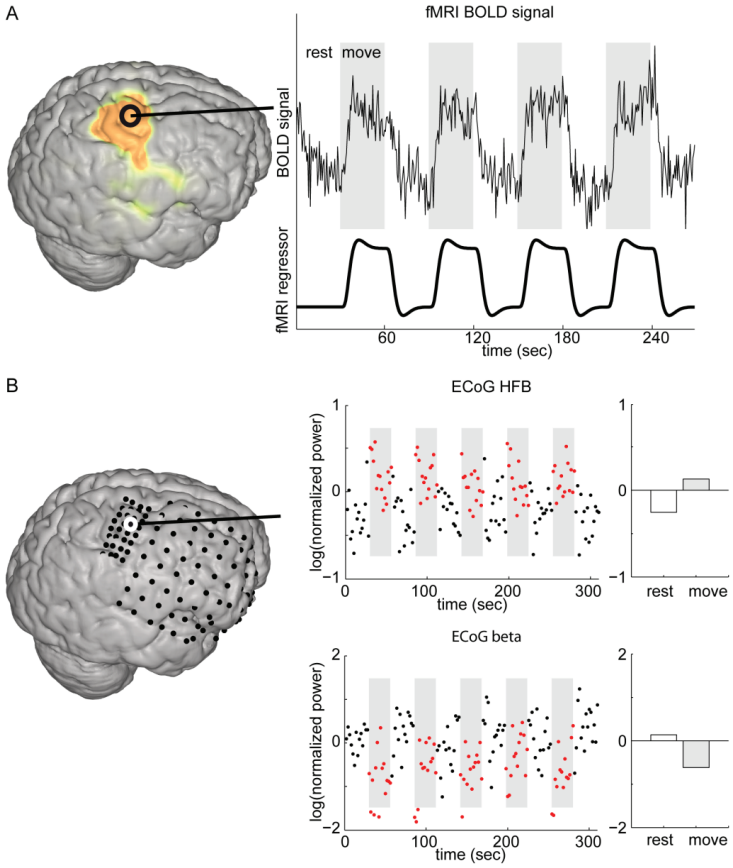

Figure S1. (*A*) The BOLD signal underneath one electrode (top) that was estimated in the GLM by a box car regressor convolved with the hemodynamic response function (bottom). The size of the BOLD signal change for finger movement compared to rest was estimated by the parameter estimates from the GLM (which is scaled as the percentage of signal change with respect to the global mean). For each electrode these parameter estimates (percentage of signal change) were averaged across gray matter voxels in an 8 mm radius of the electrode. Gray matter voxels were estimated from the gray/white matter segmentation by thresholding the gray matter probability map. **(*B*)** The HFB and β power change for the same electrode. Bar graphs show the average log(normalized power) across rest and movement epochs. The ECoG signal changes for the regression analyses were calculated by taking the difference between log(normalized power) in movement and rest blocks and dividing this by the standard deviation across all epochs to control for possible differences in variance over epochs between different frequency bands.

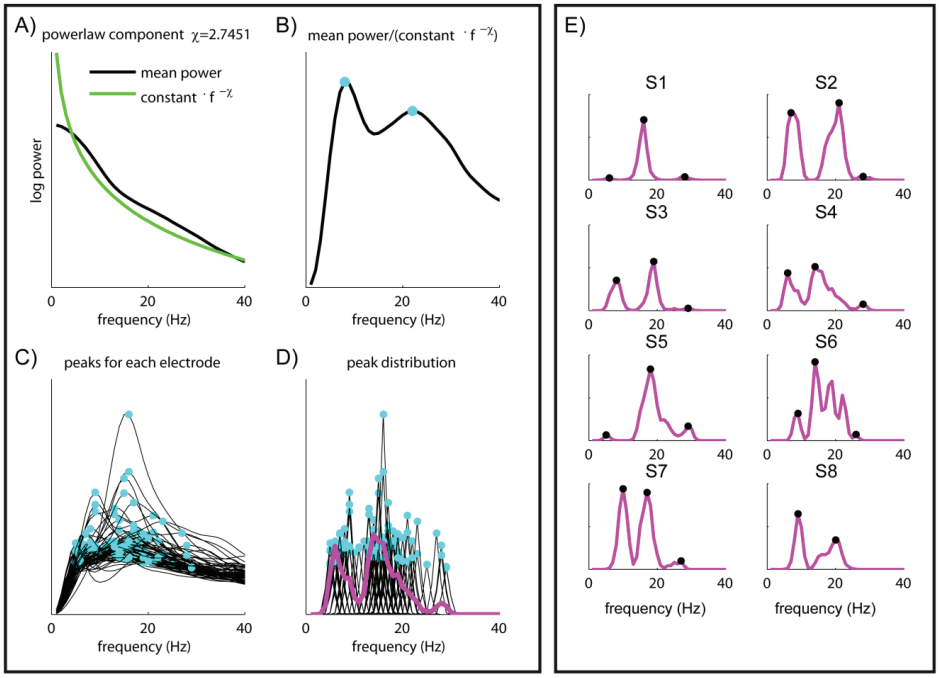

Figure S2. Estimation of α, β1 and β2 bands for each subject. (*A*) A powerlaw (constant·f^{X}) was fit to the data from the rest period for each electrode. **(*B*)** The power was normalized with respect to this powerlaw, and peaks (cyan) in this normalized powerspectrum were detected. **(*C*)** This procedure was performed for each electrode. **(*D*)** A small Gaussian was set around each peak on each electrode and the average over these peaks was calculated (purple). The frequency bands were defined as the largest peak for α ≤ 13Hz, 13Hz > β1 ≤ 24Hz, 24 Hz < β2 < 30Hz. **(*E*)** The peaks for each subject (S1-S8), only in subject S8 a β2 band could not be detected.

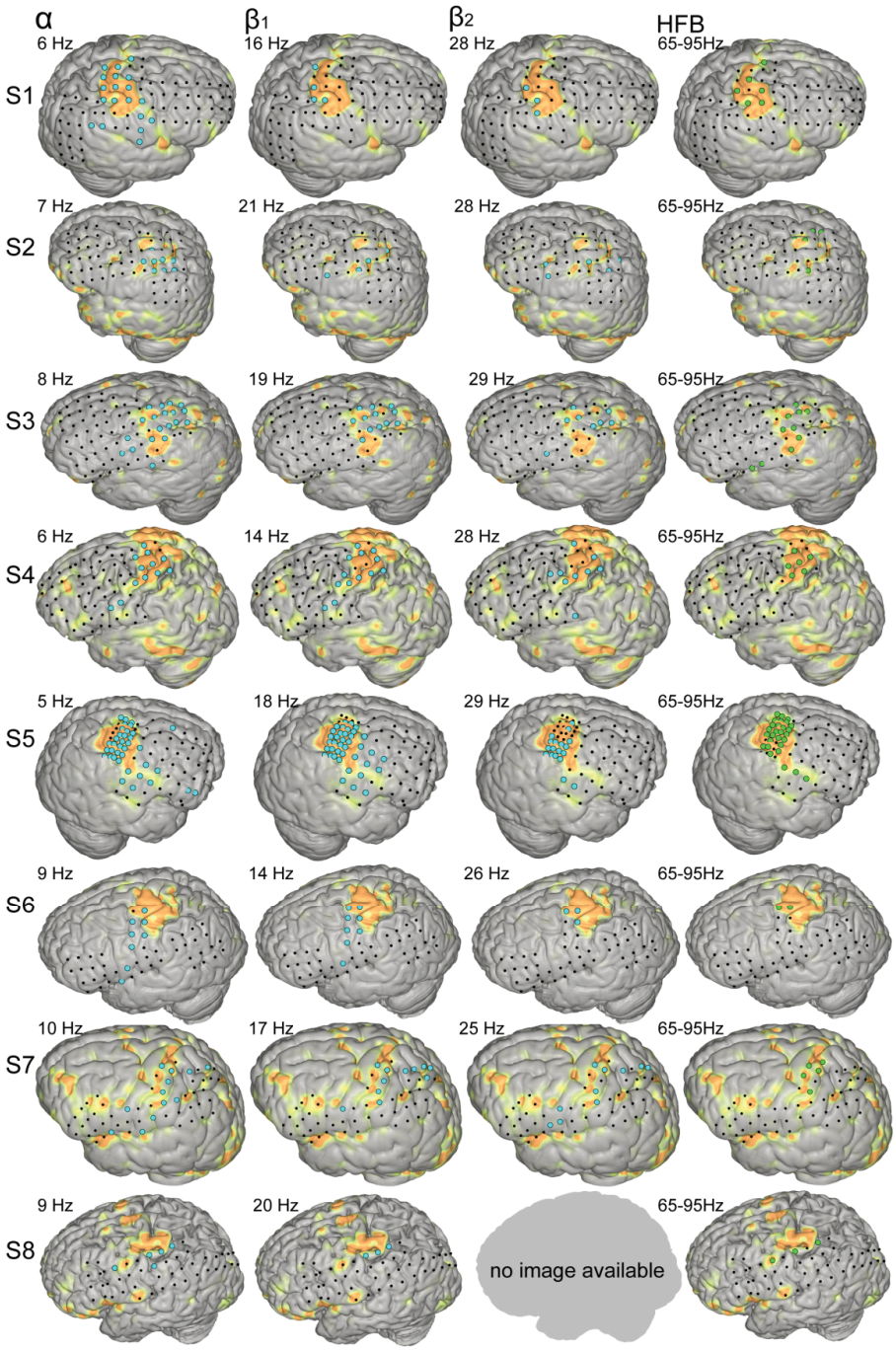

Figure S3. Overlap between brain-surface fMRI results (yellow-orange) and electric potential change in different frequency bands. For all eight subjects the rendering with smoothed fMRI results mapped on the surface is shown (fMRI t-values for movement versus rest, smoothed with 6 mm cosine kernel for display). Green denotes significant ($p<0.05$, Bonferroni corrected) increase in power in the HFB, and cyan denotes significant decrease in power in the low frequency bands. For subject 8 no β2 band was found (see Fig. S2).

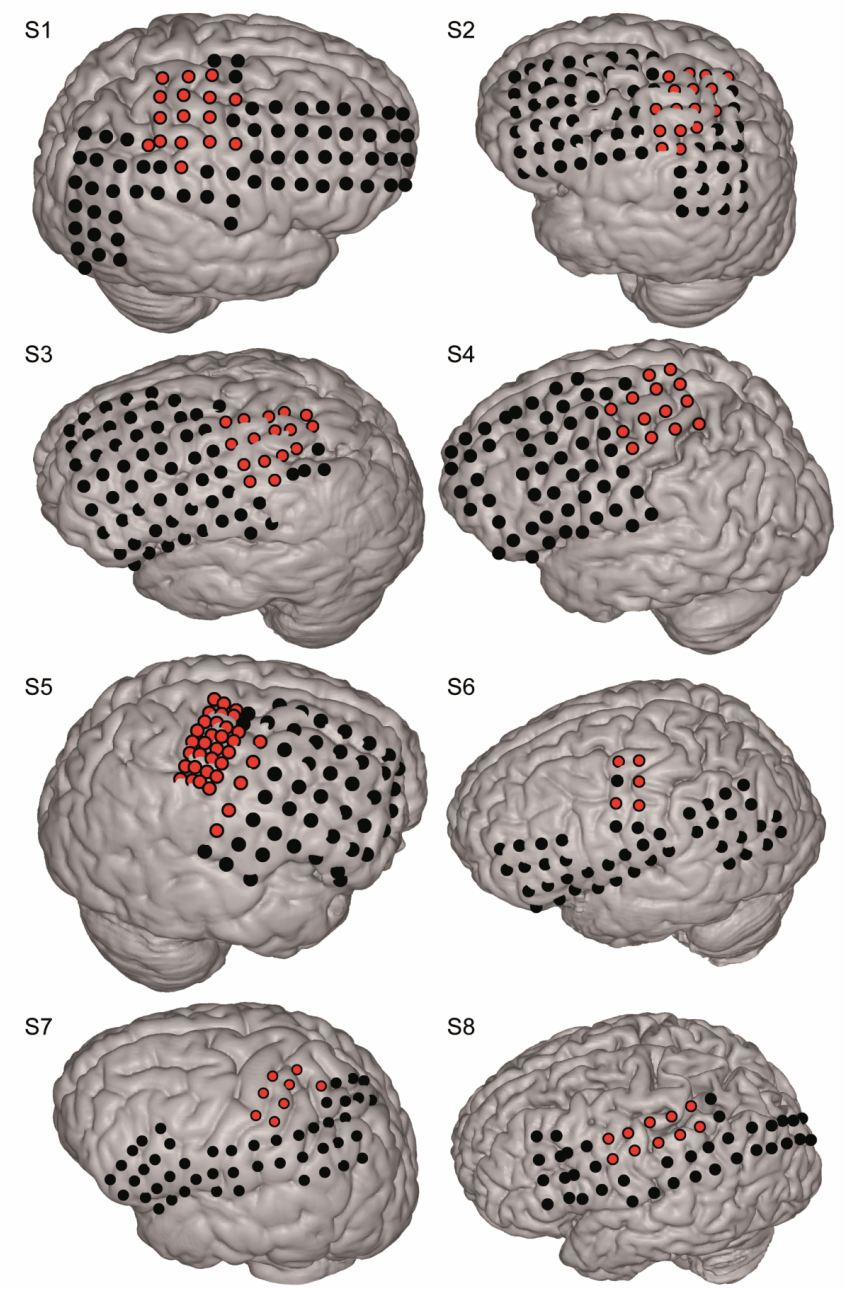

Figure S4. For each subject, the sites in red indicate electrodes where bipolar electrocortical stimulation between this electrode and any adjacent electrode elicited either hand movement or sensory hand sensation. This is a relatively liberal evaluation, as with bipolar stimulation all tissue between electrodes is stimulated, and effects are attributed to both electrodes even if only tissue underneath one is associated with motor or sensory function.

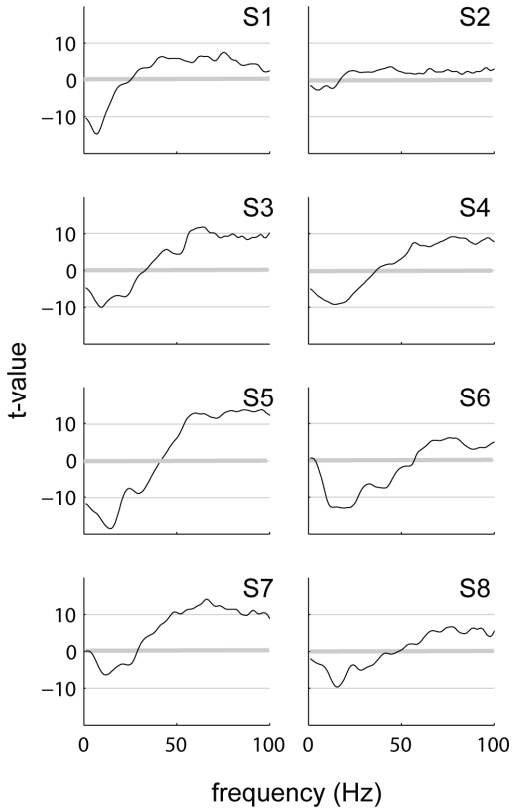

Figure S5. To get an estimate for the contrast-to-noise ratio across the power spectrum, the difference between movement and rest was calculated, normalized and then averaged across the electrodes on primary sensorimotor areas. A t-test was performed for epochs during movement versus baseline for every 1Hz frequency band. For all 8 subjects (S1-S8), the t-values are plotted as a function of frequency. Although there are differences between subjects, note that t-scores have similar magnitude for low frequency power decreases and high frequency power increases.

Table S2. For each subject, a linear regression model ($Y = X\beta + \varepsilon$) was fitted, where Y was the BOLD signal change for each electrode and X contained regressors for spectral power changes and an intercept. This table displays the explained variance (R^2 and R^2 adjusted for the number of regressors k, $R^2_{adjusted}=1-(n-1)/(n-k-1)*(1-R^2)$ where n denotes the sample size (number of electrodes) and k the number of regressors) and the *F*-test of the regression model. Regression coefficients (*B*-values) for the different frequency bands added in the model are shown.

Model 1: $X = [X_{HFB}]$						
Subject	R^2	adjusted R^2	*F*	p	$B_{65\text{-}95Hz}$	
1	0.26	0.26	28.96	<0.001	1.27	
2	0.15	0.12	11.85	<0.001	0.90	
3	0.07	0.06	5.80	<0.05	0.17	
4	0.29	0.28	27.06	<0.001	1.98	
5	0.55	0.54	95.59	<0.001	4.18	
6	0.31	0.29	20.36	<0.001	0.55	
7	0.01	-0.01	0.53	0.47	0.39	
8	0.18	0.16	9.66	<0.005	0.84	
Model 2: $X = [X_{HFB}\ X_{\alpha1}]$						
Subject	R^2	adjusted R^2	*F*	p	$B_{65\text{-}95Hz}$	B_{α}
1	0.56	0.55	50.12	<0.001	0.74	-1.13
2	0.16	0.14	7.42	<0.005	1.08	-0.40
3	0.27	0.25	13.93	<0.001	0.09	-0.25
4	0.47	0.46	28.61	<0.001	1.21	-1.56
5	0.66	0.66	75.88	<0.001	3.53	-2.54
6	0.54	0.52	26.65	<0.001	0.55	-0.46
7	0.02	-0.02	0.06	0.57	0.45	-0.44
8	0.18	0.14	4.88	<0.05	0.89	0.13
Model 3: $X = [X_{HFB}\ X_{\beta1}]$						
Subject	R^2	adjusted R^2	*F*	p	$B_{65\text{-}95Hz}$	$B_{\beta1}$
1	0.51	0.50	41.16	<0.001	1.08	-1.13
2	0.14	0.11	5.87	<0.005	0.88	0.05
3	0.15	0.12	6.28	<0.005	0.17	-0.21
4	0.53	0.52	36.31	<0.001	1.27	-1.84
5	0.75	0.74	113.53	<0.001	2.84	-2.84
6	0.59	0.58	32.87	<0.001	0.40	-0.47
7	0.02	-0.02	0.49	0.62	0.45	-0.39
8	0.19	0.15	5.00	<0.05	0.89	0.18
Model 4: $X = [X_{HFB}\ X_{\beta2}]$						
Subject	R^2	adjusted R^2	*F*	p	$B_{65\text{-}95Hz}$	$B_{\beta2}$
1	0.38	0.36	24.26	<0.001	1.42	-0.95
2	0.14	0.12	6.31	<0.005	0.73	0.32
3	0.07	0.05	3.04	0.05	0.19	-0.05
4	0.47	0.44	27.43	<0.001	1.98	-2.02
5	0.70	0.70	91.79	<0.001	4.21	-2.16
6	0.62	0.60	36.06	<0.001	0.31	-0.62
7	0.01	-0.03	0.35	0.71	0.44	-0.24
8	/					

Table S3. Regression analysis for electrodes on primary sensorimotor areas. For each subject, a linear regression model ($Y = XB+\varepsilon$) was fitted, where Y is the BOLD signal change for each electrode and X contained a regressor for power change in HFB and an intercept. This table displays the explained variance (R^2 and adjusted R^2) and *F*-test of the regression model. The regression coefficients (*B* -values) for every subject are shown.

Model 1: $X = [X_{HFB}]$						
Subject	R^2	adjusted R^2	*F*	p	*B* 65-95Hz	
1	0.55	0.51	11.23	<0.01	0.76	
2	0.27	0.21	4.1	0.07	0.97	
3	0.07	-0.02	0.83	0.38	2.24	
4	0.79	0.76	30.00	<0.001	0.34	
5	0.24	0.21	8.07	<0.05	0.11	
6	0.28	-0.09	0.76	0.48	1.47	
7	0.75	0.70	14.75	<0.05	1.2	
8	0.69	0.55	4.54	0.17	0.85	
Model 1: $X = [X_{HFB}\ X_{\alpha}]$						
Subject	R^2	adjusted R^2	*F*	p	*B* 65-95Hz	*B* α
1	0.57	0.46	5.32	<0.05	0.81	-0.32
2	0.27	0.13	1.86	0.21	1.20	0.01
3	0.07	-0.12	0.37	0.69	0.11	-0.01
4	0.79	0.73	13.12	<0.005	1.46	-0.02
5	0.26	0.19	4.11	<0.05	2.46	-0.81
6	0.93	0.79	6.53	0.27	1.02	-1.76
7	0.76	0.63	6.16	0.06	0.88	0.13
8	0.90	0.69	4.31	0.32	0.91	0.53
Model 1: $X = [X_{HFB}\ X_{\beta 1}]$						
Subject	R^2	adjusted R^2	*F*	p	*B* 65-95Hz	*B* β1
1	0.56	0.45	5.00	<0.05	0.84	-0.03
2	0.33	0.19	2.45	0.14	0.96	0.53
3	0.24	0.09	1.57	0.26	0.01	0.29
4	0.81	0.76	15.28	<0.005	1.44	-0.33
5	0.33	0.28	5.99	<0.01	2.48	-2.47
6	0.96	0.87	11.19	0.21	0.65	-2.02
7	0.75	0.62	5.93	0.06	0.98	-0.04
8	0.92	0.75	5.44	0.29	0.78	0.69

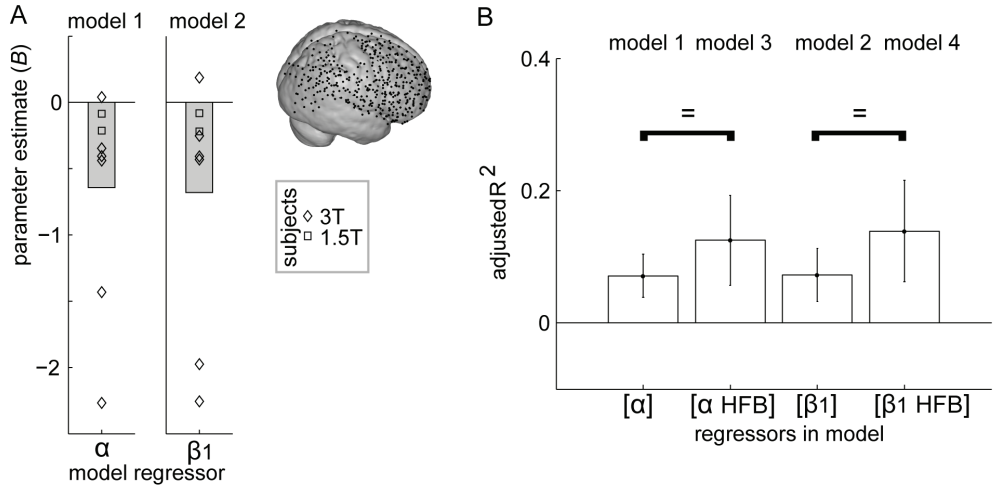

Figure S6. Parameter estimates for regression analysis for electrodes that were not on primary sensorimotor areas. For each subject, two linear regression model (Y = X*B*+ε) were fitted. In model 1, Y was the BOLD signal change for each electrode and X contained a regressor for power change in the α band. In model 2, Y was the BOLD signal change for each electrode and X contained a regressor for power change in the β1 band and an intercept. **(*A*)** The parameter estimates (*B* -values) for these two models were negative in all but 1 subject: across subjects there was a negative trend for both the α band (t(7)=-2.29, *P*=0.06) and the β1 band (t(7)=-2.11, *P*=0.07). The rendering shows the distribution of the electrodes not on primary sensorimotor hand areas. Since the ventral border of the primary sensorymotor cortex was defined based on electrocortical stimulation and due to normalization of electrode coordinates, it may appear that a couple of electrodes are more dorsal than others. **(*B*)** The mean R^2 (+/- standard error of the mean) for model 1 and model 2 and model 3 and 4, in which an HFB regressor was added. Adding an HFB regressor did not significantly explain extra variance in the BOLD signal change (adding HFB to model 1 ΔR^2=0.05, *P*=0.19, adding HFB to model 2: ΔR^2=0.07, *P*=0.14, by a permutation test with factorial 8 iterations of reshuffling across models).

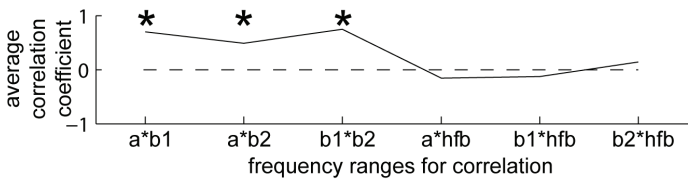

Figure S7. Spatial correlation between spectral power changes in different frequency bands. The y axis shows the average correlation across subjects between the different frequency bands. Across subjects low frequencies were significantly correlated ($p < 0.001$, indicated by an asterisk), high and low frequencies did not correlate significantly across subjects.

Chapter 5

Dissociation between neural activity in sensorimotor cortex and hand movement revealed as a function of movement rate

Dora Hermes[1], Jeroen Siero[1], Erik Aarnoutse[1], Frans Leijten[1], Natalia Petridou[1], Nick Ramsey[1]

[1] Rudolf Magnus Institute of Neuroscience, University Medical Center Utrecht, Department of Neurology and Neurosurgery, section Brainfunction and Plasticity, Utrecht, The Netherlands

Manuscript submitted

Abstract

It is often assumed that similar behavior is generated by the same brain activity, but this does not take into account the brain state or recent behavioral history, and movement initiation and continuation may not be similarly generated in the brain. In order to study whether similar movements are generated by the same brain activity, we measured neuronal population activity during movements repeated at different rates. Three subjects performed a motor repetition task in which they moved their hand at four different rates (0.3 Hz, 0.5 Hz, 1 Hz and 2 Hz). From high resolution ECoG arrays implanted on motor and sensory cortex high frequency power (65-95Hz) was extracted as a measure of neuronal population activity. During the two faster movement rates there was a significant suppression of high frequency power while movement parameters remained highly similar. This suppression was non-linear: after the first movement brain activity was reduced most strongly and the data fit a model where activity converges to an asymptote. The amplitude of the beta band suppression did not change with different rates. However, at the faster rates beta power did not return to baseline between movements but remained suppressed. We take these findings to indicate that beta power declines to release inhibition of motor cortex, and that at faster rates movement initiation is facilitated due to the extended beta power suppression. These results show that the relationship between behavior and neuronal activity is not consistent: recent movement influences the state of motor cortex and facilitates next movements by reducing the required level of neural activity.

Introduction

In daily life we often make series of similar movements: knocking on a door, walking, clapping our hands, stirring a spoon in a cup, but the exact same movements can also be made just once. It is often assumed that one action results from a specific pattern of neuronal activity. In motor cortex, this would assume that similar, repeated movements are induced by the same amount and pattern of motor cortex activity. However, behavioral and functional imaging studies have discussed whether a single movement is generated in the same way when it is carried out in a series of repetitions of the same movement [1-3]. Specific problems with the initiation or perseveration of movements in several neurological disorders and specifically in Parkinson's disease suggest that in the case of repeated movements not all movements are generated in the same way [4-7]. The assumption of a one-to-one correspondence between action and motor cortex activity can therefore be questioned.

Previous research has shown that corticospinal excitability is suppressed during repetitive movements as compared to constant contraction [8]. Decreased corticospinal excitability and difficulty to induce a hand movement by motor cortex stimulation has also been related to increased beta rhythm amplitude [9]. Similarly, the success rate to stop unwanted actions is related to the beta rhythm [10]. This suggests that during increased beta power motor cortex is inhibited. The beta rhythm decreases during motor tasks [11, 12] and previous scalp EEG research has shown that beta rhythm activity does not return to baseline between fast movements, but remains suppressed [13]. These studies may thus indicate that during fast, repetitive action the motor cortex is continuously released from inhibition. Movements have also been linked to transient increases in high frequency power of over 60 Hz [14, 15] associated with local processing in motor cortex. Whether the release from inhibition during repeated movement is also linked to differences in the actual local neuronal activity that is associated with a movement is yet unknown.

We recorded brain signals from high-resolution implanted electrode grids in epilepsy patients (electrocorticography, ECoG) from motor and somatosensory cortex and calculated beta power (12-28Hz) as a measure of brain state and high frequency band activity (HFB, 65-95Hz) as a measure of local neuronal activity. Broadband high frequency activity is associated with neuronal population firing rate [16-18] and correlates well with the fMRI signal [19]. We hypothesize that during fast, repeated movements, when motor cortex is in a different state, the amount of high frequency activity related to repeated movements will change. Three subjects made movements at 4 different rates (0.3. 0.5, 1 and 2 Hz). During fast movements (1-2 Hz) behavior changed from cue triggered into more self paced, continuous, movement. Also during the fast movements, beta power remained suppressed, not returning to baseline between movements. This suggests that during the fast movements motor cortex

is in a continuously active state, released from inhibition. During these faster movement rates there was a significant suppression of high frequency power in motor cortex after the initial movement. These data suggest that the correspondence between neuronal activity in sensorimotor cortex and hand movement changes with movement rate.

Materials and Methods

Subjects and procedure

Three right handed patients (1 female, 2 men; mean age, 27 years; range, 19-43) who were scheduled for the implantation of ECoG arrays for the clinical purpose of epilepsy monitoring gave informed consent to participate in this study. The study was approved by the ethical committee of the University Medical Center Utrecht, in accordance with the Declaration of Helsinki 2008. On average 125 electrodes were implanted, of which 32 in each patient were high resolution mini grids located on left sensorimotor cortex. Mini grids had an inter electrode spacing of 3.3 mm center to center and a spherical measurement surface of 1 mm diameter. To localize the electrodes with high accuracy we used the method presented in Hermes et al,. (2010) [20], where electrodes were localized from a high resolution CT scan (Philips Tomoscan SR7000) and projected to the cortical surface rendering generated from a preoperative MRI scan of each patient (Philips 3T Achieva, Best, The Netherlands).

Experimental paradigm

The experiment consisted of two parts, the first to map ECoG responses during one movement (Fig. 1), the second to test repeated movement effects (Fig. 2). The first part started and ended with a 30 sec rest period during which a red circle was presented on a computer screen and subjects relaxed with their right hand open, palm facing up. After the first 30 sec rest the circle turned green 54 times for 500ms at intertrial intervals varying from 3-18 sec, with an average of 8 sec. When the circle turned green the subjects closed and opened their right hand.

The second part of the experiment consisted of four movement repetition tasks where subjects moved at 4 different rates (0.33Hz, 0.5 Hz, 1Hz and 2Hz, see Fig. 2A). In the first task, each trial consisted of 3 visual cues (the red circle turning green similar as in the first part, for 400 ms), presented at 3 sec inter cue interval, instructing the subject to close and open their hand, thus resulting in 0.33Hz movement. In the 2nd, 3rd and 4th task respectively 4, 7 or 13 cues were given with 2, 1 and 0.5 sec inter cue interval. Each trial was followed by a rest period until a total trial duration of 19 sec was reached. Each task consisted of 13-15 trials of 19 sec.

Behavioral measurement and analysis

Finger movements were measured using a five degrees of freedom dataglove (5 DT Inc., Irvine, CA). The onset of each movement was visually detected for optimal accuracy. To extract a measure for whole hand movement in addition to each individual finger, we used the first component from a principal component analysis on all 5 channels. The movement amplitude and speed of flexion were calculated as follows. The average baseline was subtracted from each trial to correct for baseline offset. Hand movement amplitude was defined as the maximum deviation (when the hand is completely closed) within 500 ms after movement onset. The speed of flexion for each movement was defined as the lag between movement onset and the maximum deviation.

ECoG acquisition and analysis

ECoG data were acquired with a 128 channel recording system (Micromed, Treviso, Italy) with 512 Hz sampling rate and 0.15–134.4 Hz band-pass filter. Data were re-referenced to the common average of all electrodes recorded from the same amplifier (including electrodes on the regular grids to get a better estimate for the background noise for subjects 1 and 2). To extract power changes in high frequencies and the beta band, ECoG data were filtered for high frequencies (65-95Hz) and for the beta band using a 3rd order Butterworth filter in two directions to minimize phase distortion (using the filtfilt function in Matlab). The beta band was defined based on peaks in the power spectrum from the first single movement task and ran from 12-18 Hz for subjects 1 and 2 and from 22-28 Hz for subject 3. After filtering, the log power of the analytic amplitude (by Hilbert transform) was calculated and the signal was smoothed with a 250 ms Gaussian window (standard deviation of 42 ms). The smoothed log power from the first task was then normalized (z-score) with respect to the mean and standard deviation of 20 sec rest before the start of the task. The log power from the repetition tasks was normalized (z-score) with respect to the mean and standard deviation of all 15-19 sec periods at the end of the trials, this baseline was thus the same for all trials within a task and potential changes with repetition cannot be attributed to differences in the baseline.

To map basic ECoG responses on sensory and motor areas we selected electrodes on motor and sensory areas based on anatomical boundaries (the central sulcus and pre- and post-central sulci); electrodes located over a sulcus were not included (see Fig. 1A). The z-scored log-power was then averaged across electrodes on motor cortex and sensory cortex.

Subsequently we studied the effects of repetition and movement rate on behavioral data and beta and HFB amplitude. Using a repeated measures ANOVA we tested for significant changes in movement amplitude and speed (dataglove onset to maximum

flexion), beta amplitude and HFB amplitude across repeated movements within a task. The repeat factor was movement number: for task 1 (0.3 Hz) flexion number 1, 2 and 3, for tasks 2-4 (0.5 Hz, 1 Hz and 2 Hz) flexion number 1, 2, 3 and the last flexion. Since there were three subjects, statistics from individual subjects are reported. Results are considered significant if statistics showed significant effects in all 3 subjects (at $p < 0.05$) and effects were in the same direction.

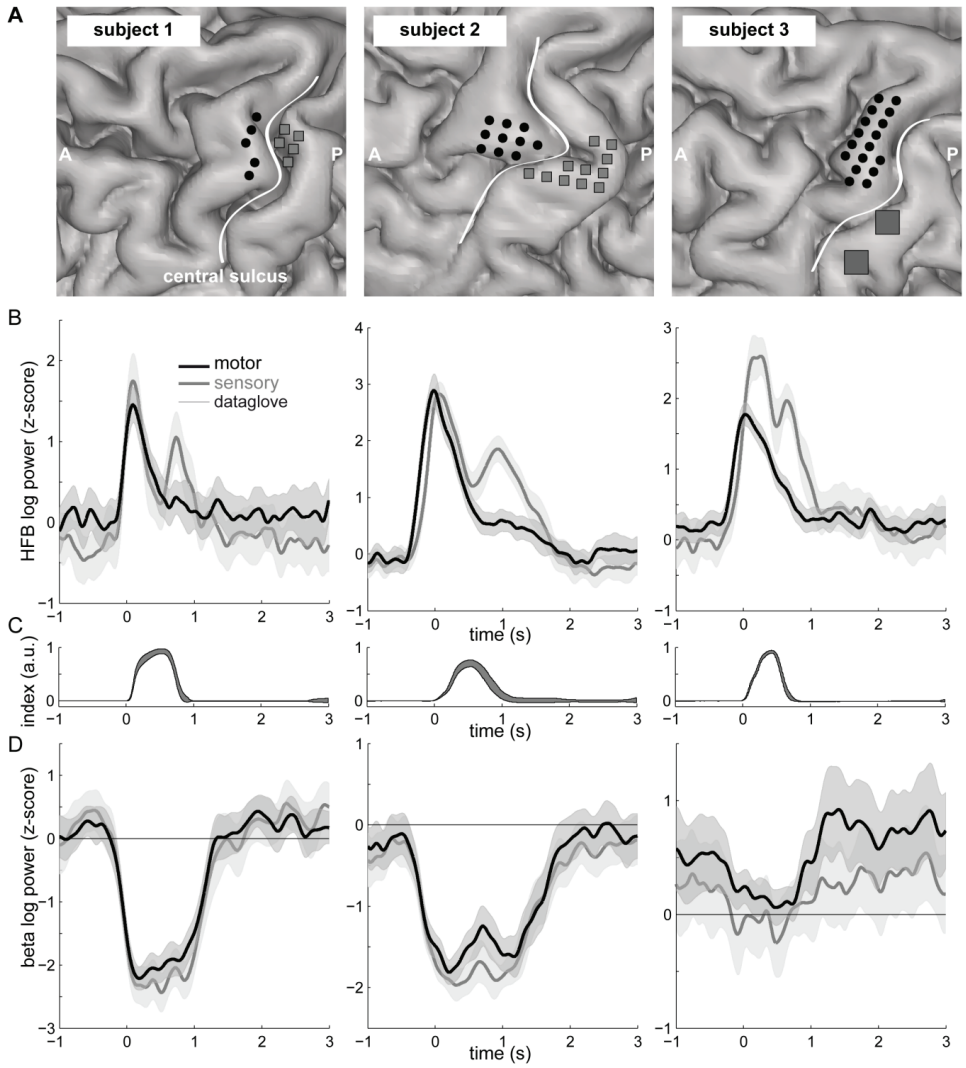

Figure 1. Responses in HFB and beta power on motor cortex and sensory cortex. **A)** The distribution of electrodes on motor and sensory cortex (A=anterior, P=posterior). Subject 3 did not have coverage of high resolution electrodes on sensory cortex and larger electrodes from the regular grid were selected. **B)** The HFB response upon movement onset at 0 ms averaged for electrodes on motor cortex (black) and sensory cortex (gray), light gray areas indicate +/- 3*standard error. **C)** The index finger movement from the dataglove. **D)** Beta response after movement onset.

Results

ECoG responses in sensory and motor cortex during 1 movement

In the first part of the experiment subjects performed a task in which 1 hand movement was made to localize and map basic ECoG responses. The subjects' average reaction time was 475 ms (+/-90 ms standard deviation across the 3 subjects, see Table 1). The ECoG signal was filtered for HFB and the beta band. Fig. 1 shows the HFB and beta response for electrodes on motor cortex and sensory cortex and the average behavioral response from the index finger of the data glove. On average, HFB responses in motor cortex reached 50% of the peak amplitude 147 ms (+/- 91 ms) before movement onset and in sensory cortex 60 ms (+/- 51 ms) before movement onset. Previous ECoG studies have observed similar lags between high frequency increase and movement onset [21, 22]. Surprisingly, the first sensory response starts before the onset of movement. Also note that while in motor cortex there is only one peak in the HFB response, in sensory cortex there are two subsequent peaks.

Table 1. Behavioral results. Reaction times during the first task in which patients made 1 hand movement. For the repetition tasks, the average number of hand movements for each trial is shown. Note that patients started to miss cues or make too many movements (holding their own pace) with movement rates of 1 Hz and 2 Hz.

Subject	1 movement RT (ms)		0.3 Hz (3 cues) # movements	0.5 Hz (4 cues) # movements	1 Hz (7 cues) # movements	2 Hz (13 cues) # movements
	mean	std				
1	404	77	3	4	7.9	13.5
2	577	73	2.9	3.9	4.8	11.2
3	445	77	3	4	7	9.2

Behavioral data during movement repetition

Hand movement was measured with a dataglove during the movement repetition task. Table 1 shows that during 0.33 Hz and 0.5 Hz movement the patients followed the cues and when shown 3 or 4 cues they made respectively 3 and 4 movements on average. During the faster movements of 1 Hz and 2 Hz behavior changed: they sometimes moved before a cue or missed a cue. This indicates that they were moving more continuously at their own pace. As a result, when 7 cues were given at 1 Hz the 3 subjects made 8, 5 or 7 movements on average, when 13 cues were given at 2 Hz they made 14, 11 and 9 movements. Fig. 2A demonstrates this effect in the dataglove responses for subject 3 during the four different tasks.

Subsequently, we tested whether subsequent movements within a task differed in movement amplitude or speed (onset to maximum flexion). Fig. 2B shows the average hand movement for the 3 subjects for flexion number 1, 2 and 3 from task 1 (0.3Hz), flexion 1, 2, 3 and 4 from task 2 (0.5Hz), flexion number 1, 2, 3 and the last 2 flexions from task 3 (1Hz), flexion number 1, 2, 3 and the last 3 flexions from task 4 (2Hz). Repeated movements look

highly similar. To test for effects of repetition on movement size and speed within a task a repeated measured ANOVA was performed. No significant changes in movement amplitude or speed were noted that were consistent across the 3 subjects (Fig. 2B shows the results of the ANOVA for each individual subject).

Changes in the beta and HFB response with repeated movement

First, we studied the effect of movement rate on beta power. Fig. 3 shows the average beta response during the movement repetition task in motor cortex and sensory cortex for all 3 subjects. It can be seen that at the faster movement rates (1Hz and 2 Hz), the beta band

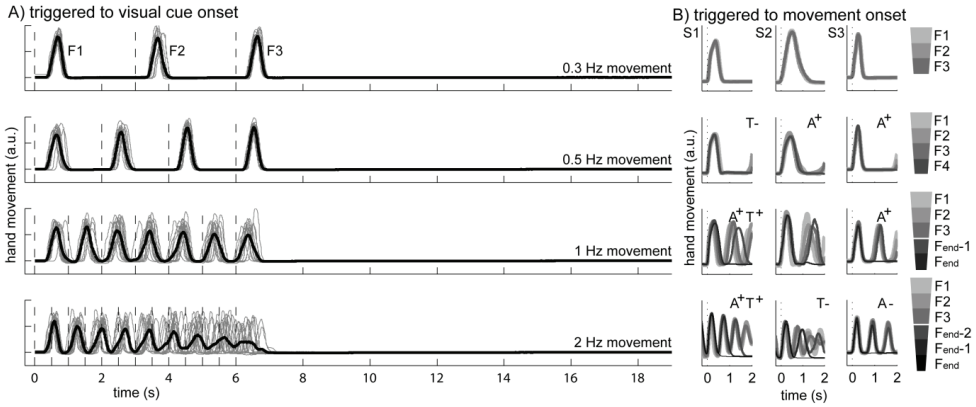

Figure 2. Repetition task design and behavioral responses. **A)** Hand movement during the 4 different repetition tasks as measured with a dataglove. The top panel shows that in the first task 3 visual cues (dashed lines) were given to open and close the hand with a 3 sec inter cue intervals (~0.3Hz). The other panels show the 2nd-4th task respectively and subjects opened and closed their hand at ~0.5Hz, ~1Hz and ~2Hz. In each trial a series of respectively 3, 4, 7 or 13 cues was followed by a rest period until 19 seconds. The average response is shown in black, individual trials are shown in gray for trials were respectively >2, >3, >5 and >7 responses were made. Note that for the 1Hz and 2Hz movements this patient started to make mistakes: movements were made too early or too late and cues were missed. Therefore in the average response (black) it seems as if movements were smaller, while the individual trials do not show this effect. **B)** To resolve this apparent reduction in movement response size trials were triggered with respect to movement onsets (t=0, dotted lines). The gray scale indicates the hand flexion number (F). For the 3 different subjects (S1-S3) the average index finger movement for respectively the 1st, 2nd and 3rd and 1st, 2nd, 3rd and 4th response are shown, for the 0.3 and 0.5 Hz task. Since mistakes started to be made for the 1 Hz and 2 Hz tasks, these show respectively the 1st, 2nd, 3rd, next to last (end-1) and last (end) response and the 1st, 2nd, 3rd, second to last (end-2), next to last (end-1) and last (end) response. All plots for the same subject have the same scale. Note that when index finger movement is locked to response onset the amplitude for subsequent movements in one task remains similar. At the faster rates with inter cue interval of <2 sec the HFB responses to the subsequent stimuli are also visible, but since these are locked to the previous hand movement and not to their response, they are not relevant for analyses. An A or T indicates significant effects of flexion number on movement amplitude or speed (time to maximum flexion), a + or - indicates an increase or decrease in either A or T with flexion number.

activity remains continuously suppressed: power does not return to baseline after every individual movement, but only after the last movement of a series.

To test whether there were any significant changes in beta amplitude with repeated movement within one task the beta power was averaged from 0ms to 300ms after movement onset (time window chosen based upon Fig . 1D). A repeated measured ANOVA on beta amplitude for each task showed no significant effect of repetition on beta amplitude across the 3 subjects, indicating that the amplitude change was the same regardless of movement rate.

Second, we then studied the effect of movement rate on high frequency power. High frequency power was extracted from electrodes on motor and sensory cortex as a measure of local neuronal activity. Fig. 4A and B show the average HFB response in motor and sensory cortex during the different movement repetition tasks. It can be seen that during the faster movements of 1 Hz and 2 Hz the first HFB response is larger than the subsequent responses. Note that this effect is most pronounced in motor cortex. To test whether this change in HFB activity with repeated movements was significant the HFB power was averaged from -100ms to 300ms around movement onset (time window chosen based upon Fig . 1B). Fig. 4C and D show the change in HFB amplitude with respect

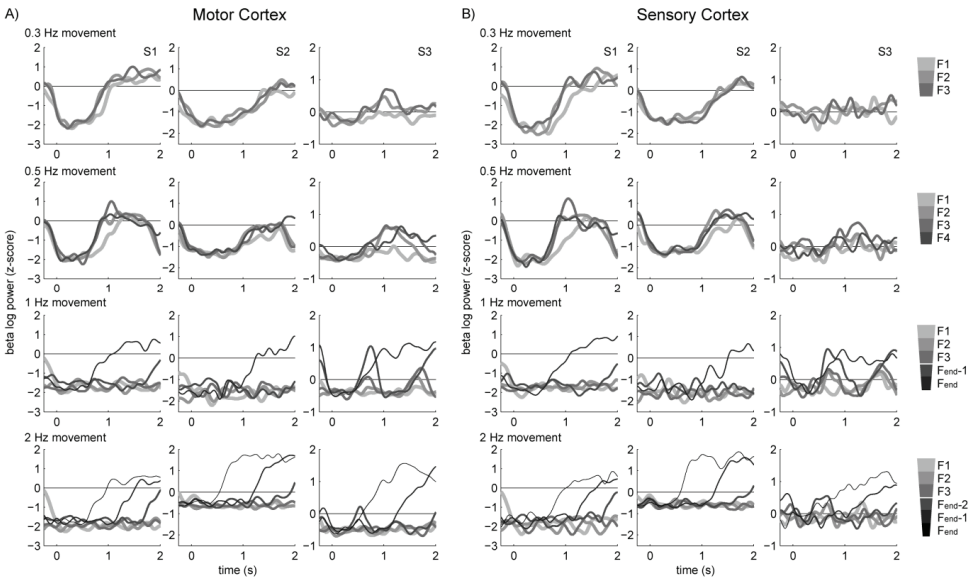

Figure 3. Beta responses on motor cortex and sensory cortex. **A)** Beta responses on motor cortex as a function of time after movement onset for subjects 1-3 from left to right and during the different movement rates from top to bottom. Note that at the faster rates with inter cue interval of <2 sec the beta responses to the subsequent stimuli are also visible. The gray scale indicates the hand flexion number (F) as in Fig. 2 and 3. **B)** Beta responses on sensory cortex for subjects 1-3 from left to right and during the different movement rates from top to bottom.

to the size of the first response. Similarly as in Fig 4A and B, a decrease in response size for subsequent movements can be noted, especially for the faster movement conditions of 1 Hz and 2 Hz. As shown in Fig. 4C, a repeated measured ANOVA indicated that in motor cortex, this decrease in HFB amplitude with subsequent movements was significant in 1 patient for the 0.3 Hz task, and for all 3 patients in the 0.5Hz, 1Hz and 2Hz tasks. In sensory cortex (Fig. 4D) a repeated measured ANOVA indicated the decrease in HFB amplitude with subsequent movements was significant in 1 patient for the 0.3Hz and 0.5Hz tasks, and for all 3 patients in the 1Hz task and for 2 patients in the 2Hz task. With faster movement repetition rate, there is thus a clear decrease in HFB amplitude after the first response; in sensory cortex this effect is similar, but less pronounced.

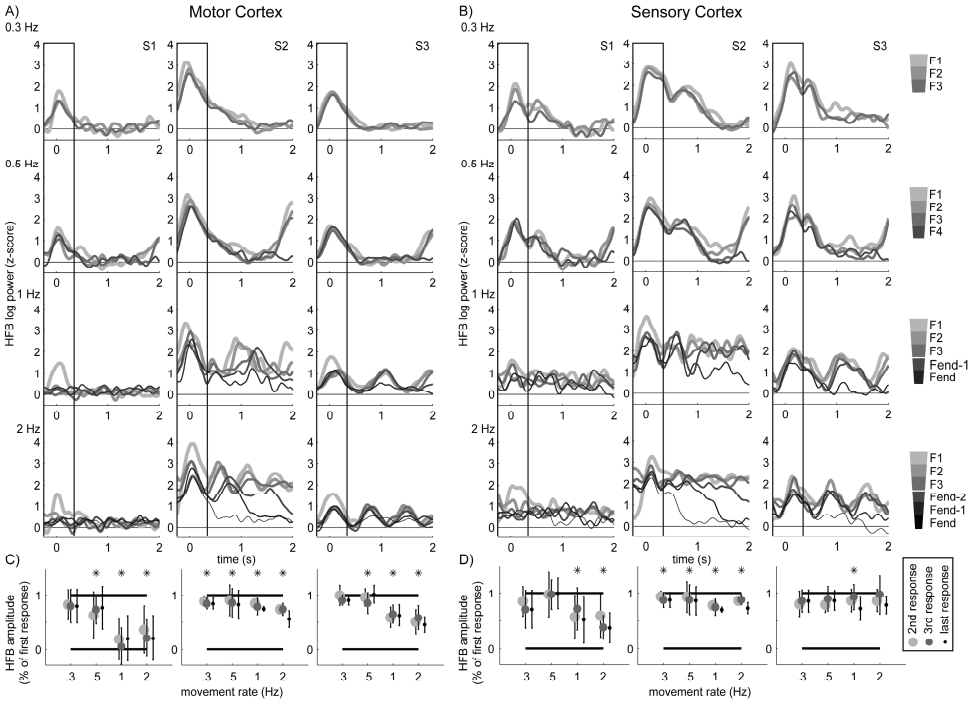

Figure 4. HFB responses on motor cortex and sensory cortex. **A)** HFB responses on motor cortex as a function of time after movement onset for subjects 1-3 from left to right and during the different movement rates from top to bottom. The gray scale indicates the hand flexion number (F) as in Fig. 2. The box accentuates the response related to onset of the current movement (at the faster rates with inter cue interval of <2 sec the responses to the subsequent stimuli are also visible, but these are irrelevant for analysis). **B)** HFB responses on sensory cortex for subjects 1-3 from left to right and during the different movement rates from top to bottom. **C)** The relative change from the first response amplitude -100 ms to 300 ms around movement onset during the 2nd, 3rd and last responses in motor cortex during the 4 different repetition tasks (0.3Hz, 0.5Hz, 1Hz and 2Hz). A * above the task denoted that flexion number had a significant effect on HFB amplitude ($p<0.05$ by a repeated measures ANOVA). **D)** The same results but in sensory cortex. Note that during the faster repetition tasks the 2nd, 3rd and last responses are suppressed. Note also that this suppression is more pronounced on motor cortex compared to sensory cortex.

Is the change in the high frequency response with repeated movement linear or non-linear?
Next, we assessed the nature of the repetition effect by fitting a linear and a non-linear model to the data. Fig. 5 shows the HFB amplitude as a function of time. Two different models were fitted to the HFB response sizes as a function of time. The first, linear model was of the form: $Y_{HFB} = bt + c$ and the second, non-linear model was of the form: $Y_{HFB} = a\frac{1}{t} + bt + c$, where t is the time of movement onset after the first cue and Y is the HFB amplitude of each movement. Other non-linear models could be fitted, this one was chosen because it converges to the linear function and has a sharp, non-linear decrease in case a is positive, but except for its non-linearity we do not attempt to draw any conclusions about the actual shape of the non-linear decrease. To test whether the non-linear model explained the data better, an F-test was performed on the difference in explained variance between the 2 models adjusted for the number of parameters ($\Delta R^2_{adjusted}$). In all subjects, in the faster 1 and 2 Hz movement tasks the motor cortex HFB amplitude was better explained by a non-linear model compared to a linear model ($p<0.01$ for all subjects), see Fig. 5. In sensory cortex the non-linear model explained the data better than the linear model in the first 2 subjects ($p<0.005$ for these 2 subjects). Only in 1 subject in motor cortex, the 0.5 Hz movement was better explained by a non-linear model $p<0.05$). This indicates that in motor cortex there is a significant, non-linear suppression of high frequency activity with repeated movements at higher rates that converges to an asymptote.

Spatial distribution of nonlinear decrease during fast movement
The decrease in HFB response amplitude in the previous analysis was based on the averaged HFB response across electrodes on motor cortex and sensory cortex. We further explored whether this decrease was seen across all individual electrodes on motor and sensory areas. The non-linear regression model ($Y_{HFB} = a\frac{1}{t} + bt + c$) was fitted for each electrode individually and spatial distribution of the non-linear regression coefficient, α, is shown in Fig. 6. A positive regression coefficient, indicating that the HFB response shows a non-linear decrease, can be noted for the faster tasks. Using the F-test approach as explained above, a significant increase in the model-fit was found for 5%, 24%, 67% and 82% of the electrodes on average after adding the non-linear parameter for the 0.3Hz, 0.5Hz, 1Hz and 2Hz tasks across the 3 subjects in motor cortex. For sensory cortex the non-linear model improved the fit in 17%, 20% 36% and 39% of electrodes.

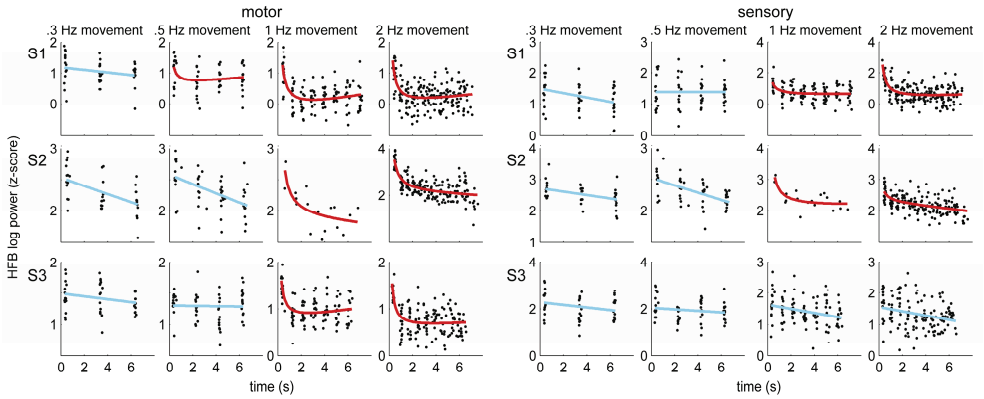

Figure 5. Fitting a linear or non-linear model to the HFB change. The gray dots in every single plot display the HFB amplitude during one movement on the y-axis and the timing of that movement on the x-axis. Subjects are shown in rows and the 4 different movement repetition tasks in columns; the average of the electrodes on motor cortex is shown on the left, the sensory cortex on the right. The linear model ($Y_{HFB} = bt + c$) fitted to the data is shown in the cyan line, but if the non-linear model ($Y_{HFB} = a\frac{1}{t} + bt + c$) fitted significantly better ($p<0.05$ by an F-test) a red line shows the non-linear model.

Discussion

In this study neuronal population activity in sensorimotor cortex was assessed during hand movement (flexion-extension) at different rates in order to understand whether the link between neuronal activity and behavior is maintained with repetitive actions. We found that high frequency (HFB) power exhibits a transient increase (response) in motor and somatosensory cortex during a movement, and that this response, which reflects neuronal population activity, decreases after the initial movement at rates of over 1 Hz. This decrease was non-linear: after activity related to the initial movement, activity dropped significantly for the subsequent repeated movement and then converged to a linear asymptote. In motor cortex, the non-linear decrease in response size with faster movement rates was noted for a large percentage of electrodes and not in a small subset. Since broadband high frequency power changes have been linked to population firing rate [16-18], this suggests that after movement initiation less motor cortex neurons have to fire or firing rates decline when multiple similar movements are made at a fast rate.

Sensory cortex showed some suppression with repetition that was not as strong as in motor cortex. In sensory cortex, this suppression can potentially be explained by accumulation of presynaptic inhibition of afferent input [21], which occurs with active movements. The suppression in motor cortex activity, which would be necessary to generate movements, can however not be explained by this phenomenon. During the single movement task sensory responses differed from motor responses (Fig. 1). While in motor

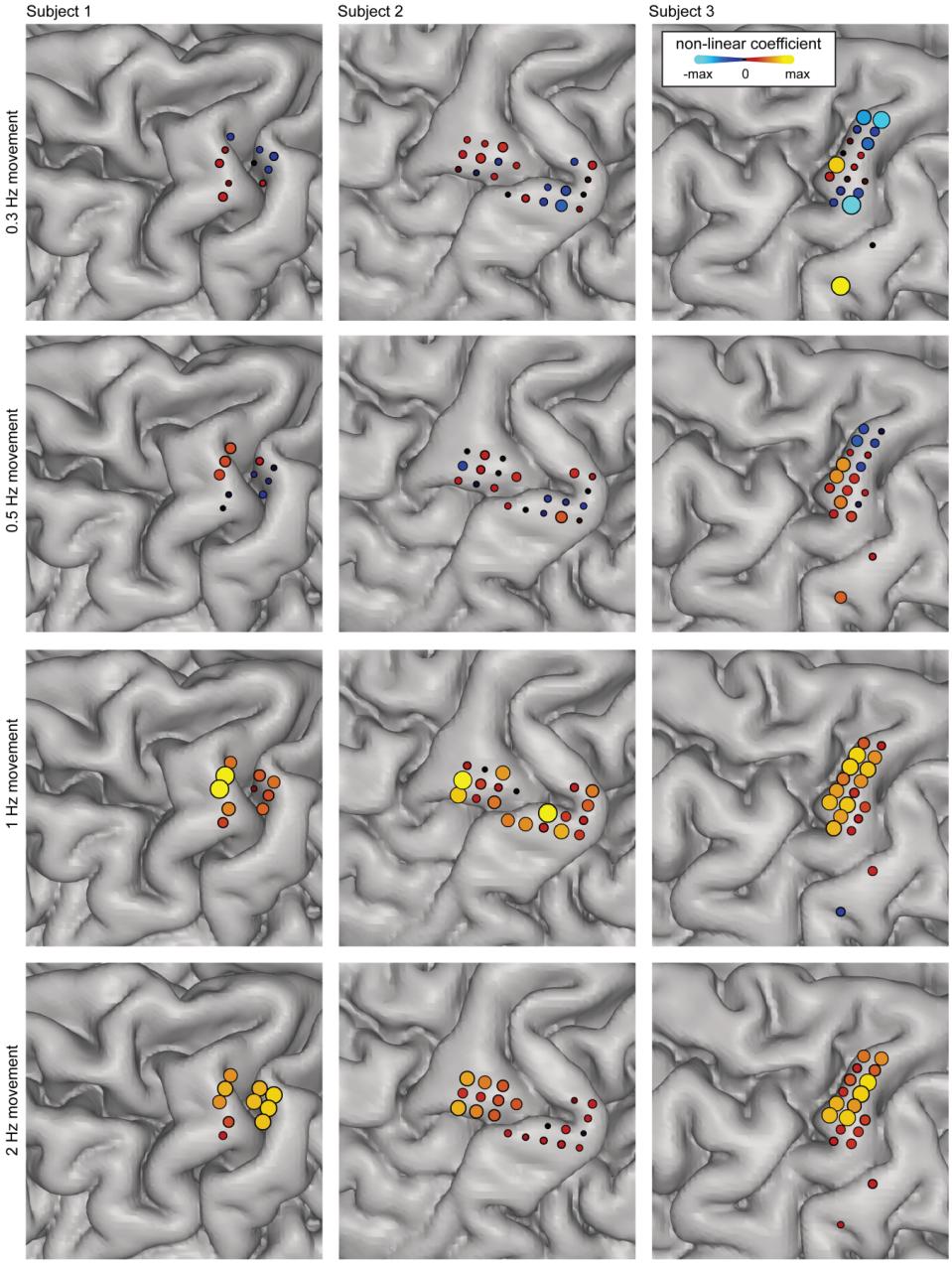

Figure 6. Spatial distribution of non-linear coefficient. Spatial distribution of the amplitude of the non-linear coefficient (*a*) from the model $Y_{HFB} = a\frac{1}{t} + bt + c$. Subjects are shown in columns and rows display different movement rates. Note that at 1Hz and 2Hz there is an overall increase in the non-linear parameter, indicating that responses became non-linearly reduced across the grid.

cortex there was only one peak in the HFB response, sensory cortex showed two subsequent peaks. Cells on the post-central gyrus are known to fire with two directions of movement [22, 23], which may explain the two peaks in the sensory response. Surprisingly, our results showed that the first sensory response started before the onset of movement. Cells in sensory cortex can fire about 60 ms before movement onset, which is a similar time-lag as shown in our results. Recent research has shown that sensory cortex may indeed be involved in motor control [24], which may require some pre-movement activity. Whether the suppression we noted in sensory cortex can be fully explained by presynaptic inhibition or also partially by changes in the pre-movement motor control component has to be further investigated.

While we found a significant decrease in high frequency responses for subsequent movements at high repetition rates, we found no repetition effect for the beta band response. However, beta band suppression did not return to baseline at faster movement rates, in contrast with the slower movement rates. This agrees with an earlier study with scalp EEG [13] and confirms that the phenomenon is present in primary sensorimotor cortex. Since previous studies reported decreased corticospinal excitability with high beta power [8, 9], continuous beta band suppression activity may reflect a continuous release of inhibition. It is possible that this release of inhibition may result in more efficient information processing requiring less neuronal activity: ongoing beta oscillations only need to be suppressed during the first movement in the fast movement conditions and initiation of movement may therefore require more activity than subsequent ones [25]. This mechanism may explain why movements at slower rates are avoided [26] and fast movements are more efficiently processed.

Our results are important for the interpretation of fMRI and PET results during movement repetition. Previous fMRI and PET studies have found that increases in repetition rate are correlated with respectively increased blood oxygen level dependent (BOLD) activity and cerebral blood flow in motor areas, reaching a ceiling at fast repetition rates [27-32]. These studies generally assume that underlying neuronal activity is the same for repeated movements and often contribute the ceiling effects to non-linearity in the BOLD response. Similarly, the duration of movement repetition affects the fMRI signal, which has also been attributed to non-linear effects in the BOLD response [33]. The BOLD response correlates well with high frequency activity [19, 34-36]. Considering our results of non-linear effects in high frequency activity with faster movements, it may well be that the reported non-linearity in the BOLD signal is overestimated. Hence, the relationship between neuronal activity and the vascular response (‘neurovascular coupling’) may be more linear than what has been reported.

It is important to understand the neurophysiology of repeated movements, since specific errors with movement initiation and perseveration are symptoms of several

neurological disorders and in Parkinson's disease in particular [4-7]. We showed that for fast, repeated movements less primary motor cortex activity is generated after the initiation of the first movement. Also, after the first movement, there was a continuous desynchronization of the beta rhythm, potentially indicating that the brain is in a different state. Interestingly, in patients with Parkinson's disease the suppression of the beta rhythm during movement is decreased [37] and when deep brain stimulation alleviates the Parkinson symptoms and normalizes the beta suppression, it is easier for these patients to stop unwanted actions [38]. Also, the onset of the beta decrease is delayed in these patients [39]. Medication reduces this delay and also facilitates movement initiation. Parkinson's disease mainly affects subcortical structures and beta rhythms have been related to subcortical-cortical interactions [40-44]. The combination of continuous beta desynchronization and a reduced high frequency response after the initiation of repeated movements may thus suggests a dynamic interplay between subcortical structures and motor cortex.

The suppression of high frequency power effect could be associated with differences in hand movement. However, hand movement amplitude or speed did not show any significant differences with repetition. We were unable to obtain electromyographic (EMG) measures, but since we did not notice significant differences in movement speed and subjects were not required to press against anything, it seems unlikely that force can explain this suppression effect. In addition, previous studies have not noticed any differences in EMG between subsequent movements [45] or movements made at different rates [13].

In conclusion, our data show that the relationship between motor actions and underlying neural activity is not consistent. The findings of repetition rate-dependent dynamics of neurophysiological parameters suggest that the amplitude of the HFB response in motor cortex depends on the degree of synchronization of the beta rhythm. At slow rates beta has time to return to baseline and a subsequent movement required a strong HFB response. At rates equal to, and higher than, 1 Hz, beta power remains depressed, and subsequent movements require a smaller HFB response. This mechanism may explain why movements at slower rates are avoided [26] and repetitive movements at higher rates are easier to execute.

Acknowledgements

The authors thank Eb Fetz, Kai Miller and Peter Brunner for their valuable comments and proofreading of the manuscript, Mariska Vansteensel, Martin Bleichner, Cyrille Ferrier, Geertjan Huiskamp, Herke Jan Noordmans and Tineke Gebbink for their help in collecting the data, Peter Gosselaar and Peter van Rijen for implanting the electrodes and the staff of the clinical neurophysiology department for their time and effort. This research is supported by the Dutch Technology Foundation STW, applied science division of NWO and the Technology Program of the Ministery of Economic Affairs, and the University of Utrecht, grant UGT7685.

References

1. Levy-Tzedek, S., Tov, M.B. & Karniel, A. Early switching between movement types: indication of predictive control? *Brain research bulletin* **85**, 283-288 (2011).
2. Schaal, S., Sternad, D., Osu, R. & Kawato, M. Rhythmic arm movement is not discrete. *Nature neuroscience* **7**, 1136-1143 (2004).
3. Miall, R.C. & Ivry, R. Moving to a different beat. *Nature neuroscience* **7**, 1025-1026 (2004).
4. Redgrave, P.*, et al.* Goal-directed and habitual control in the basal ganglia: implications for Parkinson's disease. *Nature reviews* **11**, 760-772 (2010).
5. Praamstra, P., Stegeman, D.F., Cools, A.R. & Horstink, M.W. Reliance on external cues for movement initiation in Parkinson's disease. Evidence from movement-related potentials. *Brain* **121 (Pt 1)**, 167-177 (1998).
6. Ebersbach, G., Hattig, H., Schelosky, L., Wissel, J. & Poewe, W. Perseverative motor behaviour in Parkinson's disease. *Neuropsychologia* **32**, 799-804 (1994).
7. Ridley, R.M. The psychology of perserverative and stereotyped behaviour. *Progress in neurobiology* **44**, 221-231 (1994).
8. Carroll, T.J., Baldwin, E.R., Collins, D.F. & Zehr, E.P. Corticospinal excitability is lower during rhythmic arm movement than during tonic contraction. *J Neurophysiol* **95**, 914-921 (2006).
9. Hummel, F., Andres, F., Altenmuller, E., Dichgans, J. & Gerloff, C. Inhibitory control of acquired motor programmes in the human brain. *Brain* **125**, 404-420 (2002).
10. Swann, N.*, et al.* Intracranial EEG reveals a time- and frequency-specific role for the right inferior frontal gyrus and primary motor cortex in stopping initiated responses. *J Neurosci* **29**, 12675-12685 (2009).
11. Jasper, H.H. & Andrews, H.L. Electro-Encephalography III. Normal differentiation of occipital and precentral regions in man. *Arch Neurol Psychiatry* **39**, 96-115 (1938).
12. Pfurtscheller, G. Central beta rhythm during sensorimotor activities in man. *Electroencephalography and clinical neurophysiology* **51**, 253-264 (1981).
13. Toma, K.*, et al.* Movement rate effect on activation and functional coupling of motor cortical areas. *J Neurophysiol* **88**, 3377-3385 (2002).
14. Crone, N.E., Miglioretti, D.L., Gordon, B. & Lesser, R.P. Functional mapping of human sensorimotor cortex with electrocorticographic spectral analysis. II. Event-related synchronization in the gamma band. *Brain* **121 (Pt 12)**, 2301-2315 (1998).
15. Miller, K.J.*, et al.* Spectral changes in cortical surface potentials during motor movement. *J Neurosci* **27**, 2424-2432 (2007).
16. Miller, K.J., Sorensen, L.B., Ojemann, J.G. & denNijs, M. Power-Law Scaling in the Brain Surface Electric Potential. *PLoS Comput Biol* **5**, e1000609 (2009).
17. Ray, S. & Maunsell, J.H. Different origins of gamma rhythm and high-gamma activity in macaque visual cortex. *PLoS biology* **9**, e1000610 (2011).
18. Manning, J.R., Jacobs, J., Fried, I. & Kahana, M.J. Broadband shifts in LFP power spectra are correlated with single-neuron spiking in humans. *Journal of Neuroscience* **29**, 13613–13620 (2009).
19. Hermes, D.*, et al.* Neurophysiologic correlates of fMRI in human motor cortex. *Human brain mapping* (2011).
20. Hermes, D., Miller, K.J., Noordmans, H.J., Vansteensel, M.J. & Ramsey, N.F. Automated electrocorticographic electrode localization on individually rendered brain surfaces. *Journal of neuroscience methods* **185**, 293-298 (2010).
21. Seki, K., Perlmutter, S.I. & Fetz, E.E. Sensory input to primate spinal cord is presynaptically inhibited during voluntary movement. *Nature neuroscience* **6**, 1309-1316 (2003).
22. Soso, M.J. & Fetz, E.E. Responses of identified cells in postcentral cortex of awake monkeys during comparable active and passive joint movements. *J Neurophysiol* **43**, 1090-1110 (1980).
23. Fetz, E.E., Finocchio, D.V., Baker, M.A. & Soso, M.J. Sensory and motor responses of precentral cortex cells during comparable passive and active joint movements. *J Neurophysiol* **43**, 1070-1089 (1980).
24. Matyas, F.*, et al.* Motor control by sensory cortex. *Science* **330**, 1240-1243 (2010).
25. Baker, S.N. Oscillatory interactions between sensorimotor cortex and the periphery. *Current opinion in neurobiology* **17**, 649-655 (2007).
26. van der Wel, R.P., Sternad, D. & Rosenbaum, D.A. Moving the Arm at Different Rates: Slow Movements are Avoided. *Journal of motor behavior* (2009).
27. Sadato, N.*, et al.* Frequency-dependent changes of regional cerebral blood flow during finger movements: functional MRI compared to PET. *J Cereb Blood Flow Metab* **17**, 670-679 (1997).
28. Blinkenberg, M.*, et al.* Rate dependence of regional cerebral activation during performance of a repetitive motor task: a PET study. *J Cereb Blood Flow Metab* **16**, 794-803 (1996).
29. Sadato, N.*, et al.* Frequency-dependent changes of regional cerebral blood flow during finger movements. *J Cereb Blood Flow Metab* **16**, 23-33 (1996).
30. Turner, R.S., Grafton, S.T., Votaw, J.R., Delong, M.R. & Hoffman, J.M. Motor subcircuits mediating the control of movement velocity: a PET study. *J Neurophysiol* **80**, 2162-2176 (1998).
31. Wildgruber, D., Ackermann, H. & Grodd, W. Differential contributions of motor cortex, basal ganglia, and cerebellum to speech motor control: effects of syllable repetition rate evaluated by fMRI. *NeuroImage* **13**, 101-109 (2001).

32. Riecker, A., Wildgruber, D., Mathiak, K., Grodd, W. & Ackermann, H. Parametric analysis of rate-dependent hemodynamic response functions of cortical and subcortical brain structures during auditorily cued finger tapping: a fMRI study. *NeuroImage* **18**, 731-739 (2003).
33. Birn, R.M., Saad, Z.S. & Bandettini, P.A. Spatial heterogeneity of the nonlinear dynamics in the FMRI BOLD response. *NeuroImage* **14**, 817-826 (2001).
34. Lachaux, J.P.*, et al.* Relationship between task-related gamma oscillations and BOLD signal: new insights from combined fMRI and intracranial EEG. *Human brain mapping* **28**, 1368-1375 (2007).
35. Logothetis, N.K., Pauls, J., Augath, M., Trinath, T. & Oeltermann, A. Neurophysiological investigation of the basis of the fMRI signal. *Nature* **412**, 150-157 (2001).
36. Niessing, J.*, et al.* Hemodynamic signals correlate tightly with synchronized gamma oscillations. *Science* **309**, 948-951 (2005).
37. Lim, V.K., Hamm, J.P., Byblow, W.D. & Kirk, I.J. Decreased desychronisation during self-paced movements in frequency bands involving sensorimotor integration and motor functioning in Parkinson's disease. *Brain research bulletin* **71**, 245-251 (2006).
38. Swann, N.*, et al.* Deep brain stimulation of the subthalamic nucleus alters the cortical profile of response inhibition in the beta frequency band: a scalp EEG study in Parkinson's disease. *J Neurosci* **31**, 5721-5729 (2011).
39. Magnani, G., Cursi, M., Leocani, L., Volonte, M.A. & Comi, G. Acute effects of L-dopa on event-related desynchronization in Parkinson's disease. *Neurol Sci* **23**, 91-97 (2002).
40. Brown, P. Oscillatory nature of human basal ganglia activity: relationship to the pathophysiology of Parkinson's disease. *Movement disorders* **18**, 357-363 (2003).
41. Feige, B.*, et al.* Cortical and subcortical correlates of electroencephalographic alpha rhythm modulation. *J Neurophysiol* **93**, 2864-2872 (2005).
42. Pfurtscheller, G. & Lopes da Silva, F.H. Event-related EEG/MEG synchronization and desynchronization: basic principles. *Clin Neurophysiol* **110**, 1842-1857 (1999).
43. Schnitzler, A., Timmermann, L. & Gross, J. Physiological and pathological oscillatory networks in the human motor system. *Journal of Physiology-Paris* **99**, 3-7 (2006).
44. Jones, S.R.*, et al.* Quantitative analysis and biophysically realistic neural modeling of the MEG mu rhythm: rhythmogenesis and modulation of sensory-evoked responses. *J Neurophysiol* **102**, 3554-3572 (2009).
45. Muthukumaraswamy, S.D. Functional properties of human primary motor cortex gamma oscillations. *J Neurophysiol* **104**, 2873-2885 (2010).

Chapter 6

Semantic processing disrupts prominent intracranial phase-amplitude coupling in the language network: a new role for theta?

Dora Hermes[1], Kai J. Miller[2], Mariska J. Vansteensel[1], Erik Edwards[3], Cyrille H. Ferrier[1], Martin G. Bleichner[1], Peter C. van Rijen[1], Erik J. Aarnoutse[1], Nick F. Ramsey[1].

[1] Rudolf Magnus Institute of Neuroscience, University Medical Center Utrecht, Department of Neurology and Neurosurgery, section Brainfunction and Plasticity, Utrecht, The Netherlands

[2] Department of Neurobiology and Behavior, University of Washington, Seattle, WA, United States

[3] Department of Electrical Engineering, University of Washington, Seattle, WA, United States

Manuscript submitted

Abstract

The role of low frequency oscillations in language areas is not yet understood. Using ECoG, we studied the interaction between low frequencies and local neuronal activity reflected in high frequencies. Broca's area and temporal language areas were localized in individual subjects using fMRI. In these areas theta power significantly decreased during verb generation and correlated negatively with high frequency activity across verb generation trials. During baseline, high frequency power was coupled to theta phase, but this coupling significantly decreased during verb generation. These results suggest a dynamic interaction between the neuronal mechanisms underlying the theta rhythm and local neuronal activity in language areas, which may reflect inhibitory gating. Since language areas have known connections to the thalamus and basal ganglia, and our fMRI results showed significant activation in these areas, the thalamus may play an important role in theta modulation in language areas.

Introduction

Understanding the basic neurophysiological changes in language areas is necessary to understand language processing. Language function is largely unique to humans, precluding animal research. In comparison with other cognitive functions, such as working memory and attention, not as much is known about the neurophysiology of language. Recent years have seen an increasing interest in the role of electrophysiological phenomena in the frequency domain in brain functions, exploiting developments in imaging technology and signal processing. High frequency broadband (HFB) power, measured in the frequency range over 30-60Hz is closely linked to local neuronal activity as well as mean firing rate [1-4]. The role of HFB for language has been investigated with intracranial recordings in humans and it was shown that changes in this range are highly specific for areas that are critical for language production such as Broca's and Wernicke's area [5]. In these areas, HFB changes are time locked to reading, hearing and speech production stages, indicating functional significance of HFB [6-9]. HFB power and gamma oscillations in the high frequency range are modulated by low frequency oscillations (LFO, < 20Hz) as was shown in several studies addressing other brain functions where fluctuations in frontal cortex, hippocampus and visual cortex were coupled to the phase of LFO [10-14]. It has been postulated that LFO may serve to facilitate neuronal computation [15, 16].

In temporal language areas, language stimuli evoked a HFB increase which was followed by a LFO power decrease 100-600 ms later [17, 18], suggesting a functionally relevant interaction. Interestingly, a decrease in LFO was first noted in 1981 as a flattening of the intracranial potential during naming [19] and was later demonstrated to be a decrease in amplitude of low frequencies [20]. Ojemann and colleagues proposed that the decrease in LFO reflected the gating function of the thalamocortical activation system.

Within the LFO range, theta oscillations (~5Hz) have been implicated in language processing in a magnetoencephalography (MEG) study, where the theta phase in auditory cortex tracked the envelope of spoken language [21]. With electrocorticography (ECoG), where brain signals are recorded with electrodes on the surface of the cortex, it has been shown that during a language task theta oscillations are more coherent across areas of cortex compared to other LFO, suggesting a specific role for theta in inter-regional communication [17]. Moreover, HFB power fluctuations in frontal areas are coupled to the phase of theta oscillations [11]. Coupling between theta phase and HFB or gamma power has been examined in other regions and functions, notably related to memory. In hippocampus, theta to gamma coupling has been characterized as a neural code for memory formation and retrieval [22, 23], and both theta and gamma power and coupling increase during memory tasks. Similarly, a theta increase has been reported for working memory function in humans with both

intracranial recordings [24] and MEG [25]. These studies show that theta and HFB or gamma power both increase during activity and suggest that the theta rhythm plays an important role in information transfer. While in hippocampus this hypothesis has been extensively tested, in frontal areas it has also been shown that the theta increase is rather moderate and not coherent across sites [26]. Theta rhythms may thus exhibit different behaviors across brain regions and functions, implying that theta in different areas of cortex may not be driven by the same mechanism.

To further explore the electrophysiological mechanisms in the language system, we measured ECoG and fMRI signal changes during covert verb generation. Verb generation is a standard task in neuroimaging for inducing semantic processing and is known to reliably activate language areas with both ECoG and fMRI [6, 7, 27]. We have shown that fMRI reliably localizes ECoG activity on a single subject basis [28, 29] and we therefore used fMRI to localize the frontal and temporal language areas. We found that in these areas, the theta band exhibited the most pronounced power changes. In contrast with frontal theta power during working memory, theta power decreased during verb generation in all three language regions investigated, and was anti-correlated with HFB increase. Furthermore, the theta phase was coupled to the power in HFB at baseline, but this coupling decreased significantly during verb generation.

Results

Six subjects performed a verb generation task where a noun was presented on a computer screen and subjects had to covertly generate a verb. Epochs of nouns were compared to epochs of rest were symbols were presented on the screen and subjects relaxed (baseline).

fMRI results

To localize language areas involved in the covert verb generation task an fMRI group analysis was performed. The fMRI group analysis showed significant activation ($p_{uncorrected}<0.001$, cluster size>10 voxels) during verb generation compared to rest in Broca's area, in the left and right middle temporal gyrus (MTG), the medial frontal gyrus, the right cerebellum and left basal ganglia and thalamus (see Table 1 and supplemental Fig. S1A). The temporal parietal junction (TPJ), which contains Wernicke's area, was not significantly activated on the group level, which may be related to high variability of the location of Wernicke's area across subjects [30] in combination with the small number of subjects (6) in the group analysis. Note that we used a covert verb generation task to reduce fMRI motion artifacts due to mouth movement. Also note that therefore no significant activity in motor mouth areas was found.

For localization of language regions of interest on an individual subject basis (Broca's area and left MTG based on fMRI group results, and TPJ since it contains Wernicke's area), single subject fMRI results for verb generation compared to rest were calculated and electrodes with the largest fMRI signal change in these areas were selected. All 6 subjects had electrodes on Broca's area and in 5 subjects electrodes covered TPJ and MTG. Fig. 1A shows in an example subject that these areas were significantly activated (see supplemental Fig. S1B for fMRI results in all subjects).

Table 1. FMRI group results for verb generation compared to rest are reported at $p_{uncorrected}<0.001$ (t>5.89), cluster size larger than 10 voxels. MNI coordinates of local maxima in each region are shown, the T value at this coordinate and the total cluster size in number of voxels.

Anatomical region	Hemisphere	MNI coordinates			T-value	Cluster Size
		x	y	z		
Inferior Frontal Gyrus	L	-48	20	-16	15,46	61
		-48	36	4	9,92	
		-36	24	0	7,59	
Middle Temporal Gyrus	L	-64	-48	0	17,49	56
	R	56	-40	-4	10,78	11
		48	-40	-12	8,59	
Medial Frontal Gyrus	L and R	8	24	48	16,08	21
Cerebellum	R	4	-40	-28	9,50	14
Cerebellum	R	28	-64	-36	20,73	126
		24	-68	-48	20,21	
		32	-72	-32	12,02	
Basal Ganglia/Thalamus	L	-12	0	8	8,90	15

ECoG results

To test which low frequency showed the most prominent power changes in language areas and to investigate whether theta power increased or decreased during a language task, the spectral power change during verb generation and rest was calculated for Broca's area, TPJ and MTG (see Fig. 1B and Fig. 2A). Fig. 2A shows the difference in power for verb generation versus rest: within the LFO range the theta band (4-7Hz) showed the strongest spectral power changes (i.e. a decrease) during verb generation compared to rest in all areas, in all subjects. Spectral power increases in high frequencies (>65Hz) were largest in Broca's area and were only noted in some subjects in TPJ and MTG (for spatial distribution of theta and HFB changes see Fig. 1C-D and supplemental Fig. S2 for all subjects).

To investigate spectral power changes over time, the signals were filtered for HFB (65-95Hz) and for theta (4-7Hz) since the theta band showed most robust changes in the previous analysis (see Fig. 1 E-G and Fig. 2B). Fig 2B shows how the power changed in

these bands over time during verb generation epochs. Power increases in HFB were largest in Broca's area and peaked on average at 1 sec after noun onset. TPJ showed smaller HFB power increases with an earlier peak (0.5 sec). MTG showed small, sustained HFB power increases that did not show a clear peak. In all areas, theta power decreased after the onset of the noun and showed the largest drop just after 1 sec (1.1 sec).

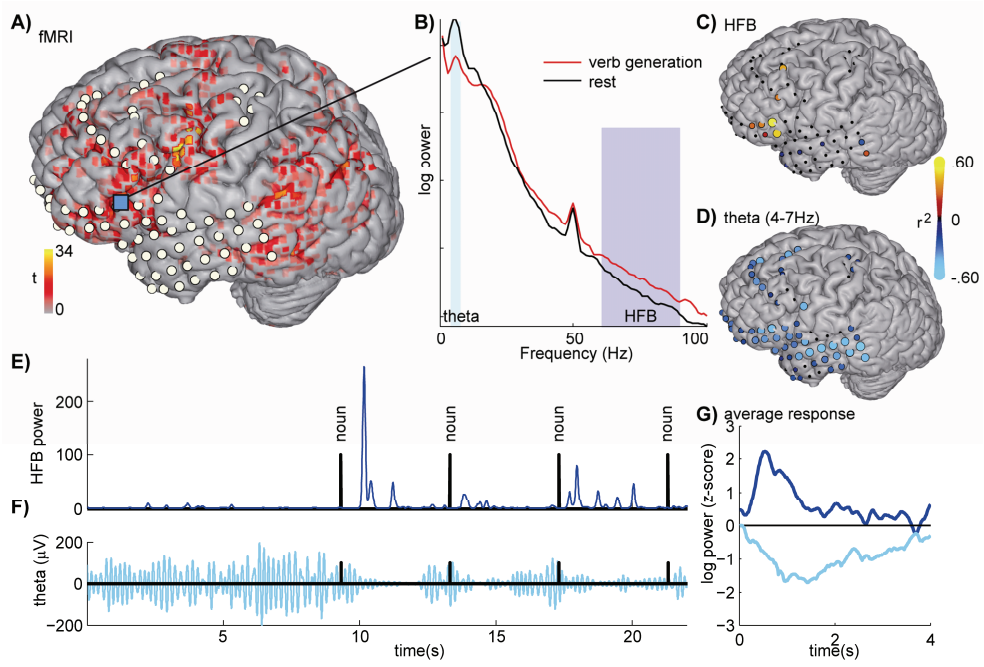

Figure 1. Example of fMRI and ECoG signal change during verb generation. **A)** Shows the areas that showed significant fMRI activity during verb generation compared to rest (t>4.5). The electrode with the largest fMRI signal change on Broca's area is indicated with a blue square. **B)** Shows the log power spectra from the ECoG signal measured from this electrode during verb generation and rest epochs. Power decreases in low frequencies (such as theta, 4-7Hz, indicated in cyan) and power increases in HFB from 65-95Hz can be noted. At 50Hz a line noise peak is visible. **C)** and **D)** For each electrode the size of the spectral power change (r2) in the theta band and in HFB was calculated. Note clear localized power increases in HFB in Broca's area and widespread power decreases in theta. **E)** From the same electrode on Broca's area the power of the signal filtered from 65-95Hz and resampled at 100Hz shows clear increases after noun presentation. **F)** The signal filtered for 4-7Hz shows large amplitude oscillations during rest. The amplitude drops after noun presentation. **G)** The average power change in HFB and theta for the verb generation epochs z-scored with respect to the power during rest.

Amplitude-amplitude correlation (AAC)

As a first measure of interaction between theta and high frequencies, we tested whether there was a direct correlation between HFB and theta power (AAC). Theta and HFB power, averaged across time within each trial, were correlated across trials. Fig. 3A shows for subject 1 that during verb trials, theta power was negatively correlated with HFB power increase. During rest trials this AAC disappeared. The spatial distribution of the correlation during verb and rest trials showed that this negative correlation during verb trials was most robust in Broca's area and MTG. This is shown in Fig. 3A where all electrodes were normalized to MNI space using the parameters generated by normalization of the anatomical MRI [31] and are displayed on and MNI template brain (http://mouldy.bic.mni.mcgill.ca/brainweb/selection_normal.html). To test whether the AAC was specific for theta, HFB power was correlated with power in the range of 1 to 40 Hz, in

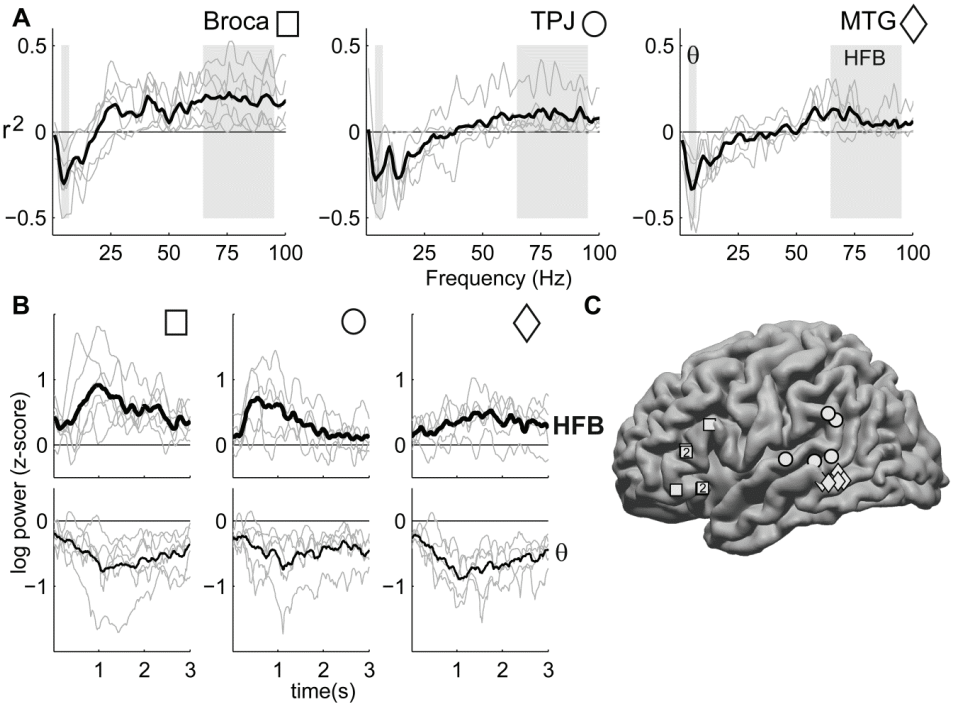

Figure 2. ECoG spectral power changes. **A)** For the selected electrodes on Broca's area, TPJ and MTG the power changes for verb generation compared to rest are shown in the signed r^2 for every single subject (light gray), and averaged over all subjects (black). Theta (4-7Hz) and HFB (65-95Hz) bands are indicated vertically. **B)** Log power change z-scored with respect to rest in the signal filtered for HFB (top) and theta (bottom). Plotted for every individual subject in light gray and averaged for all subjects in black. **C)** Locations of selected electrodes on Broca's area (squares), TPJ (circles) and MTG (diamonds) plotted on a standardized MNI brain. A '2' within an electrode indicates that in 2 subjects the electrodes were in the same location.

1Hz bins. Fig 3B shows that in the language areas the negative correlation between HFB and low frequencies was most specific for the theta range and was significantly negative across subjects ($p<0.05$ by t-test on the Fisher transform of the correlation coefficients). This significant correlation indicates that there may be a direct interaction between the processes reflected in HFB and theta.

The temporal resolution with which power changes in a theta rhythm (4-7Hz) can be estimated is much lower than that of high frequency power changes and to calculate interactions between high frequencies and theta at smaller timescales (<3 sec) we further investigated the coupling of theta phase to high frequency amplitude.

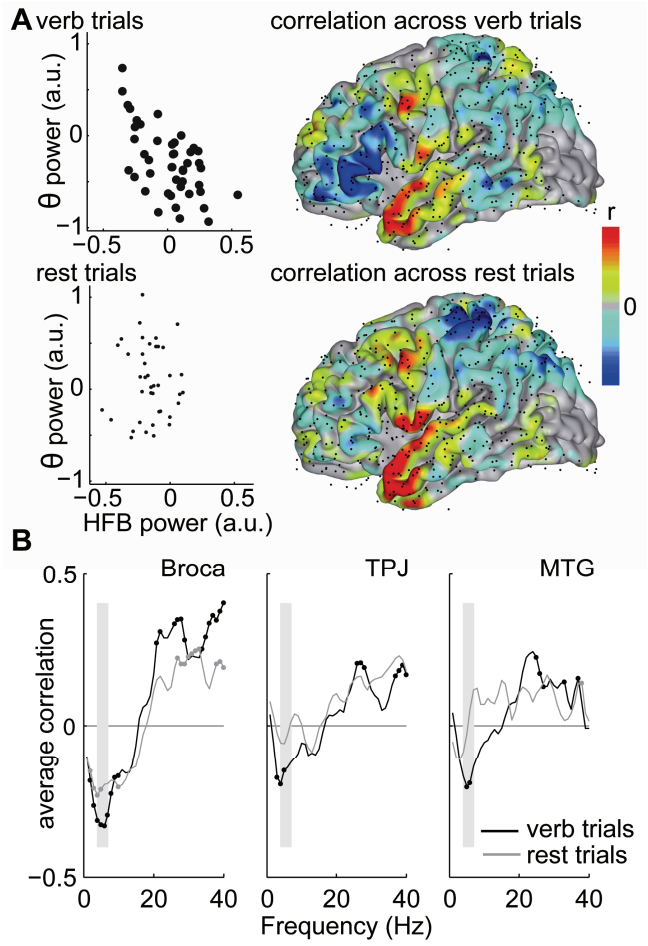

Figure 3: Amplitude-amplitude correlation (AAC). **A)** Average HFB power (x-axis) versus theta power (y-axis) during verb generation trials (top - dark circles) and rest trials (bottom – small circles) in the electrode on Broca's area of subject 1. Renderings show the average correlations per electrode rendered on the MNI brain (http://mouldy.bic.mni.mcgill.ca/brainweb/selection_normal.html) for all subjects and electrodes (black dots). Positive correlations are red, negative correlations blue. **B)** The average correlation (y-axis) between 1Hz low frequency bins (x-axis) and HFB across subjects for during verb trials (black) and rest trials (light gray) in Broca's area, TPJ and MTG. A black/gray dot on the line indicates that the correlation was significant (either negative or positive, puncorrected<0.05 by t-test on the Fisher transform of the correlation coefficient).

Phase amplitude coupling (PAC)

To test whether the theta rhythm is coupled to local neuronal activity and whether the theta rhythm drives the HFB increase during a task, we studied the relationship between theta phase and HFB power (PAC). Fig. 4 shows for subject 1 that HFB power peaked at the rising phase of the theta rhythm during rest in language areas. Fig. 4 shows the same for the average across subjects. Surprisingly, PAC decreased during verb generation compared to rest (no changes in phase were noted). Trial by trial statistics on the coupling between theta and HFB are shown in Fig 5. The decrease in PAC magnitude during verb generation was significant in Broca, TPJ and MTG (by paired t-test, Broca: $p<0.01$, TPJ: $p<0.05$, MTG: $p<0.05$). The spatial distribution of the PAC shift illustrates that the decrease in PAC was most robust in these a-priori selected language regions.

To test whether the theta rhythm in the three areas was modulated by one and the same source, we calculated theta coherence between these areas. Coherence between Broca, TPJ and MTG (see supplemental Fig. S3) showed no significant shifts in theta coherence during verb generation compared to rest (only in 1 subject an increase in theta coherence between Broca and TPJ during verb generation was noted).

Spatial correlation with fMRI

In order to bridge the gap with non-invasive human fMRI recordings, and to further investigate the relation of theta and HFB with respect to metabolic (blood oxygen level dependent, BOLD) change as was reported in motor cortex [28], we investigated the spatial correlation between theta, HFB and BOLD. For each electrode i, the BOLD percent signal change (Y_i) and spectral power change in HFB (X_{HFBi}) and theta ($X_{\theta i}$) was calculated. These were entered in a regression model ($Y = XB+\varepsilon$, where $X=[X_{HFB} X_{\theta}]$) for each subject individually. Fig. 6B shows the relation between ECoG predicted BOLD and BOLD change across electrodes for all subjects. An F-test showed that this regression model was significant in all subjects ($p<0.01$ for all subjects). Regression coefficients for HFB and θ shown in Fig. 6A were respectively significantly positive and negative across subjects (HFB: $t=7.30$, $p<0.001$, θ: $t=-4.84$, $p<0.005$), indicating that across areas of cortex BOLD change correlated positively with HFB change and negatively with θ power change. On average 28% of the BOLD change was explained by the ECoG change ($R^2=.28$). When either HFB or θ power changes were removed from the model, the explained spatial variance in BOLD dropped significantly by 15% for HFB: $t=-2.65$, $p<0.05$, and by 5% for θ: $t=-4.20$, $p<0.01$ (an F-test showed that models explaining BOLD by only HFB or theta changes were still significant in all subjects), indicating that HFB was the strongest correlate of BOLD signal change as was the case in the motor system [28]. This indicates that HFB and θ both correlate

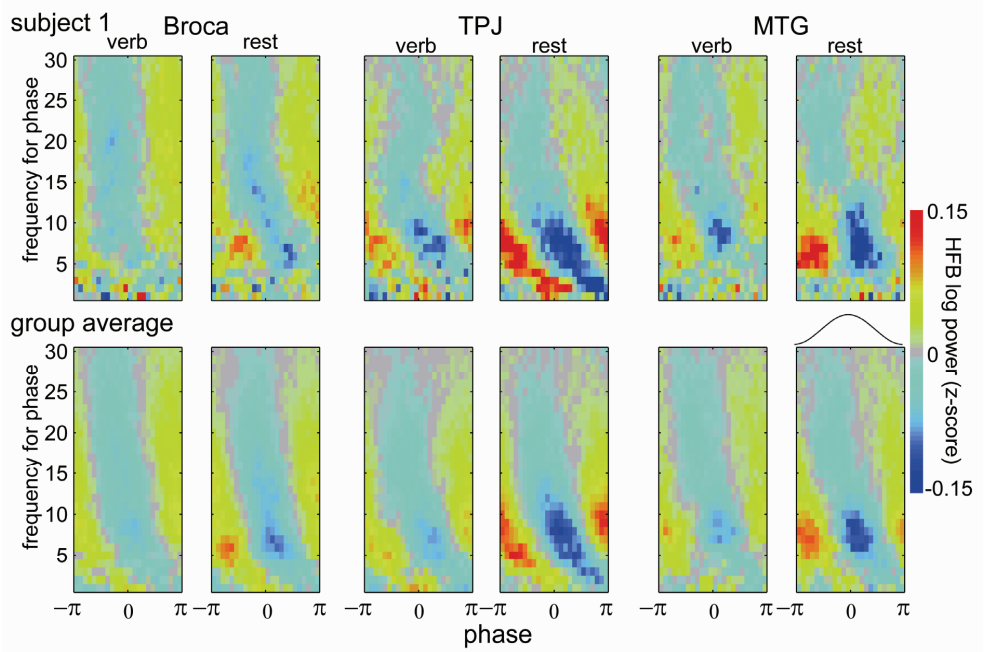

Figure 4: Phase amplitude coupling (PAC) palettes. Phase amplitude coupling palettes during verb generation and rest in subject 1 (top) and averaged across all subjects (bottom). The y-axis shows the frequency for which the phase was calculated. The phase is plotted on the x-axis. The color shows the z-scored HFB log power difference from the average. At the top of the bottom right panel an example the low frequency rhythm is plotted.

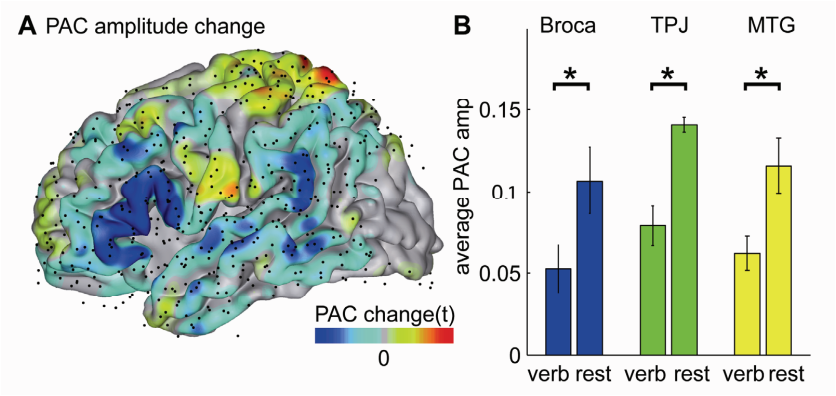

Figure 5: Trial by trial shift in theta-HFB PAC amplitude. A) A rendering of a standardized MNI brain with all electrodes in all subjects (black dots). The PAC shift between theta phase and HFB power was calculated for every electrode. The color scale indicates a PAC decrease during verb generation compared to rest in blue (negative t-values), or an increase in red (positive t-values). B) For the selected electrodes on Broca's area, TPJ and MTG the average PAC amplitude across subjects is shown (+/- SEM) during verb and rest trials. A * indicates a significant shift in PAC for verb compared to rest trials ($p<0.05$ by paired t-test).

differently with BOLD change. HFB and θ power changes were indeed spatially largely differently distributed: HFB and θ power were only significantly spatially correlated in 3 out of 6 subjects and shared 8% of variance on average.

To verify whether the correlation between BOLD and spectral power change was specific for theta and HFB, the spatial Pearson correlation was calculated for every individual frequency (Fig. 6C). It can be seen that the theta band shows a prominent negative correlation across all subjects and high frequencies correlated positively in a broad frequency range >60Hz.

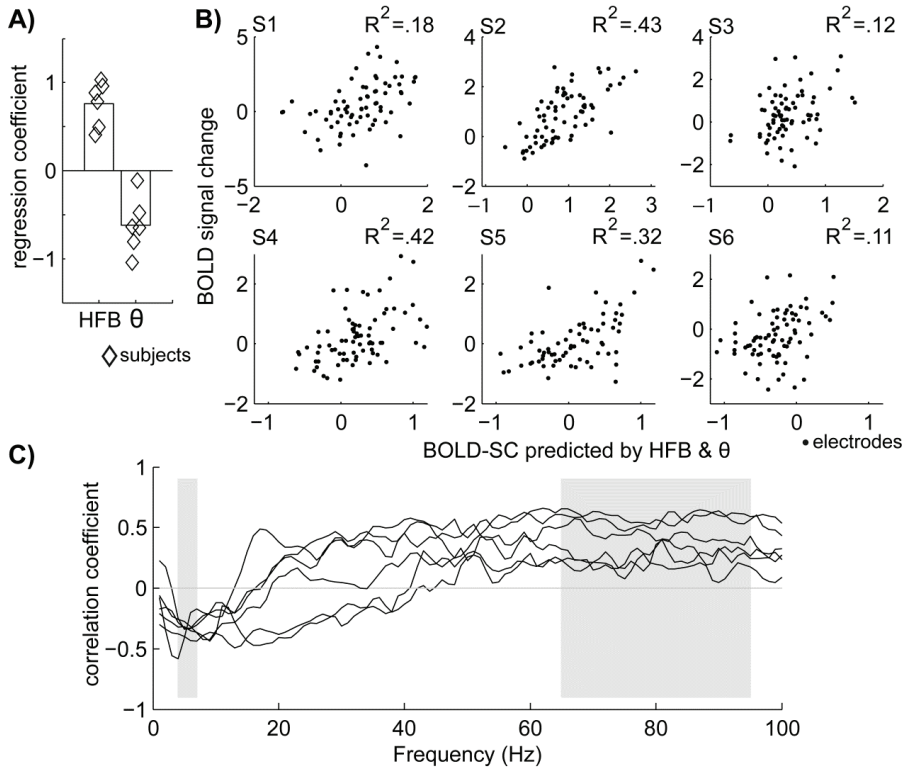

Figure 6: Relation between ECoG power change and fMRI. **A)** Regression coefficients (B) from the regression model Y = XB+ε where X = [X_{HFB} X_{θ}] for each subject show that power change in HFB correlated positively with BOLD signal change and theta correlated negatively with BOLD change. **B)** For all subjects (S1-S6), the relation between the BOLD change predicted by ECoG (x-axis) and the actual BOLD change (y-axis) is shown. In the top right of each plot the model fit ($R^2_{adjusted}$) is shown. **C)** The Pearson correlation between BOLD and ECoG calculated for every individual frequency (x-axis). Separate lined show the 6 individual subjects and theta and HFB are indicated in light gray.

Conclusion

In the present study, the basic electrophysiological mechanisms in language areas were investigated. We localized language areas on a single subject basis by fMRI and investigated which low frequencies showed the most robust spectral power changes during verb generation. Both frontal and temporal language areas showed a pronounced decrease in power in the theta band. This theta power decrease correlated with HFB power increases on a trial by trial basis. In addition, during rest HFB power was locked to the rising phase of the theta rhythm, and this coupling decreased significantly during verb generation specifically in language areas. Interestingly, no task related changes in theta coherence between language areas were noted. Last, when comparing spectral power change with fMRI BOLD change, theta power correlated negatively with BOLD increase, high frequencies correlated positively with BOLD change and each explained a different part of the BOLD change.

An interesting question is whether theta rhythm changes in different areas of cortex relate to the same neuronal mechanism. Our results showed that theta power decreases significantly in language areas during covert verb generation. In contrast, MEG and EEG studies on working memory have shown that theta power in frontal areas increases with memory load [25, 32]. Intracranial recordings in humans have shown robust theta increases in hippocampus [33], but in other cortical areas both increases [26] and decreases have been shown [34]. Furthermore, our data showed that theta power was anticorrelated with high frequency power during verb generation trials and phase amplitude coupling decreased during verb generation compared to rest. Other groups have shown that in hippocampus this is reversed: during a memory task power increases in the theta and gamma range and phase amplitude coupling increases concurrently, for review see [22]. Lastly, our results showed that theta rhythms anticorrelated with BOLD increases, and also here other studies have shown the reverse: in the human parahippocampal area BOLD correlated positively with theta power [35]. This suggests that theta rhythms in different areas of cortex, and different brain functions, may not always reflect the same underlying mechanism.

Canolty et al., 2007 proposed that theta power serves to control the amount of activity and theta phase the timing of spiking. We found that in verb generation trials with lower theta power, high frequency power was enhanced, suggesting indeed a correlation between theta power and the amount of activity. Also, theta phase was coupled to high frequency power during rest, but this coupling decreased during verb generation in all three regions. This indicates that increases in local neuronal activity are not carried by a theta rhythm, while during rest theta phase correlates with the timing of local neuronal activity. Therefore, theta phase does not seem to control the timing of population spiking in the verb generation setting. Miller et al., (2010) proposed that in addition to facilitation by synchronization, there

may also be suppression by synchronization: during rest when brain areas are in a disengaged state, local neuronal activity is inhibited by synchronizing low frequency rhythms. Similarly, Jensen and Mazaheri (2010) suggested that low frequencies may gate information processing or flow by means of inhibition. An inhibitory effect of theta rhythms would better explain both the reduced phase amplitude coupling and the decrease in theta amplitude during verb generation. In line with this notion, a decrease in phase amplitude coupling may reflect a release of inhibition by an as of yet unknown mechanism, in our data reflected by the theta rhythm.

It has been shown previously that low frequency theta or alpha power in temporal language areas is decreased during language and auditory tasks [18, 20]. Ojemann et al., (1989) suggested that the drop in low frequency power reflected the thalamocortical activation system. The involvement of the thalamocortical system in language function has been known for some time from lesion and electrical stimulation studies, described in detail by [36]). Stimulation of specific thalamic nuclei causes uncontrolled, irrelevant speech, suggesting an activating role of thalamus in speech. A recent deep brain stimulation study has shown that event related potentials during semantic errors measured in the thalamus matched accurately with the ERPs measured at the cortical level with EEG [37]. Thalamic stimulation can also trigger cortical theta oscillations measured with EEG [38]. In addition, our fMRI group results showed significant task activation in areas of the thalamus and basal ganglia and it can be hypothesized that the phase amplitude coupling we found is driven by thalamo-cortical or basal ganglia-cortical interactions. Future studies will have to verify whether this hypothesis is correct.

We cannot be sure about the origin of the measured theta rhythm and it has to be considered that theta rhythms do not necessarily have to be driven by input from other regions. Theta rhythms have been identified in isolated cortical slices in vitro and may thus also be locally generated [39]. Blatow et al. (2003) found that the theta rhythm was generated by an inhibitory network of GABAergic interneurons, which corresponds with the hypothesis that low frequency theta rhythms may also reflect a suppressing or inhibitory process. In auditory cortex, it was hypothesized that either thalamic inhibition or horizontal inhibition plays an important role in tuning neuronal activity [40]. A recent study on the theta rhythm during working memory also found a lack of theta synchronization across distant cortical cites and suggested local generators [26]. We also did not find any changes in coherence between Broca's area, TPJ and MTG during verb generation, indicating either local theta generators or input from different (subcortical) structures. Both scenarios can explain the lack of coherence: while inferior frontal language areas have reciprocal connections to the ventral anterior nucleus of the thalamus, temporoparietal areas are connected to the pulvinar nucleus [36]. For the visual alpha rhythm a recent study suggested the possibility for a

combination of both local and subcortical generation or modulation [41]. Based on this literature and our findings, we cannot exclude either local or subcortical theta generators, or a possible combination of both.

The fMRI BOLD change has been shown to correlate well with the high frequency gamma rhythm in visual cortex [42] and with HFB power change in other areas [43, 44]. However, these measures do not always match [45, 46]. Low frequency alpha power changes in visual cortex also play an important role in explaining temporal patterns of BOLD change in addition to the gamma rhythm [47, 48] and sensorimotor rhythms in motor cortex explain a different part of the BOLD signal change not explained by HFB change [28]. Our results showed that in language areas, theta power changes explain spatial variance in BOLD activation separately from HFB. As discussed above, a cortical theta rhythm may be related to interneuron activity [39], while broadband changes have been associated with average spike rate [1, 2, 4]. While we found that high frequencies and the theta rhythm dynamically interact, the limited spatial correlation also shows that the mechanisms underlying these changes are partially unrelated (similarly as found for low and high frequencies in motor and visual cortex, see [28, 48]. Our results and these studies show that the BOLD signal correlates with theta, alpha, sensorimotor and gamma rhythms and broadband change, all partly independent from each other. This indicates that the BOLD signal is influenced by a range of neurophysiological processes reflected in these spectral power changes.

In conclusion, we show that the theta rhythm is closely related to function in language areas. The theta rhythm dynamically interacts with local neuronal activity as measured in HFB, in both power and phase amplitude coupling. Both theta power and phase amplitude coupling was reduced during verb generation, suggesting an inhibitory function of the theta rhythm in language areas.

Experimental procedures

Subjects and procedure

Six subjects (mean age 28.5 years (range 19-43), 4 women) gave informed consent to participate in the study. All were patients who suffered from intractable epilepsy and were scheduled for the implantation of ECoG arrays for clinical purposes. The study was approved by the ethical committee of the University Medical Center Utrecht, in according to the Declaration of Helsinki 2008. During a preoperative fMRI session and during ECoG recordings these patients performed the same verb generation task that consisted of 30 second verb generation blocks (where every 3-4 seconds a noun was visually presented and the patient had to covertly think of a matching verb), alternated with 30 second blocks of rest (where neutral stimuli were presented every 3-4 seconds) for 4.5-5.5 minutes.

Magnetic Resonance Measurement

Preoperatively, fMRI scans were acquired on a Philips Achieva 3T scanner with a PRESTO sequence [49, 50] (482 scans, TR/TE 22.5/33.2 ms, flip angle 10 degrees, FOV = 256x224x160 mm, acquisition voxel size 4 mm isotropic). Functional images were realigned and coregistered using normalized mutual information [51] with an anatomical scan using SPM5 (http://www.fil.ion.ucl.ac.uk/spm/). The anatomical image was segmented in gray and white matter with unified segmentation [31].

fMRI analysis

Statistical analyses were performed on a single subject basis and therefore no smoothing was applied. A general linear model (GLM) was estimated with one regressor for activation related to verb generation (a 30s box car for verb generation blocks convolved with a standard hemodynamic response function), data were corrected for low frequency drifts by a 128s high pass filter and corrected for serial correlations with a first order AR model.

An fMRI group analysis was performed to test which areas were significantly active across all subjects. Functional images were smoothed with an 8 mm FWHM and the same GLM was estimated as for the individual subject analysis. Contrasts between verb generation and rest were entered in a group analysis t-test and results are reported at $p_{uncorrected}<0.001$ ($t>5.89$), cluster size >10 voxels.

Electrocorticographic measurement

Arrays of ECoG electrodes were implanted subdurally for localization of seizure focus during the course of treatment for epilepsy. These platinum electrodes had an inter electrode spacing of 1 cm (heart to heart) and an exposed surface of 2.3 mm in diameter. Electrodes were localized on a CT scan and projected to the cortical surface of each patient after corrections for brainshift [52]. ECoG data were acquired with a 128 channel recording system (Micromed, Treviso, Italy) with 512 Hz sampling rate and 0.15–134.4 Hz band-pass filter.

Spatial alignment of ECoG and fMRI

For each ECoG electrode, the magnitude of the BOLD signal change for verb generation compared to rest was estimated by taking the parameter estimates from the GLM and correcting these for the amplitude of the regressor, which results in the percentage of BOLD signal change with respect to the global mean. To correct for the 1 cm spacing in between electrodes, the estimated percentage of BOLD signal change was averaged across gray matter voxels in an 8mm radius of an electrode. This way the fMRI data directly underneath the surface of the grids were optimally matched to the electrodes. Functional MRI results are displayed on the rendered cortical surface as t-maps, which were generated by testing the

GLM verb generation parameter estimates for statistical significance. Fig. 1A shows an example of an fMRI t-maps rendered on the cortical surface, supplemental Fig. S1B shows this for all subjects.

ROI selection

To define electrodes on the different language areas we did a two-step procedure. First, we defined anatomical landmarks and second, the electrode within that area with the largest signal change during fMRI was selected. We defined three areas: Broca's area and the middle temporal gyrus (MTG) since they were most robustly activated in the fMRI group analysis and the temporal-parietal junction (TPJ) which may include Wernicke's area. The anatomical landmark used to define Broca's area was the inferior frontal gyrus and the MTG was defined as the posterior part of the middle temporal gyrus. The location of Wernicke's area is highly variable across subjects [30]. Therefore, electrodes on the superior temporal gyrus or the supramarginal gyrus that were critical for language function as defined by electrocortical stimulation were selected as TPJ. For subjects in which no stimulation was performed (subjects 3 and 4), the posterior part of the superior temporal gyrus and the supramarginal gyrus were anatomically selected. Supplemental Fig. S1B shows the selected anatomical ROI and specific electrode for each subject.

ECoG analysis

ECoG data were further analyzed in Matlab (The Mathworks, Inc., Natick, MA). Signals were re-referenced to the common average of all intracranial electrodes and 3-4 second epochs were extracted for every noun presentation during verb generation blocks and for every visual control stimulus during rest blocks. Electrodes and epochs that showed large epileptic artifacts were rejected (on average 2 electrodes per patient were rejected prior to common average referencing). Electrodes in grids that were on frontal, parietal, lateral temporal and occipital lobes were selected for further analysis (Supplemental Fig. S1B) resulting in 80 (range 71-99) electrodes on average per subject.

Spectral power analysis

To test which low frequency showed the most prominent power changes during verb generation and to calculate high frequency power changes (65-95Hz), spectral power density was calculated. For each epoch, the power spectral density was calculated every 1 Hz by Welch's method (Welch 1967) with 500 ms windows with 250 ms overlap and a Hamming window to attenuate edge effects (Fig. 1B shows log power during verb and rest blocks). Spectral power changes for verb generation compared to rest periods were then calculated. The power spectra of each epoch were normalized (by element-wise division) with respect to the mean power over all epochs at each frequency and the log was taken. If spectral power

changes were calculated for a frequency range (θ: 4-7Hz or HFB: 65-95Hz), the log normalized power was averaged across frequencies in this range. For visualization of the size of the power change between verb generation and rest epochs the r^2 was calculated [53]. The r^2 indicates the percentage of variance explained by different task conditions (verb generation versus rest). A t-test was used to indicate whether differences between rest and verb generation periods were significant, and results are reported at $p<0.05$, Bonferroni corrected for the number of electrodes.

Spectral power change over time

To investigate low and high frequency power changes over time we filtered the signal using a 3rd order Butterworth filter for the low frequency band that showed the most robust power changes during verb generation across subjects (θ, α, or β based on spectral power analysis). The log power of the envelope of the filtered signal was then calculated. For HFB power changes, we were only interested in power fluctuations on a time scale larger than 10ms. We therefore filtered in smaller bands of 5Hz from 65-95Hz, calculated the envelope of these filtered signals and averaged across the 5Hz frequency bands and calculated the log power. The log power signals (X) were then resampled at 100Hz to reduce computational load and z-scored with respect to the rest trials: $X_{z-score} = \frac{X-mean(X_{rest})}{std(X_{rest})}$. Fig. 1G shows the average z-scored high frequency power increases and theta power decreases for one electrode on Broca's area.

Phase amplitude coupling (PAC)

We tested how high frequency power was coupled to the phase of the low frequency rhythms. To visualize to which low frequency the HFB power was coupled PAC-palettes were calculated as described in [12]: phase of 1 Hz low frequency bins from 1-30Hz and power in high frequencies was calculated by calculating respectively the phase and power using Gaussian wavelets of 5 cycles. The log power in high frequencies (65-95Hz) was then z-scored and binned according to the phase of the low frequency in 24 bins from –π to π and the average binned log power was subtracted to clearly visualize increases and decreases from the mean. The low frequency phase varies between –π and π according to a cosine, such that the peak is at 0 and the through at –π and π (indicated in the lower right in Fig. 4). This power per low frequency phase bin was averaged for verb and rest epochs and stacked in a PAC-palette for visualization (Fig. 4).

Next, it was calculated on a trial-by-trial basis whether there were any significant shifts in PAC between verb and rest trials as follows, using the same method as Miller et al., 2010. Since we were interested in HFB power changes on a time scale smaller than 10 ms,

the raw signal was filtered between 65-95Hz and for a low frequency band. The analytic amplitude (absolute of the Hilbert transform) of the high frequencies and instantaneous Hilbert phase of the low frequency band was then calculated. For every trial the analytic amplitude of the high frequencies was then z-scored (*X*) and binned according to the phase of the low frequency in 24 bins from –π to π. For single rest and verb generation trials the phase amplitude coupling vector (Z_{mod}) was then calculated as follows: $Z_{mod}e^{i\varphi_c} = \frac{1}{2}K\sum_{k=1}^{K}X_k e^{i\varphi_k}$, where k is the phase interval and K is the number of intervals (24). Since φ_c is not reproducible on a trial by trial basis, the phase-amplitude coupling vector for individual trials when then projected onto the average angle $\overline{\varphi^q}$ for the condition q (verb generation or rest) the trial belonged to ($\overline{Z_{mod}^q}e^{i\overline{\varphi^q}} = \frac{1}{N}\sum_n Z_{mod}(n)e^{i\varphi(n)}$, where N is the number of trials), resulting in a reliable amplitude estimate per single trial ($Z_{mod}^q(n) = Z_{mod}(n) * \cos(\varphi(n) - \overline{\varphi^q})$). To estimate whether there were significant shifts in PAC amplitude between verb and rest trials, a paired t-test was used to compare the single trial PAC amplitudes.

Correlation between ECoG and BOLD

It was tested whether the magnitude of the BOLD signal change correlated spatially with the magnitude of the spectral power change in HFB and low frequencies using a multiple regression model similar as described in [28]. For each electrode, the BOLD signal change and spectral power change were calculated. The ECoG signal change from rest to verb generation blocks was calculated by the difference in log normalized power between verb and rest epochs and divided by the standard deviation across all epochs to control for possible differences in variance between different frequency bands. The BOLD signal change was the percent signal change for verb generation compared to rest in the gray matter in an 8 mm radius of every electrode. For each subject, a linear regression model ($Y = XB + \varepsilon$) was fitted, where Y is a vector with the percentage of BOLD signal change for each electrode and X the design matrix containing a regressor with spectral power changes in HFB for each electrode and an intercept. The degrees of freedom were given by the number of electrodes entered into the analysis (71-99 per subject). This model was tested for significance in each individual subject by an F-test. To test whether across subjects there was a significant correlation between BOLD and spectral change, it was tested whether the regression coefficients (B) differed significantly from 0 by a t-test. As an indication of the overlap between BOLD and ECoG, we calculated the percentage of BOLD variance that the model explained (R^2).

To test whether low frequency bands explained additional variance in the BOLD signal change independently of HFB change the explained variance was calculated (R^2) and adjusted for the number of regressors $R^2_{adjusted} = (1 - R^2)\frac{1-(n-1)}{n-k-1}$ where n denotes the

sample size (number of electrodes) and k the number of regressors. In a stepwise regression procedure, regressors for low frequency power changes were each added to the model and it was tested whether across subjects there was a significant increase in the explained variance ($\Delta R^2_{adjusted}$) by a paired sample t-test on the Fisher transform of the $R^2_{adjusted}$.

Acknowledgements

The authors thank Frans Leijten, Geertjan Huiskamp, Herke Jan Noordmans and Tineke Gebbink for their help in collecting the data, Peter Gosselaar for implanting the electrodes and staff of the clinical neurophysiology department for their time and effort. This research is supported by the Dutch Technology Foundation STW, applied science division of NWO and the Technology Program of the Ministery of Economic Affairs, and the University of Utrecht, grant UGT7685.

References

1. Manning, J.R., Jacobs, J., Fried, I. & Kahana, M.J. Broadband shifts in LFP power spectra are correlated with single-neuron spiking in humans. *Journal of Neuroscience* **29**, 13613–13620 (2009).
2. Miller, K.J., Sorensen, L.B., Ojemann, J.G. & denNijs, M. Power-Law Scaling in the Brain Surface Electric Potential. *PLOS Computational Biology* **5**, e1000609 (2009).
3. Crone, N.E., Korzeniewska, A. & Franaszczuk, P.J. Cortical gamma responses: searching high and low. *Int J Psychophysiol* **79**, 9-15 (2011).
4. Ray, S. & Maunsell, J.H. Different origins of gamma rhythm and high-gamma activity in macaque visual cortex. *PLoS biology* **9**, e1000610 (2011).
5. Sinai, A.*, et al.* Electrocorticographic high gamma activity versus electrical cortical stimulation mapping of naming. *Brain* **128**, 1556-1570 (2005).
6. Pei, X.*, et al.* Spatiotemporal dynamics of electrocorticographic high gamma activity during overt and covert word repetition. *NeuroImage* **54**, 2960-2972 (2011).
7. Edwards, E.*, et al.* Spatiotemporal imaging of cortical activation during verb generation and picture naming. *NeuroImage* **50**, 291-301 (2010).
8. Miller, K.J., Abel, T.J., Hebb, A.O. & Ojemann, J.G. Rapid online language mapping with electrocorticography. *J Neurosurg Pediatr* **7**, 482-490 (2011).
9. Towle, V.L.*, et al.* ECoG gamma activity during a language task: differentiating expressive and receptive speech areas. *Brain* **131**, 2013-2027 (2008).
10. Osipova, D., Hermes, D. & Jensen, O. Gamma power is phase-locked to posterior alpha activity. *PloS one* **3**, e3990 (2008).
11. Canolty, R.T.*, et al.* High gamma power is phase-locked to theta oscillations in human neocortex. *Science (New York, N.Y* **313**, 1626-1628 (2006).
12. Miller, K.J.*, et al.* Dynamic modulation of local population activity by rhythm phase in human occipital cortex during a visual search task. *Frontiers in human neuroscience* **4**, 197 (2010).
13. Lisman, J. The theta/gamma discrete phase code occuring during the hippocampal phase precession may be a more general brain coding scheme. *Hippocampus* **15**, 913-922 (2005).
14. Voytek, B.*, et al.* Shifts in gamma phase-amplitude coupling frequency from theta to alpha over posterior cortex during visual tasks. *Frontiers in human neuroscience* **4**, 191 (2010).
15. Canolty, R.T. & Knight, R.T. The functional role of cross-frequency coupling. *Trends in cognitive sciences* **14**, 506-515 (2010).
16. Jensen, O. & Mazaheri, A. Shaping functional architecture by oscillatory alpha activity: gating by inhibition. *Frontiers in human neuroscience* **4**, 186 (2010).
17. Canolty, R.T.*, et al.* Spatiotemporal dynamics of word processing in the human brain. *Frontiers in neuroscience* **1**, 185-196 (2007).
18. Edwards, E.*, et al.* Comparison of time-frequency responses and the event-related potential to auditory speech stimuli in human cortex. *Journal of neurophysiology* **102**, 377-386 (2009).
19. Fried, I., Ojemann, G.A. & Fetz, E.E. Language-related potentials specific to human language cortex. *Science (New York, N.Y* **212**, 353-356 (1981).
20. Ojemann, G.A., Fried, I. & Lettich, E. Electrocorticographic (ECoG) correlates of language. I. Desynchronization in temporal language cortex during object naming. *Electroencephalography and clinical neurophysiology* **73**, 453-463 (1989).
21. Luo, H. & Poeppel, D. Phase patterns of neuronal responses reliably discriminate speech in human auditory cortex. *Neuron* **54**, 1001-1010 (2007).
22. Lisman, J. & Buzsaki, G. A neural coding scheme formed by the combined function of gamma and theta oscillations. *Schizophrenia bulletin* **34**, 974-980 (2008).
23. Jensen, O. & Lisman, J.E. An oscillatory short-term memory buffer model can account for data on the Sternberg task. *J Neurosci* **18**, 10688-10699 (1998).
24. Raghavachari, S.*, et al.* Gating of human theta oscillations by a working memory task. *J Neurosci* **21**, 3175-3183 (2001).
25. Jensen, O. & Tesche, C.D. Frontal theta activity in humans increases with memory load in a working memory task. *The European journal of neuroscience* **15**, 1395-1399 (2002).
26. Raghavachari, S.*, et al.* Theta oscillations in human cortex during a working-memory task: evidence for local generators. *Journal of neurophysiology* **95**, 1630-1638 (2006).
27. Rutten, G.J., Ramsey, N.F., van Rijen, P.C., Noordmans, H.J. & van Veelen, C.W. Development of a functional magnetic resonance imaging protocol for intraoperative localization of critical temporoparietal language areas. *Annals of neurology* **51**, 350-360 (2002).

28. Hermes, D.*, et al.* Neurophysiologic Correlates of fMRI in Human Motor Cortex. *Hum Brain Mapp, in press* (2011).
29. Vansteensel, M.J.*, et al.* Brain-computer interfacing based on cognitive control. *Annals of neurology* **67**, 809-816 (2010).
30. Ojemann, G.A. Individual variability in cortical localization of language. *Journal of neurosurgery* **50**, 164-169 (1979).
31. Ashburner, J. & Friston, K.J. Unified segmentation. *NeuroImage* **26**, 839-851 (2005).
32. Voytek, B.*, et al.* Dynamic neuroplasticity after human prefrontal cortex damage. *Neuron* **68**, 401-408 (2010).
33. Ekstrom, A.D.*, et al.* Human hippocampal theta activity during virtual navigation. *Hippocampus* **15**, 881-889 (2005).
34. Khursheed, F.*, et al.* Frequency-specific electrocorticographic correlates of working memory delay period fMRI activity. *NeuroImage* **56**, 1773-1782 (2011).
35. Ekstrom, A., Suthana, N., Millett, D., Fried, I. & Bookheimer, S. Correlation between BOLD fMRI and theta-band local field potentials in the human hippocampal area. *Journal of neurophysiology* **101**, 2668-2678 (2009).
36. Crosson, B. Subcortical functions in language: a working model. *Brain and language* **25**, 257-292 (1985).
37. Wahl, M.*, et al.* The human thalamus processes syntactic and semantic language violations. *Neuron* **59**, 695-707 (2008).
38. Zumsteg, D., Lozano, A.M. & Wennberg, R.A. Rhythmic cortical EEG synchronization with low frequency stimulation of the anterior and medial thalamus for epilepsy. *Clin Neurophysiol* **117**, 2272-2278 (2006).
39. Blatow, M.*, et al.* A novel network of multipolar bursting interneurons generates theta frequency oscillations in neocortex. *Neuron* **38**, 805-817 (2003).
40. O'Connell, M.N., Falchier, A., McGinnis, T., Schroeder, C.E. & Lakatos, P. Dual mechanism of neuronal ensemble inhibition in primary auditory cortex. *Neuron* **69**, 805-817 (2011).
41. Bollimunta, A., Mo, J., Schroeder, C.E. & Ding, M. Neuronal mechanisms and attentional modulation of corticothalamic alpha oscillations. *J Neurosci* **31**, 4935-4943 (2011).
42. Logothetis, N.K., Pauls, J., Augath, M., Trinath, T. & Oeltermann, A. Neurophysiological investigation of the basis of the fMRI signal. *Nature* **412**, 150-157 (2001).
43. Lachaux, J.P.*, et al.* Relationship between task-related gamma oscillations and BOLD signal: new insights from combined fMRI and intracranial EEG. *Human brain mapping* **28**, 1368-1375 (2007).
44. Mukamel, R.*, et al.* Coupling between neuronal firing, field potentials, and FMRI in human auditory cortex. *Science (New York, N.Y* **309**, 951-954 (2005).
45. Muthukumaraswamy, S.D. & Singh, K.D. Functional decoupling of BOLD and gamma-band amplitudes in human primary visual cortex. *Human brain mapping* **30**, 2000-2007 (2009).
46. Sirotin, Y.B. & Das, A. Anticipatory haemodynamic signals in sensory cortex not predicted by local neuronal activity. *Nature* **457**, 475-479 (2009).
47. Maier, A.*, et al.* Divergence of fMRI and neural signals in V1 during perceptual suppression in the awake monkey. *Nature neuroscience* **11**, 1193-1200 (2008).
48. Scheeringa, R.*, et al.* Neuronal dynamics underlying high- and low-frequency EEG oscillations contribute independently to the human BOLD signal. *Neuron* **69**, 572-583 (2011).
49. Neggers, S.F., Hermans, E.J. & Ramsey, N.F. Enhanced sensitivity with fast three-dimensional blood-oxygen-level-dependent functional MRI: comparison of SENSE-PRESTO and 2D-EPI at 3 T. *NMR in biomedicine* **21**, 663-676 (2008).
50. Ramsey, N.F.*, et al.* Phase navigator correction in 3D fMRI improves detection of brain activation: quantitative assessment with a graded motor activation procedure. *NeuroImage* **8**, 240-248 (1998).
51. Maes, F., Collignon, A., Vandermeulen, D., Marchal, G. & Suetens, P. Multimodality image registration by maximization of mutual information. *IEEE transactions on medical imaging* **16**, 187-198 (1997).
52. Hermes, D., Miller, K.J., Noordmans, H.J., Vansteensel, M.J. & Ramsey, N.F. Automated electrocorticographic electrode localization on individually rendered brain surfaces. *Journal of neuroscience methods* **185**, 293-298 (2010).
53. Sheikh, H., McFarland, D.J., Sarnacki, W.A. & Wolpaw, J.R. Electroencephalographic(EEG)-based communication: EEG control versus system performance in humans. *Neuroscience letters* **345**, 89-92 (2003).

Chapter 6 supplementary material

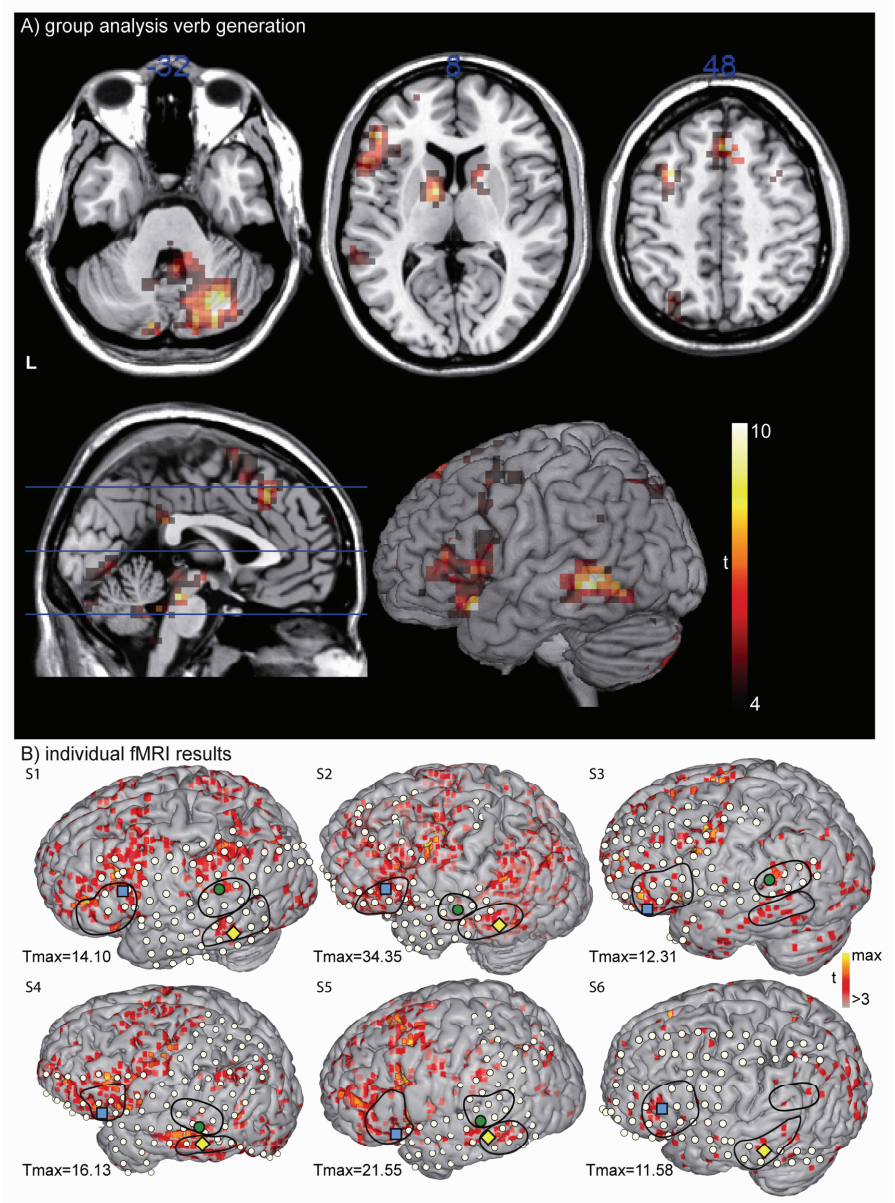

Figure S1. fMRI results. A) Group results for verb generation - rest are shown at t>4. Results were significant only at $p_{uncorrected}$<0.001 (t>5.89), cluster size > 10 voxels. **B)** In every individual subject the inferior frontal gyrus (Broca's area), the temporal-parietal junction (TPJ including Wernicke's area) and the middle temporal gyrus were anatomically marked (black outline) and for Wernicke's are restricted to the electrodes that were involved in language function as found by electrocortical stimulation (except in subjects S3 and S4 where no stimulation was performed). The electrode with the largest fMRI percent signal change within the anatomical areas was then selected. A blue square / green circle / yellow diamond indicates the electrode on Broca's area, TPJ and MTG.

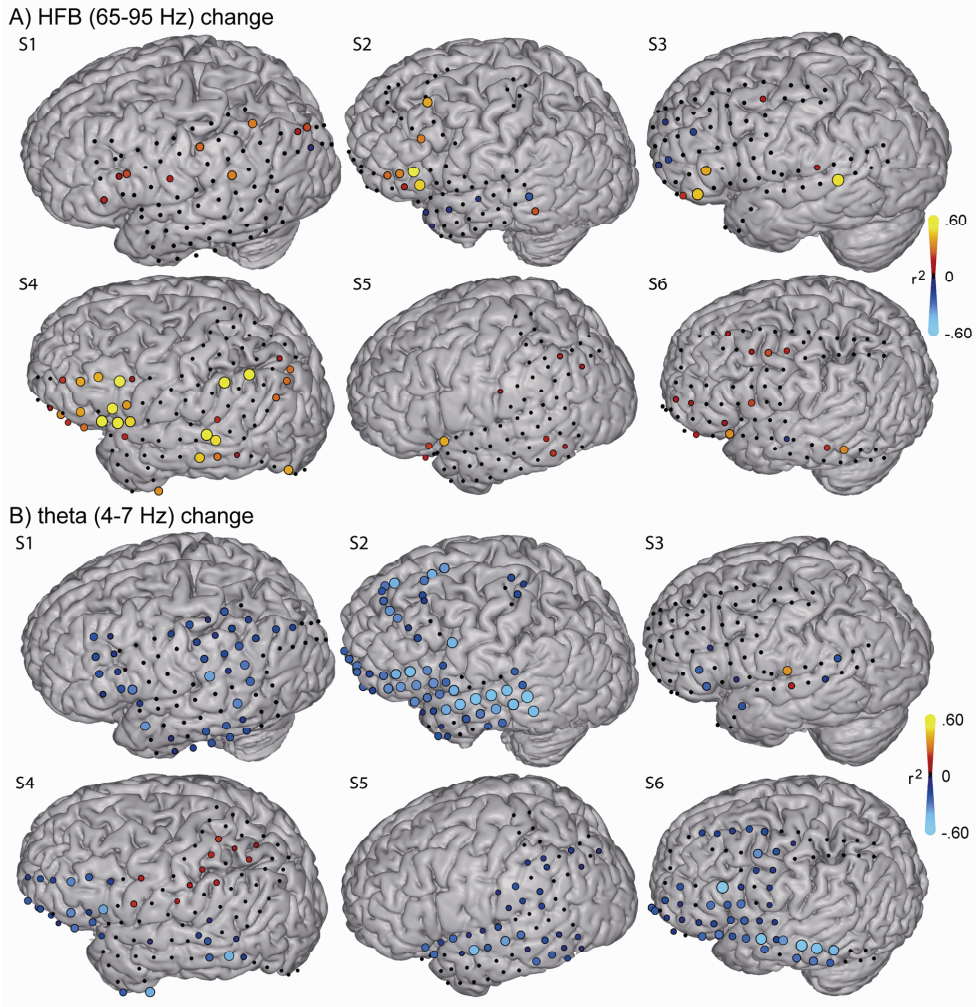

Figure S2. Individual results for ECoG HFB and theta changes. A) Electrodes are shown on the rendered cortex on each individual subject. The color scale and size of the electrodes indicates the difference in power in the HFB (65-95Hz) between verb generation and rest (signed r^2). **B)** The color scale and size of the electrodes indicates the difference in power in the theta band (4-7Hz) between verb generation and rest (signed r^2). Electrodes with an r^2>.6 are the same color as r^2=.6.

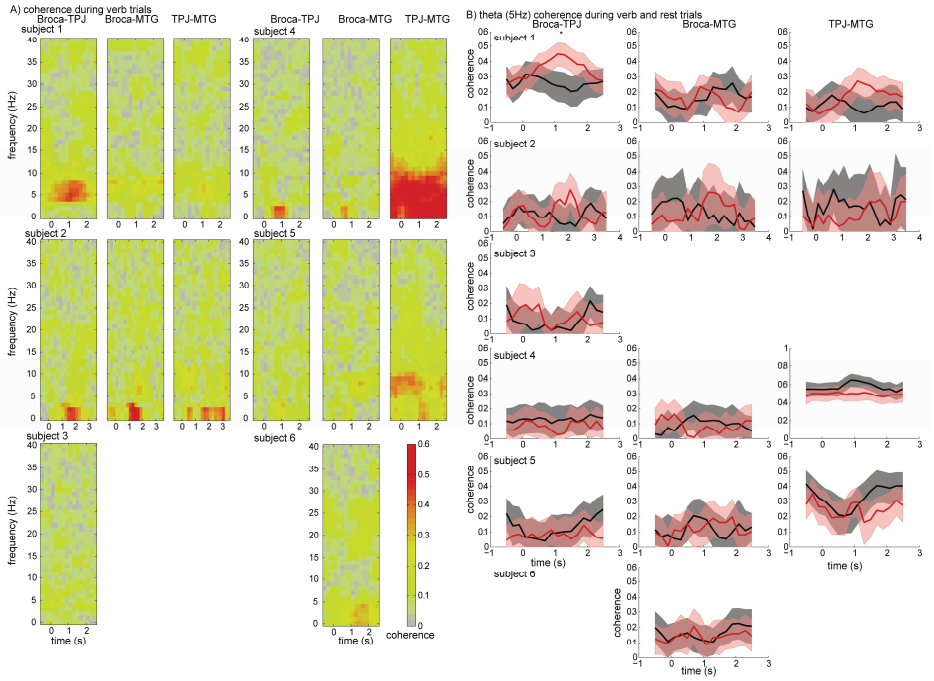

Figure S3. Coherence. To test for coherence between Broca and TPJ, Broca and MTG and TPJ and MTG we used the Chronux toolbox (http://www.chronux.org/, (Mitra and Bokil 2008)). The coherence is the absolute value of the coherency *C(f)*: $C(f) = \frac{S_{XY}(f)}{\sqrt{S_{XX}(f)S_{YY}(f)}}$, where S_{xy} is the cross spectrum and S_{xx} and S_{yy} the power spectra for signals from 2 electrodes *X* and *Y*:

$S_{XY}(f) = \frac{1}{K}\sum_{k=1}^{K} X_k(f)Y_k^*(f)$, where Y_k^* is the complex conjugate of Y_k.

$$S_{YY}(f) = \frac{1}{K}\sum_{k=1}^{K} |Y_k(f)|^2$$

$$S_{XX}(f) = \frac{1}{K}\sum_{k=1}^{K} |X_k(f)|^2$$

The power spectra and cross spectra of the signals x and y were calculated by the Fourier transform with 5 orthogonal Slepian tapers (Percival and Walden 1993), for example for X_k:

$X_k(f) = \sum_{n=1}^{N} w_n(k)x_n e^{-2\pi i f t}$, where $w_n(k)$ is the kth Slepian tapering function.

The coherence was estimated from 1 to 40 Hz in steps of 1 Hz, using a 1 sec window with 200 ms step size. The bandwidth of the tapers was set in such a way that there was a smoothing in the frequency range over +/-3 Hz.

A) The coherence during verb generation trials between electrode pairs on Broca's area and TPJ, Broca's area and MTG and TPJ and MTG. Note that in the theta range (4-7Hz) no increases in coherence can be noted that are consistent across subjects and between electrode pairs. **B)** Coherence during verb generation and rest in a 5Hz band. The 5Hz band was chosen as representative of the theta range. Coherence in 5Hz between electrode pairs is shown in red during verb generation and in black during rest trials. A jackknife procedure was used to estimate 95% confidence intervals for the coherence. In light red and gray confidence intervals for verb generation and rest trials is shown. A * was used to denote when the confidence intervals were non-overlapping.

References

Mitra P, Bokil H. 2008. Observed brain dynamics. New York: Oxford University Press.

Percival DB, Walden A. 1993. Spectral analysis for physical applications, multitaper and conventional univariate techniques. Cambrigde, UK: Cambridge UP.

Chapter 7

Summary and discussion

Summary

This thesis describes studies on the electric potential of a neuronal population of about half a million neurons. It is essential to understand neurophysiology at the millimeter scale since ECoG and fMRI studies have shown that some functional units are specifically defined at this scale. While ECoG measures neuronal activity, fMRI only reflects its vascular and metabolic correlate and it is not well understood how this relates to the underlying neurophysiology. In the setting of motor and language function we used ECoG to define the dominant neurophysiological processes at the scale of millimeters: high frequency changes that are related to local neuronal activity and low frequency changes that reflect more global processes. We studied their interaction and investigated how these are related to the fMRI BOLD change to gain a better understanding of the role of these processes.

Any ECoG study, and particularly when comparing ECoG with fMRI, starts with visualizing the location of the ECoG electrodes on the brain. After these electrodes are implanted during surgery, there is often a brain shift of order 1 to 2 cm. As a result of this brain shift, when a CT scan is made to localize the electrodes and overlaid on a preoperative MRI the electrodes seem localized underneath the surface of the brain. Chapter 2 describes a method to project these shifted electrodes to the brain surface obtained from the preoperative MRI. These projections matched accurately with the location on the operative photo, with a 2.6 mm median distance. Considering that the measurement surface of each electrode is 2.3 mm in diameter and the distance between electrodes localized on pre and post-operative photos is 1.7 mm, this is a very accurate localization method.

Previous studies have shown mismatches between the fMRI signal and neurophysiology in the location of activity. In chapter 3 we illustrated an apparent mismatch between fMRI and neurophysiology measured with EEG. In order to localize motor imagery areas we measured fMRI during motor imagery in 12 healthy subjects. Separately, EEG was measured in the same subjects while they performed the exact same task. FMRI showed clear activation only in premotor cortex and parietal areas and not in primary motor cortex, but a simple EEG analysis showed activation right above the primary sensorimotor areas. At first glance the BOLD signal and the neurophysiology thus seemed to be dissociated. To avoid inserting any assumptions on our data and trying to estimate the source of the EEG signal, we instead measured ECoG and fMRI in the same subject. ECoG high frequency power increases were clearly localized on the fMRI spot and the low frequency power decreases were slightly more distributed around this area. These data illustrate that the BOLD signal matched well with neurophysiology when both were measured with similar scale.

In chapter 4 we tested how the fMRI signal correlates with neuronal population physiology during a motor task. We measured fMRI and ECoG during a finger movement task in eight subjects. Spectral power changes in low frequencies and high frequencies were extracted from the ECoG signal and spatially correlated with the BOLD signal change. We found that the BOLD signal change is a summation of both low and high frequency change, where each explains a different part of the fMRI activation. On primary sensorimotor areas the largest peaks in the BOLD signal correlated with the amplitude of high frequency increases. More distributed, lower BOLD signal change correlated negatively with the low frequencies. This indicates that while fMRI maps represent multiple neuronal processes, the peaks give the best representation of local neuronal processing.

The study described in chapter 5 further explores the different roles of low and high frequencies for motor function. Hand movements have a close association with high frequency activity in motor cortex. However, movements are often repeated at fast rates and whether recent behavioral history influences the link between local neuronal activity and behavior is unclear. ECoG data were recorded at high resolution in three subjects while they performed repeated hand movements at four different rates of 0.3 Hz, 0.5 Hz, 1 Hz and 2 Hz. When hand movements where performed at 1 Hz or faster behavioral results showed that patients started to move in their own rhythm, sometimes moving before the cue. There were no changes in the amplitude of the low frequency beta rhythm suppression, but during the fast movements the beta power remained suppressed and did not return to baseline between movements. During the two faster movement rates high frequency power was significantly suppressed after the initial movement. We take these findings to indicate that beta power declines to release inhibition of motor cortex, and that at faster rates movement initiation is facilitated, requiring less local neuronal activity, due to the extended beta power suppression. These results show that the neuronal activity underlying a particular kind of behavior may differ among similar instances of this behavior: in a set of repeated movements each movement may enable more efficient neuronal computation for subsequent repeated movements.

The study described in chapter 6 further explores the role of low frequencies for language function. It was unclear whether language areas have a dominant low frequency rhythm which interacts with local neuronal activity and relates to BOLD changes. We measured ECoG and fMRI during a verb generation task in six patients. ECoG data showed that theta oscillations are dominant in language areas. In addition, theta oscillations were coupled in phase to the amplitude of high frequency power, with a weaker coupling during activity compared to rest. Lastly, theta power decreases correlated with BOLD increases in addition to high frequency increases. Language areas thus show a dominant theta rhythm,

which interacts dynamically with local neuronal activity and relates to fMRI signal change. This suggests that the theta rhythm may play a functional role for language processing.

General discussion

Half a million neurons (ECoG)

When the electrical potential is measured at the scale of millimeters, local and global processes can be detected simultaneously and their interaction can be studied. When subjects performed motor and language tasks, low frequency rhythms were seen across large areas of cortex while high frequency increases were highly localized. In both motor and language areas low and high frequencies were only partially correlated, indicating that the underlying mechanisms are different phenomena that may interact. We found that when the beta rhythm was continuously suppressed during fast repeated hand movements, the neuronal activity related to each movement was decreased. In language areas the phase of the theta rhythm was coupled to high frequency power fluctuations during rest and this coupling decreased during verb generation. In addition, the decrease in low frequencies correlated with BOLD increase. It is thus likely that these low frequency decreases are not just an epi-phenomenon of cortical idling, but have a specific function.

It has been hypothesized that low frequency rhythms can facilitate local neuronal activity through inhibition [1, 2]. In a disengaged state (during rest), GABA-ergic interneurons provide rhythmic inhibition of pyramidal cells. This rhythmic inhibition suppresses ongoing information processing. When inhibition is released and the synchronizing inhibitory input is reduced, neuronal populations can fire in complex patterns for active information processing. In this way, brain regions that are not relevant for the current task can be suppressed. These models thus propose that high frequency information processing can be suppressed by a low frequency rhythm and a reduction of low frequency modulatory activity is required to allow complex neuronal computation.

Several studies support the inhibitory role of the beta rhythm. It has been shown that enhanced beta band activity is related to increased ability to inhibit unwanted actions in a Go-NoGo task [3] and that during enhanced beta band activity voluntary movements are slower [4]. It has also been shown that the motor cortex is less excitable with increased beta band activity. Transcranial magnetic stimulation of the motor cortex can induce a motor evoked potential; i.e. activity of the hand muscle. Motor evoked potentials were decreased when beta band activity was significantly enhanced during a motor inhibition task [5] or when sensorimotor rhythms were enhanced during resting fluctuations [6]. These slower movements, easy inhibition of action and less excitable motor cortex indicate an inhibited state of motor cortex with increased beta power.

The gating by inhibition hypothesis suggests that inhibitory interneurons play a role in the generation of the beta rhythm. It is important to make the distinction between different beta rhythms: in chapter 4 for example we found two beta rhythms: beta 1 from 13-24 Hz and beta 2 from 24-30 Hz and these different rhythms may not have the same function and physiology. There is evidence that inhibitory interneurons play a role in the generation of the beta 1 rhythm. For example, it has been shown that GABA agonists increase beta band power [7, 8]. Jensen et al. used a modeling approach that indicated a specific role for inhibitory interneurons in generating the beta rhythm. The beta 2 rhythm on the other hand may be generated by gap junctions between pyramidal neurons and not by synaptic processing [9].

It has been hypothesized that sensorimotor rhythms are driven by thalamocortical interactions [10-13], but as of yet, there is no direct evidence for this model and local generators have been suggested as an alternative [14]. Still, two lines of indirect evidence indicate that subcortical-cortical interactions are involved in beta rhythm generation. First, the beta rhythm is present in the complete motor circuit: from cortex [15-17] to striatum and thalamus [18, 19] and the beta oscillations are synchronous between thalamus and cortex [20]. Second, neurological diseases that affect subcortical structures, such as Parkinson's, specifically disrupt the beta rhythm [21-24]. Projections from subcortical structures to inhibitory interneurons in motor cortex may thus drive beta oscillations.

Throughout the cortex, different rhythms may have similar inhibitory functions. In motor areas the beta band may play a role for the release of inhibition. We suggested in chapter 6 that in language areas the theta rhythm serves this function and in visual areas the visual alpha rhythm may play this role [2]. Considering the distinct cytoarchitecture in cortical areas [25], it seems possible that in different areas of neocortex the oscillatory frequency of the inhibitory rhythm differs, while the inhibitory gating role is the same. Also, different thalamic nuclei project to different cortical areas. The lateral geniculate nucleus of the thalamus projects to visual areas and may be involved in the alpha rhythm [26]. For motor cortex on the other hand, the ventrolateral nucleus of the thalamus may be important for the beta rhythm [24]. Even within the language network it has been hypothesized that different subcortical areas project to the two major language areas in frontal and temporal cortex [27]. If thalamocortical interactions generate these low frequency rhythms, these differences can result in different oscillatory frequencies across areas.

While task related decreases in the coupling between low frequency phase and high frequency amplitude may suggest inhibitory gating by low frequency rhythms, increases in this phase amplitude coupling suggest a different function for low frequencies. Increases in theta-gamma coupling have been shown numerous times in hippocampus, where theta oscillations may serve as a carrier wave for memory coding and retrieval (for review see [28]). Not all brain regions show such a clear role. In some cortical areas studies showed both

increases and decreases in phase amplitude coupling with a task. For example, in visual areas decreases in alpha-gamma coupling were found by Osipova et al. when subjects opened their eyes [29]. In contrast, increases in phase amplitude coupling during visual tasks compared to non-visual tasks were noted by others [30] and both increases and decreases have also been shown [1]. In frontal language areas we noted a decrease in theta phase to high frequency amplitude coupling during a verb generation task, while increases in phase amplitude coupling in frontal areas during working memory have also been shown [31]. It can thus be questioned whether these studies measure the same rhythms. Laminar recordings have indeed indicated that there can be multiple sources that generate the visual alpha rhythm: both subcortical and local [26]. Also, intracranial recordings in humans have shown that the cortical theta rhythm may have multiple local generators [32]. Potentially, different studies address entirely different rhythms. Future research will have to show which low frequencies serve inhibitory functions and which provide carrier waves for information processing or have other functions.

A neuronal population and the fMRI signal

When the neuronal population within an fMRI voxel is activated, there is not just one neurophysiological mechanism that plays a role: high frequency power may increase and low frequency power may decrease. In chapter 4 and 6 we showed that in motor and language areas both low and high frequency mechanisms need to be taken into account in order to explain the BOLD signal. A very recent study in which fMRI and EEG were measured concurrently showed the same in visual cortex: alpha and gamma correlated independently with the BOLD change [33]. Also, in monkey V1 a mismatch was found between fMRI and high frequency activity during perceptual suppression [34]. They noted a significant BOLD increase, while there was no change in high frequency activity. When they carefully looked at low frequency power changes the BOLD increase could be explained. A combination of global and local neurophysiological mechanisms thus explains BOLD better than either by itself.

In chapter 3 we showed that fMRI and neurophysiology matched when both were measured at similar scale and different processes were extracted apart from the powerspectrum. A similar example was shown in a recent ECoG study. First, the authors reported a mismatch between fMRI and event related potentials (ERP) [35]. The authors recently readdressed their ECoG data and decomposed the signal into spectral power changes in low and high frequencies [36]. In contrast with the ERP, high frequency modulations matched the fMRI signal changes.

In chapter 4 and 6 we described that in both motor and language areas low and high frequencies explained different parts of the BOLD signal. This indicates that while low and high frequency processes interact, they are only partially related. We proposed that low

frequency changes are related to a release of inhibition and that different rhythms suppress distinct functional areas. When low frequency power decreases in a task-relevant area, there may thus be local neuronal activity only in this area that is released from inhibition. This suggests a two-stage process for brain function: release from inhibition in a larger cortical area and local neuronal processing within this area. A summation of these two processes seems reflected in the BOLD signal: small, distributed BOLD increases related to low frequency decrease and, superimposed on that, large BOLD peaks correlated with the amplitude of high frequency activity. Similar differences between local and distributed patterns in fMRI activation maps have been noted in other studies: reliable and reproducible BOLD peaks with surrounding smaller activity [37]. Since the BOLD signal is partially related to metabolism [38], this two stage process may serve efficient processing in the brain. Since decreases in low frequency rhythms in motor areas were related to small BOLD increases, releasing a larger area of cortex from inhibition may require only a small metabolic cost compared to high frequency activity, which was related to large BOLD changes. Releasing only a specific network of areas from inhibition to perform a certain task may thus decrease the likelihood that non-task relevant areas are activated. Also, as noted in the previous section, research in Parkinson's patients shows that it is increasingly difficult to generate a movement when cortex is not released from inhibition. Releasing inhibition may thus be a necessary requirement for local neuronal processing.

It is unclear through which mechanism low frequency rhythms influence the BOLD signal. If low frequency rhythms are driven by thalamocortical interactions, it is possible that thalamic projections influence the BOLD signal. Deep brain stimulation studies have shown that subcortical stimulation can alter metabolism in cortical projection sites [39, 40]. A recent optogenetic study also showed that thalamic activation may result in BOLD change in motor cortex [41]. However, whether this BOLD activation is related to thalamocortical interactions and sensorimotor rhythms or simply through local processing in the cortical projection sites is unclear [42].

For the mechanisms by which high frequencies relate to BOLD change, an explicit distinction should be made between broadband high frequency power increases versus the gamma rhythm. Importantly, gamma rhythms and broadband activity are distinct phenomena and may even be anticorrelated: in visual cortex power in the gamma rhythm increases and broadband activity decreases for larger visual stimuli [43]. The underlying neuronal dynamics that generate either a broadband change or gamma rhythms are also different [43-46]: broadband activity is linked to population firing rate whereas gamma rhythms are thought to arise from coherent firing of inhibitory interneurons. A recent study confirmed the role of inhibitory interneurons for the gamma rhythm and their relation to BOLD change [47]. They showed that the oscillatory frequency of the gamma rhythm correlates positively with the

GABA concentration and negatively with the size of the BOLD response. In future research it is therefore essential to separate power changes in the gamma rhythm from broadband effects.

Since the LFP is the major correlate of the BOLD signal [48-50] and the LFP mainly represents synaptic activity, it had been suggested that the BOLD signal reflects input to a region. However, the LFP is not only influenced by synaptic input into a region, but also by effects of neuromodulation and local excitatory-inhibitory loops, which also affect the BOLD signal [51]. In rat hippocampus the BOLD change could not be explained by either input or firing output [52]. Angenstein et al. used the well defined hippocampal circuit and varied the amount of input into the dendate gyrus and found that there were specific cases in which the size of the BOLD response did not correlate with the amount of input into this region. In addition, the spiking output did not always correlate directly with BOLD changes. This indicates that the local circuitry, and not just the input or output, modulates the BOLD response. A recent modeling study showed that both synaptic activity and spiking output are necessary to explain the BOLD response [53]. They concluded that if baseline spiking is low, BOLD change can be largely explained by synaptic activity, if baseline spike rate is high, spiking activity also needs to be considered. Based on these results it is likely that the complete circuitry within a voxel has to be taken into account to explain BOLD changes.

These data demonstrate that global and local neurophysiology have independent contributions to BOLD change. The input, output, and local processing in a region may all differently affect hemodynamic changes. This illustrates the necessity to tease apart all mechanisms and consider them separately in order to fully understand the neuronal correlates of fMRI.

Limitations & Future directions

A major issue that is often neglected in ECoG research is the fact that the signal is measured from the brain surface. Measuring at the brain surface neglects differences between layers of cortex. Processes in neurons in the different layers of cortex may contribute to the ECoG signal in different manner and there may even be phase cancelation for rhythms from different cortical layers. Laminar recordings can grasp a better understanding of processes driving low frequency oscillations [26]. Since the BOLD signal has been shown to have different characteristics in the layers of cortex [54], the layering of cortex cannot be neglected either when comparing electrophysiology and fMRI. A recent study has shown the possibility to concurrently record laminar signals and vascular changes in humans [55], giving the potential to further elucidate these issues.

Another limitation is that the ECoG signal is sparsely sampled, potentially missing small patches in between electrodes and missing activity in the sulci. Depending on the size

of the electrodes there may be different, smaller functional units underneath one electrode. Mini and micro ECoG recordings can partially address these issues [56, 57].

For the comparison between fMRI and ECoG, we have focused on the spatial correlation and explaining increases in the BOLD response in motor and language areas. To get a more complete understanding of the BOLD signal, future studies should also investigate the temporal relation between BOLD and ECoG and study different brain functions and regions.

A clinical application

The studies described in this thesis were done in a clinical setting with a brain computer interface (BCI) application in mind. These studies are relevant for at least two questions from the BCI field. First, which part of the ECoG signal is optimal for BCI and whether the optimal location for a BCI device can be predicted with fMRI. This thesis has shown several characteristics of the fMRI and ECoG signal that can help to answer these questions.

First, chapter 4 showed that in the subjects who were scanned on a 1.5 T scanner instead of on a 3 T scanner, the signal in primary sensorimotor cortex did not correlate as well with high frequencies. It is thus necessary to have a good signal to noise ratio to be able to use fMRI as a localizer for high frequencies. Second, chapter 4 shows that large fMRI signal changes in primary sensorimotor areas corresponded best with high frequency increases, similar as what we have shown in chapter 3 for premotor cortex during motor imagery and for dorsolateral prefrontal cortex during working memory [58]. However, in non-primary areas, there may be BOLD changes that do not correspond to high frequency power change, but only to low frequency power changes. It is thus essential to choose areas with a primary involvement in a task, with a large BOLD signal change, before implantation of an electrode is considered. Furthermore, it is often assumed for brain computer interfaces that every action is linked to the same neuronal activity. Chapter 5 shows a drastic decrease in high frequency activity during fast repeated movement. It may be much more difficult to classify these faster movements compared to slower movement.

In short, using fMRI to localize target areas for BCI seems possible when people are scanned on a 3T machine or at even higher field strength, provided that a) an electrode is placed on an area primarily involved in the task at hand, b) high frequency power changes are used to control a BCI and c) repetition effects are well understood before an electrode is placed.

Conclusion

In this thesis we used electrocorticography (ECoG) to study neuronal populations of about half a million neurons in motor and language areas. Understanding the neurophysiology at this scale can provide unique insights into brain function: local and global processes interact at this level and can be studied independently. Low frequency decreases and high frequency increases during motor and language processing showed dynamic interactions in which decreases in low frequencies may facilitate high frequency activity by releasing inhibition. In addition, the combined contribution of low and high frequencies explained BOLD changes better than each contribution individually. The fMRI signal thus seems to reflect both global and local neurophysiological processes and the neuronal mechanisms reflected in different frequencies have to be considered simultaneously in order to understand the fMRI signal.

References

1. Miller, K.J., *et al.* Dynamic modulation of local population activity by rhythm phase in human occipital cortex during a visual search task. *Frontiers in human neuroscience* **4**, 197 (2010).
2. Jensen, O. & Mazaheri, A. Shaping functional architecture by oscillatory alpha activity: gating by inhibition. *Frontiers in human neuroscience* **4**, 186 (2010).
3. Swann, N., *et al.* Intracranial EEG reveals a time- and frequency-specific role for the right inferior frontal gyrus and primary motor cortex in stopping initiated responses. *J Neurosci* **29**, 12675-12685 (2009).
4. Gilbertson, T., *et al.* Existing motor state is favored at the expense of new movement during 13-35 Hz oscillatory synchrony in the human corticospinal system. *J Neurosci* **25**, 7771-7779 (2005).
5. Hummel, F., Andres, F., Altenmuller, E., Dichgans, J. & Gerloff, C. Inhibitory control of acquired motor programmes in the human brain. *Brain* **125**, 404-420 (2002).
6. Sauseng, P., Klimesch, W., Gerloff, C. & Hummel, F.C. Spontaneous locally restricted EEG alpha activity determines cortical excitability in the motor cortex. *Neuropsychologia* **47**, 284-288 (2009).
7. Jensen, O., *et al.* On the human sensorimotor-cortex beta rhythm: sources and modeling. *NeuroImage* **26**, 347-355 (2005).
8. Baker, M.R. & Baker, S.N. The effect of diazepam on motor cortical oscillations and corticomuscular coherence studied in man. *The Journal of physiology* **546**, 931-942 (2003).
9. Roopun, A.K., *et al.* A beta2-frequency (20-30 Hz) oscillation in nonsynaptic networks of somatosensory cortex. *Proceedings of the National Academy of Sciences of the United States of America* **103**, 15646-15650 (2006).
10. Pfurtscheller, G. & Lopes da Silva, F.H. Event-related EEG/MEG synchronization and desynchronization: basic principles. *Clin Neurophysiol* **110**, 1842-1857 (1999).
11. Brown, P. Oscillatory nature of human basal ganglia activity: relationship to the pathophysiology of Parkinson's disease. *Movement disorders* **18**, 357-363 (2003).
12. Schnitzler, A., Timmermann, L. & Gross, J. Physiological and pathological oscillatory networks in the human motor system. *Journal of Physiology-Paris* **99**, 3-7 (2006).
13. Jones, S.R., *et al.* Quantitative analysis and biophysically realistic neural modeling of the MEG mu rhythm: rhythmogenesis and modulation of sensory-evoked responses. *J Neurophysiol* **102**, 3554-3572 (2009).
14. Nunez, P.L., Wingeier, B.M. & Silberstein, R.B. Spatial-temporal structures of human alpha rhythms: theory, microcurrent sources, multiscale measurements, and global binding of local networks. *Human brain mapping* **13**, 125-164 (2001).
15. Crone, N.E., *et al.* Functional mapping of human sensorimotor cortex with electrocorticographic spectral analysis. I. Alpha and beta event-related desynchronization. *Brain* **121 (Pt 12)**, 2271-2299 (1998).
16. Murthy, V.N. & Fetz, E.E. Coherent 25- to 35-Hz oscillations in the sensorimotor cortex of awake behaving monkeys. *Proceedings of the National Academy of Sciences of the United States of America* **89**, 5670-5674 (1992).
17. Sanes, J.N. & Donoghue, J.P. Oscillations in local field potentials of the primate motor cortex during voluntary movement. *Proceedings of the National Academy of Sciences of the United States of America* **90**, 4470-4474 (1993).
18. Cassidy, M., *et al.* Movement-related changes in synchronization in the human basal ganglia. *Brain* **125**, 1235-1246 (2002).
19. Courtemanche, R., Fujii, N. & Graybiel, A.M. Synchronous, focally modulated beta-band oscillations characterize local field potential activity in the striatum of awake behaving monkeys. *J Neurosci* **23**, 11741-11752 (2003).
20. Paradiso, G., *et al.* Involvement of human thalamus in the preparation of self-paced movement. *Brain* **127**, 2717-2731 (2004).
21. Lim, V.K., Hamm, J.P., Byblow, W.D. & Kirk, I.J. Decreased desychronisation during self-paced movements in frequency bands involving sensorimotor integration and motor functioning in Parkinson's disease. *Brain research bulletin* **71**, 245-251 (2006).
22. Swann, N., *et al.* Deep brain stimulation of the subthalamic nucleus alters the cortical profile of response inhibition in the beta frequency band: a scalp EEG study in Parkinson's disease. *J Neurosci* **31**, 5721-5729 (2011).
23. Magnani, G., Cursi, M., Leocani, L., Volonte, M.A. & Comi, G. Acute effects of L-dopa on event-related desynchronization in Parkinson's disease. *Neurol Sci* **23**, 91-97 (2002).

24. Van Der Werf, Y.D., Sadikot, A.F., Strafella, A.P. & Paus, T. The neural response to transcranial magnetic stimulation of the human motor cortex. II. Thalamocortical contributions. *Experimental brain research. Experimentelle Hirnforschung* **175**, 246-255 (2006).
25. Brodmann. *Vergleichende Lokalisationslehre der Grosshirnrinde.* (Barth JA, Leizig, 1909).
26. Bollimunta, A., Mo, J., Schroeder, C.E. & Ding, M. Neuronal mechanisms and attentional modulation of corticothalamic alpha oscillations. *J Neurosci* **31**, 4935-4943 (2011).
27. Crosson, B. Subcortical functions in language: a working model. *Brain and language* **25**, 257-292 (1985).
28. Lisman, J. & Buzsaki, G. A neural coding scheme formed by the combined function of gamma and theta oscillations. *Schizophrenia bulletin* **34**, 974-980 (2008).
29. Osipova, D., Hermes, D. & Jensen, O. Gamma power is phase-locked to posterior alpha activity. *PloS one* **3**, e3990 (2008).
30. Voytek, B.*, et al.* Shifts in gamma phase-amplitude coupling frequency from theta to alpha over posterior cortex during visual tasks. *Frontiers in human neuroscience* **4**, 191 (2010).
31. Canolty, R.T.*, et al.* High gamma power is phase-locked to theta oscillations in human neocortex. *Science* **313**, 1626-1628 (2006).
32. Raghavachari, S.*, et al.* Theta oscillations in human cortex during a working-memory task: evidence for local generators. *J Neurophysiol* **95**, 1630-1638 (2006).
33. Scheeringa, R.*, et al.* Neuronal dynamics underlying high- and low-frequency EEG oscillations contribute independently to the human BOLD signal. *Neuron* **69**, 572-583 (2011).
34. Maier, A.*, et al.* Divergence of fMRI and neural signals in V1 during perceptual suppression in the awake monkey. *Nature neuroscience* **11**, 1193-1200 (2008).
35. Huettel, S.A.*, et al.* Linking hemodynamic and electrophysiological measures of brain activity: evidence from functional MRI and intracranial field potentials. *Cereb Cortex* **14**, 165-173 (2004).
36. Engell, A.D., Huettel, S. & McCarthy, G. The fMRI BOLD signal tracks electrophysiological spectral perturbations, not event-related potentials. *NeuroImage* (2011).
37. Saad, Z.S., Ropella, K.M., DeYoe, E.A. & Bandettini, P.A. The spatial extent of the BOLD response. *NeuroImage* **19**, 132-144 (2003).
38. Ogawa, S., Menon, R.S., Kim, S.G. & Ugurbil, K. On the characteristics of functional magnetic resonance imaging of the brain. *Annual review of biophysics and biomolecular structure* **27**, 447-474 (1998).
39. Asanuma, K.*, et al.* Network modulation in the treatment of Parkinson's disease. *Brain* **129**, 2667-2678 (2006).
40. Eidelberg, D.*, et al.* Regional metabolic correlates of surgical outcome following unilateral pallidotomy for Parkinson's disease. *Annals of neurology* **39**, 450-459 (1996).
41. Lee, J.H.*, et al.* Global and local fMRI signals driven by neurons defined optogenetically by type and wiring. *Nature* **465**, 788-792 (2010).
42. Logothetis, N.K. Bold claims for optogenetics. *Nature* **468**, E3-4; discussion E4-5 (2010).
43. Ray, S. & Maunsell, J.H. Different origins of gamma rhythm and high-gamma activity in macaque visual cortex. *PLoS biology* **9**, e1000610 (2011).
44. Miller, K.J., Sorensen, L.B., Ojemann, J.G. & denNijs, M. Power-Law Scaling in the Brain Surface Electric Potential. *PLoS Comput Biol* **5**, e1000609 (2009).
45. Crone, N.E., Korzeniewska, A. & Franaszczuk, P.J. Cortical gamma responses: searching high and low. *Int J Psychophysiol* **79**, 9-15 (2011).
46. Manning, J.R., Jacobs, J., Fried, I. & Kahana, M.J. Broadband shifts in LFP power spectra are correlated with single-neuron spiking in humans. *Journal of Neuroscience* **29**, 13613–13620 (2009).
47. Muthukumaraswamy, S.D., Edden, R.A., Jones, D.K., Swettenham, J.B. & Singh, K.D. Resting GABA concentration predicts peak gamma frequency and fMRI amplitude in response to visual stimulation in humans. *Proceedings of the National Academy of Sciences of the United States of America* **106**, 8356-8361 (2009).
48. Viswanathan, A. & Freeman, R.D. Neurometabolic coupling in cerebral cortex reflects synaptic more than spiking activity. *Nature neuroscience* **10**, 1308-1312 (2007).
49. Logothetis, N.K., Pauls, J., Augath, M., Trinath, T. & Oeltermann, A. Neurophysiological investigation of the basis of the fMRI signal. *Nature* **412**, 150-157 (2001).
50. Lippert, M.T., Steudel, T., Ohl, F., Logothetis, N.K. & Kayser, C. Coupling of neural activity and fMRI-BOLD in the motion area MT. *Magnetic resonance imaging* **28**, 1087-1094 (2010).
51. Logothetis, N.K. What we can do and what we cannot do with fMRI. *Nature* **453**, 869-878 (2008).

52. Angenstein, F., Kammerer, E. & Scheich, H. The BOLD response in the rat hippocampus depends rather on local processing of signals than on the input or output activity. A combined functional MRI and electrophysiological study. *J Neurosci* **29**, 2428-2439 (2009).
53. Rosa, M.J., Kilner, J.M. & Penny, W.D. Bayesian comparison of neurovascular coupling models using EEG-fMRI. *PLoS Comput Biol* **7**, e1002070 (2011).
54. Siero, J.C., Petridou, N., Hoogduin, H., Luijten, P.R. & Ramsey, N.F. Cortical depth-dependent temporal dynamics of the BOLD response in the human brain. *J Cereb Blood Flow Metab* (2011).
55. Keller, C.J.*, et al.* Intracranial microprobe for evaluating neuro-hemodynamic coupling in unanesthetized human neocortex. *Journal of neuroscience methods* **179**, 208-218 (2009).
56. Flinker, A., Chang, E.F., Barbaro, N.M., Berger, M.S. & Knight, R.T. Sub-centimeter language organization in the human temporal lobe. *Brain and language* **117**, 103-109 (2010).
57. Kellis, S.*, et al.* Decoding spoken words using local field potentials recorded from the cortical surface. *Journal of neural engineering* **7**, 056007 (2010).
58. Vansteensel, M.J.*, et al.* Brain-computer interfacing based on cognitive control. *Annals of neurology* **67**, 809-816 (2010).

List of abbreviations

µm	micrometer
ANOVA	analysis of variance
AR	auto regressive
BCI	brain computer interfacing
BOLD	blood oxygen level dependent
CT	computed tomography
ECoG	electrocorticography
EEG	electroencephalography
EMG	electromyography
fMRI	functional magnetic resonance imaging
FA	flip angle
FOV	field of view
FWHM	full width half max
GABA	gamma-aminobutyric acid
GLM	general linear model
HFB	high frequency band
Hz	Hertz
LFP	local field potential
LFO	low frequency oscillations
M1	primary motor cortex
MEG	magnetoencephalography
MNI	Montréal neurological institute
MTG	middle temporal gyrus
ms	milliseconds
PMc	premotor cortex
PRESTO	principle of echo shifting with a train of observations
ROI	region of interest
s/sec	seconds
S	subject
SMA	supplementary motor areas
SPM	statistical parametric mapping
TE	echo time
TR	repetition time
TPJ	temporal parietal junction

Nederlandse samenvatting

Lokalisatie van hersenfuncties vormt een essentieel onderdeel van de hulp aan sommige patiënten. Bij patiënten met een tumor, bijvoorbeeld, of bij patiënten met epilepsie die door een bepaald gebied in het brein wordt veroorzaakt, is het nodig om te weten dat het te verwijderen hersenweefsel niet bij essentiële functies betrokken is. Elektrocorticografie (ECoG) en functionele Magnetische Resonantie Imaging (fMRI) zijn veel gebruikte technieken om hersenfuncties te lokaliseren. Beide meten de hersenfunctie in gebiedjes ter grootte van een paar millimeter, ongeveer een half miljoen neuronen, een schaal waarop verschillende belangrijke functionele units in de hersenen gerepresenteerd zijn. Het fMRI-signaal meet alleen hemodynamische veranderingen en welke neuronale processen er in zo'n gebiedje plaatsvinden, is veelal onbekend. Daarom gaat dit proefschrift over de potentiaal van een half miljoen neuronen. Wij hebben ECoG gebruikt om op deze millimeterschaal de dominante neurofysiologische processen in motor- en taalgebieden te meten: hoog-frequente veranderingen die lokale neuronale activiteit weergeven, en laag-frequente veranderingen die meer globale processen reflecteren. We hebben de interactie tussen deze twee processen bestudeerd en gerelateerd aan het fMRI-signaal om de rol van deze processen beter te begrijpen.

Iedere ECoG-studie begint met het nauwkeurig lokaliseren van de elektrodes op het brein. Dit is niet vanzelfsprekend, omdat door de implantatie van ECoG-elektrodes het brein één tot twee centimeter kan verschuiven. Wanneer de computertomografie (CT) scan waarop de elektrodes te zien zijn over de preoperatieve MRI-scan wordt heengelegd, lijkt het er als gevolg van deze verschuiving van het brein op dat de elektrodes onder de oppervlakte van het brein geïmplanteerd zijn. Hoofdstuk twee beschrijft een methode die de elektrodes naar het oppervlak van het brein terugprojecteert en zo voor de verschuiving van het brein corrigeert. De locatie van deze geprojecteerde elektrodes kwam goed overeen met de locatie van de elektrodes zoals die te zien was op de foto's die gemaakt waren tijdens de operatie.

Vorig onderzoek heeft laten zien dat de locatie van fMRI-activiteit niet altijd overeenkomt met die van de neurofysiologie. In hoofdstuk 3 laten we een voorbeeld zien waarop het erop lijkt dat de fMRI-activiteit niet overeenkomt met de neurofysiologie zoals die met elektro-encephalografie (EEG) gemeten werd. Om de gebieden te lokaliseren die betrokken zijn bij het zich inbeelden van een beweging voerden twaalf gezonde vrijwilligers een taak uit tijdens een fMRI-scan waarbij ze handbewegingen uitvoerden en inbeeldden. Daarnaast voerden ze precies dezelfde taak uit terwijl het EEG gemeten werd. De fMRI-scan liet zien dat de premotorgebieden en de pariëtale gebieden betrokken waren bij het zich inbeelden van beweging. Het EEG daarentegen liet activiteit zien precies boven de primaire sensorimotorcortex. Op het eerste gezicht leken de neurofysiologie en het fMRI-signaal dus niet overeen te komen. Om dit probleem op te lossen zonder enige aannames te doen die nodig zijn voor het localiseren van de EEG-bron, hebben we het ECoG en de fMRI-activiteit

gemeten gedurende de ingebeelde handbewegingen in één patiënt. Toenames in de power van hoge frequenties van het ECoG waren direct gelokaliseerd op de fMRI spots, terwijl afnames van de power van lage frequenties iets meer hieromheen verspreid lagen. Deze data latendus zien dat het fMRI-signaal wel goed overeenkwam met de neurofysiologie, wanneer beide op eenzelfde schaal gemeten werden.

In hoofdstuk 4 hebben we vervolgens getest hoe het fMRI-signaal correleert met de neurofysiologie van populaties van neuronen in de motor cortex. We hebben fMRI en ECoG gemeten in acht patiënten terwijl ze een taak uitvoerden waarbij ze hun vingers bewogen. Uit het ECoG-signaal hebben we de veranderingen in power in hoge en lage frequenties afgeleid en spatieel gecorreleerd met de veranderingen in het fMRI-signaal. De resultaten laten zien dat de veranderingen in het fMRI-signaal een optelling zijn van de veranderingen in power in zowel de lage als de hoge frequenties: ieder verklaarde een afzonderlijk gedeelte van de fMRI-activiteit. Op de primaire sensorimotorcortex correleerden de grootste pieken in het fMRI-signaal positief met de toenames in power van de hoge frequenties. Meer verdeelde, minder sterke veranderingen in het fMRI-signaal correleerden negatief met de power in de lage frequenties. Deze resultaten laten zien dat, hoewel fMRI-activatiepatronen meerdere processen weergeven, de grootste pieken het best overeenkomen met lokale neuronale processen.

In hoofdstuk 5 hebben we de verschillende functies van hoge en lage frequenties in het EcoG tijdens het uitvoeren van motortaken verder bestudeerd. Fluctuaties in de power van hoge frequenties zijn strak gekoppeld aan handbewegingen. In het dagelijks leven worden bewegingen met wisselende snelheden herhaald en het is niet bekend of de koppeling tussen beweging en hersenactiviteit daarmee verandert. In drie proefpersonen hebben we ECoG-data verzameld terwijl ze handbewegingen uitvoerden met vier verschillende herhalingsfrequenties: 0.3 Hz, 0.5 Hz, 1 Hz en 2 Hz. Bij het herhalen van handbewegingen sneller dan 1 Hz begonnen de proefpersonen meer in hun eigen ritme te bewegen, en soms bewogen ze ook voordat de cue om te bewegen op het scherm te zien was. In de motorcortex nam tijdens beweging de power in de hoge frequenties toe en de power in laag-frequente bèta-oscillaties af. Tussen de verschillende herhalingsfrequenties waren er gedurende beweging geen veranderingen in de amplitude van de afname in bèta-power, maar bij de twee hoogste herhalingsfrequenties keerde de bèta-power tussen de verschillende bewegingen niet terug naar de baseline en bleef onderdrukt. Tevens was bij deze twee hoogste herhalingsfrequenties de power in de hoge frequencties na de eerste beweging significant onderdrukt. Dit zou kunnen betekenen dat na de eerste beweging in een serie van snel herhaalde bewegingen de volgende bewegingen gefaciliteerd worden en minder neuronale activiteit vergen, mogelijk door de continue onderdrukking van bèta-power. Deze resultaten laten zien dat hetzelfde gedrag gekoppeld kan zijn aan verschillende

neuronale activiteit: iedere beweging in een set herhaalde bewegingen faciliteert mogelijk de volgende beweging.

In hoofdstuk 6 hebben we verder gekeken naar de rol van lage frequenties bij het uitvoeren van taalfuncties. Het was onduidelijk of taalgebieden ook een dominant laag-frequent ritme hebben dat interactie vertoont met lokale neuronale activiteit en veranderingen in het fMRI-signaal. In zes patiënten maten we de fMRI- en ECoG-activiteit tijdens een taaltaak waarin werkwoorden bedacht werden bij een zelfstandig naamwoord. De ECoG data lieten zien dat thèta-oscillaties dominant waren in de taalgebieden en dat de power van deze thèta-oscillaties afnam tijdens het uitvoeren van de taaltaak. Daarnaast was de fase van deze thèta-oscillaties gekoppeld aan de amplitude van de power in de hoge frequenties en deze koppeling nam af gedurende het uitvoeren van een taalfunctie ten opzichte van rust. Toenames in power van de hoge frequenties en afnames in thèta-power correleerden op verschillende wijze met toenames in het fMRI-signaal. Taalgebieden laten dus een dominant thèta-ritme zien dat interacties met lokale neuronale activiteit vertoont en correleert met fMRI-activiteit. Dit geeft aan dat het thèta-ritme een belangrijke functionele rol zou kunnen spelen voor taalfunctie.

In de neurofysiologie die we met het ECoG hebben bestudeerd spelen twee processen een belangrijke rol tijdens het uitvoeren van motor- en taalfuncties: globale afnames in de power van lage frequenties en lokale toenames in de power van hoge frequenties. Deze twee processen lieten verschillen zien, maar waren soms ook aan elkaar gekoppeld. Het is mogelijk dat de afname in de power van lage frequenties een toename in lokale neuronale activiteit faciliteert door het verlagen van inhibitie. De som van deze verschillende processen verklaart het fMRI-signaal beter dan ieder voor zich, en beide moeten dus tegelijkertijd in ogenschouw worden genomen om het fMRI-signaal te verklaren.

Dankwoord

Bij dit onderzoek zijn een heleboel mensen betrokken geweest, die ik allemaal graag wil bedanken.

Nick, heel erg bedankt voor alle discussies, ik heb heel veel van je geleerd. Ik begon bij jou als stagiare en jij creëerde zoveel mogelijkheden voor leuk en spannend onderzoek met combinaties van brain-computerinterface studies, klinische toepassingen, neuro-imaging en signaalverwerking dat ik heel blij was dat ik kon blijven. Bedankt voor de grote hoeveelheid vrijheid en het vertrouwen die je me hebt gegeven. Als we ergens tegenaan liepen, kwamen we er altijd uit. Je wilt altijd overal plaatjes van zien en ik heb veel plezier gehad aan het tot in de details bekijken van alle data. Het was inspirerend om samen te brainstormen over nieuwe ideeën en er zijn nog zo veel meer dingen die we zouden kunnen uitzoeken. Ik verheug me erop om in de toekomst de samenwerking voort te kunnen zetten!

De BCI en 7T groep, bedankt voor alle gesprekken, feedback op de inhoud van dit proefschrift, discussies, en gezellige tijden tijdens de vele uren dataverzameling, de lunch en de conferenties. Erik, je hebd mij wegweis gemaakd in de BCI werelt, je redden ons alteid als er weer eens een BCI programa crasjte en als we iets bedagte wat niet met Matlab kon dan wist jei alteid wel een C^{++} oplosing. Mariska, toen jij kwam werden we een groep, het was erg gezellig om samen met veel dropjes de ECoG-experimenten te runnen, jouw zorgvuldige manier van onderzoek doen was onmisbaar. Lenny, samen hebben we de eerste EEG-BCI-experimenten gedaan, bedankt voor alle demo's. Martin, bedankt voor alle discussies en natuurlijk voor het zorgen voor mijn mandarijnenplant (leeft ie nog?). Jeroen and Natalia, it was very much fun to work with you on the high-resolution project; thank you for the input and the thorough feedback! Patrik, thank you for being there during all the real-time fMRI experiments and for letting us use your software. Aldemar, I always enjoyed seeing you in your red shoes. Carolina, Anke-Marit, Marije, jullie waren geweldige stagiares, bedankt voor de vele uren op de IEMU en het doorstaan van alle EEG problemen (waar komt de brom nu weer vandaan?). Annemiek, toen jij er was liepen allerlei dingen plotseling veel soepeler; heel erg bedankt voor alle ondersteuning. Je zei altijd 'natuurlijk, geen probleem', maar zonder jouw steun was het voor mij een heel stuk lastiger geweest om van een afstand alles af te ronden!

Bas, jij hebt me tijdens mijn master de eerste fMRI en Matlab kneepjes bijgebracht, je hebt mij een degelijke basis meegegeven waar ik heel erg veel aan heb gehad. Je bent altijd enthousiast, en ik heb veel plezier beleefd aan het helpen organiseren van de fMRI-cursus en de journal club.

Collega's van de RIBS, psychiatrie en psychonomie, bedankt voor de feedback tijdens meetings, discussies tijdens de journal club, de gesprekken en de gezelligheid; Gerry, Erika (jouw overzicht van alle ECoG taken was de basis voor meerdere experimenten uit dit proefschrift), Matthijs B, Floor (jammer genoeg maar heel kort kamergenootjes), Martijn,

Mathijs R., Gert, Joost, Tom, Casper, Suzanne, Peter (het was erg leuk om in het begin heel kort kamergenoot te zijn, jouw vrolijkheid is aanstekelijk), Maartje, Floris, Niek, Branka (you were the first to give me an introduction to fMRI), Marijn, Antoin, Janna, Janna-Marie, Matthijs V. en Tamar. Tjerk, Cédric, Bram en Marriët, ik kon altijd de kantoortuin binnenlopen als dat nodig was, en SfN en HBM waren erg gezellig! Kelly, dank voor alle kopjes thee. fMRI flow-managers, Erika, Peter, Marys, David en Estrella, bedankt voor het scannen in weekenden en avonden. Systeem beheerders, Vincent (gelukkig vond je mijn 'verloren' data zonder enig probleem terug), Pieter en Roger, bedankt voor het op de been houden van de server op de cruciale momenten.

Afdeling klinische neurofysiology, het was geweldig boeiend om met jullie samen te werken; bedankt voor alle hulp bij de ECoG-dataverzameling! Frans en Cyrille, het was altijd erg inspirerend om jullie klinische blik op ons onderzoek te horen. Geertjan, Nizare, Nico en Willy, bedankt voor alle hulp met het EEG- en ECoG-onderzoek en het maken van mooie BCI-filmpjes. Tineke, Marjolein, de laboranten en verpleegkundigen, bedankt voor jullie hulp en de gezellige uren op de IEMU. Van de afdeling Medische Technologie & Klinische Fysica, Patrick, bedankt voor het herhaaldelijk doormeten en fixen van onze EEG-cap.

Neurochirurgen, Peter van Rijen, Peter Gosselaer, Bon Verweij, bedankt voor jullie kennis en vakmanschap.

Herke Jan, bedankt voor je hulp bij het lokaliseren van alle electrodes.

Speciale dank aan alle patiënten die in moeilijke tijden hebben bijgedragen aan het wetenschappelijk onderzoek.

Alle proefpersonen die mee hebben gedaan aan het EEG-BCI-onderzoek, bedankt!

Lieve familie en vrienden, bedankt voor alle steun en afleiding die soms hard nodig was. Bedankt voor de vele kopjes thee, chocola, gevulde speculaas, het gezellig samen eten, het luisteren naar mijn verhalen, en het meeleven met mijn onderzoek, etc… Bedankt voor het proeflezen van sommige stukken, het verwijderen van spelfouten, het passen op Max zodat ik mijn proefschrift af kon ronden. Max, zo fijn dat je zo lief op mijn buik wilde slapen terwijl ik aan het werk was. Lieve Floor en Feikje, jullie zijn er gewoon altijd voor mij en ik ben heel blij dat jullie mijn paranimfen zijn!

Kai, thank you for showing up in Utrecht and working with me day and night. And yes, you were the one who taught me how to make real nice figures (amongst many other things). I love you.

Gerv, Peter, thank you for helping to set up the BCI experiments and the ECoG data collection. It is a lot of fun to work with you!

Jeff, thank you for hosting me in Seattle, Marcel, bedankt voor de discussies met echte Nederlandse stroopwafels, Bill, Larry, Kurt, Erik, Felix, Adam, Lise, Tim, Miah, thanks for the interesting discussions at the lab meetings and the good times.

Er zijn zoveel mensen bij dit onderzoek betrokken geweest en veel dank aan iedereen die ik vergeten ben.

For the future, Josef Parvizi, Brett Foster, Mo Dastjerdi, Vinitha Rangarajan, Bob Knight, you made me feel very welcome in the bay area and I am very much looking forward to work with all of you!

List of publications

Journal Articles:

Hermes D, Miller KJ, Vansteensel MJ, Aarnoutse EJ, Leijten FSS, Ramsey NF (2011). Neurophysiologic correlates of fMRI in human motor cortex. *Human Brain Mapping.* doi: 10.1002/hbm.21314

Bleicher MG, Vansteensel MJ, Huiskamp GM, **Hermes D**, Aarnoutse EJ, Ferrier CH, Ramsey NF (2011). The effects of blood vessels on electrocorticography. *Journal of Neural Engineering*, 8, 4. doi: 10.1088/1741-2560/8/4/044002

Hermes D, Vansteensel MJ, Albers AM, Bleichner MG, Benedictus MG, Mendez Orellana C Leijten FSS, Aarnoutse EJ, Ramsey NF (2011). fMRI based identification of brain areas involved in motor imagery for implantable BCIs. *Journal of Neural Engineering,* 8, 2. doi:10.1088/1741-2560/8/2/025007

Miller KJ, **Hermes D**, Honey CJ, Sharma M, Rao RP, den Nijs M, Fetz EE, Sejnowski TJ, Hebb AO, Ojemann JG, Makeig S, Leuthardt EC (2010). Dynamic modulation of local population activity by rhythm phase in human occipital cortex during a visual search task. *Front. Hum. Neurosci.* 4:197 doi:10.3389/fnhum.2010.00197

Vansteensel MJ, **Hermes D**, Aarnoutse EJ, Bleichner MG, Schalk G, van Rijen PC, Leijten FSS, Ramsey NF (2010). Brain-computer interfacing based on cognitive control. *Annals of Neurology* 67(6): 809-816

Hermes D, Miller KJ, Noordmans HJ, Vansteensel MJ, Ramsey NF (2010). Automated electrocorticographic electrode localization on individually rendered brain surfaces. *Journal of Neuroscience Methods* 185: 293-298

Baeken C, De Raedt R, Ramsey N, Van Schuerbeek P, **Hermes D**, Bossuyt A, Leyman L, Vanderhasselt MA, De Mey J, Luypaert R (2009). Amygdala responses to positively and negatively valenced baby faces in healthy female volunteers: influences of individual differences in harm avoidance. *Brain Research* 1296: 94-103.

Osipova D, **Hermes D**, Jensen O (2008) Gamma Power Is Phase-Locked to Posterior Alpha Activity. *PLoS ONE* 3(12): e3990.

Submitted manuscripts:

Hermes D, Miller KJ, Vansteensel MJ, Edwards E, Ferrier CH, Bleichner MJ, Van Rijen PC, Aarnoutse EJ, Ramsey NF. Semantic processing disrupts prominent intracranial phase-amplitude coupling in the language network: a new role for theta?

Hermes D, Siero J, Aarnoutse EJ, Leijten FSS, Petridou N, Ramsey NF. Dissociation between neural activity in sensorimotor cortex and hand movement revealed as a function of movement rate.

Miller KJ, **Hermes D,** Honey CJ, Hebb AO, Ramsey NF, Knight RT, Ojemann JG, Fetz EE. Human motor cortical activity is selectively phase-entrained on underlying rhythms.

Johnson LA, Blakeley T, **Hermes D**, Hakimian S, Ramsey NF, Ojemann JG. Sleep spindles are locally modulated by training on a brain-computer interface.

Bauer PR, Vansteensel MJ, Bleicher MG, **Hermes D**, Ferrier CH, Aarnoutse EJ, Ramsey NF. Mismatch between electrocortical stimulation and electrocorticography frequency mapping of language.

Vansteensel MJ, Bleichner MG, Dintzner LT, Aarnoutse EJ, Leijten FSS, **Hermes D**, Ramsey NF. Task-free electrocorticography frequency mapping of the motor cortex.

Shum J, Dastjerdi M, Foster BL, Winawer J, Rangarajan V, **Hermes D**, Miller KJ, Parvizi J. A human brain area for seeing numbers.

Conference papers:

Miller KJ, Hebb AO, **Hermes D**, den Nijs M, Ojemann JG, Rao RPN, 2010. Brain surface electrode co-registration using MRI and x-ray. IEEE Eng Med Biol Soc 2010, 6015-6018.

Miller KJ, **Hermes D**, Schalk G, Ramsey NF, Jagadeesh B, den Nijs M, Ojemann JG, Rao RP (2009). Detection of spontaneous class-specific visual stimuli with high temporal accuracy in human electrocorticography. Conf Proc IEEE Eng Med Biol Soc. 2009;1:6465-8.

Conference abstracts:

Hermes D, Miller KJ, Vansteensel MJ, Edwards E, Ferrier CH, Bleichner MJ, Van Rijen PC, Aarnoutse EJ, Ramsey NF. Dynamic interaction between theta and high frequencies in language areas. Poster presentation at SfN 2011.

Hermes D, Miller KJ, Edwards E, Weaver K, Ramsey NF & Ojemann JG. Repetition of a language task shows decreased high frequency power response in the ECoG signal. Poster presentation at SfN 2011.

Hermes D, Miller KJ, Vansteensel MJ, Ferrier CH, Bleichner MJ, Aarnoutse EJ, Ramsey NF. Spatiotemporal correlation between BOLD and electrophysiology in language function. Poster presentation at HBM 2011.

Hermes D, Bleichner MJ, Vansteensel MJ, Aarnoutse EJ, Albers AM, Benedictus MR, Mendez Orellana C, Schalk G, Ramsey NF. Changes in thalamic activity after controlling a sensorimotor rhythm-based BCI: an EEG and fMRI study. Poster presentation at SfN 2010.

Hermes D, Miller KJ, Vansteensel MJ, Albers AM, Bleichner MG, Aarnoutse EJ, Leijten FSS, Ramsey NF. 3D-BOLD fMRI as a presurgical localization technique for BCI implants: validation with ECoG. Oral presentation at the fourth International Brain-Computer Interface Meeting, Asilomar Conference Center, Monterey, CA. Student Scholarship Award.

Hermes D, Miller KJ, Vansteensel MJ, Aarnoutse EJ, Leijten FSS, Ramsey NF. Neurophysiological correlates of BOLD signal changes: an ECoG and fMRI study. Poster presentation at SfN 2009.

Hermes D, Discrepancy between EEG and fMRI in motor imagery: are high frequencies the answer? Oral presentation at the Donders Discussions 2009, Donders Institute for Brain, Cognition and Behavior, Nijmegen, The Netherlands.

Hermes D, Miller KJ, Noordmans HJ, Vansteensel MJ, Ramsey NF. Localizing electrodes on an individual MRI for ECoG research. Poster presentation at HBM 2009. NeuroImage, Volume 47, Supplement 1.

Hermes D, Vansteensel MJ, Ferrier CH, Leijten FSS, Aarnoutse EJ, Gosselaar PH, Ramsey NF. Defining language specific features for brain computer interfaces by comparing electrocorticography to electrical cortical stimulation. Poster presentation at SfN 2008.

Hermes D, Brass M, Zysset S, Theeuwes J, Neggers SFW. Cortical control of visual selection in saccade preparation: fMRI analysis of visual search errors. Poster presentation at HBM 2007. NeuroImage, Volume 36, Supplement 1.

Curriculum Vitae

Dora Hermes werd op 13 juli 1982 geboren in Nijmegen. In 2000 behaalde zij haar VWO-diploma aan het Strabrecht College in Geldrop, en begon aan een studie wiskunde aan de Universiteit van Utrecht. Ze behaalde haar propedeuse wiskunde en stapte over naar een studie psychologie, eveneens in Utrecht. In 2005 reisde ze af naar Auckland, Nieuw Zeeland, om haar bacheloronderzoek te doen bij Prof. Dr. Michael Corballis and Dr. Jeff Hamm betreffende de line-motion illusion, waarna ze haar bachelordiploma behaalde. In hetzelfde jaar begon ze aan de Master Neuroscience and Cognition in Utrecht. Tijdens deze master deed ze fMRI-onderzoek aan oogbewegingen onder begeleiding van Dr. Bas Neggers bij het Helmholtz Instituut in Utrecht, en reisde voor dit onderzoek naar het Max Planck Instituut in Leipzig in het kader van een samenwerkingsproject met Dr. Marcel Brass. Tijdens haar tweede stage verdiepte ze zich in brain-computer interfaces onder begeleiding van Prof. Dr. Nick Ramsey bij het Universitair Medisch Centrum (UMC) in Utrecht. Nadat ze in 2007 haar MSc afrondde, bleef ze in dit lab werken als AiO, en begon aan het promotie-onderzoek beschreven in dit proefschrift. Dora trouwde op 20 maart 2011 met Kai Miller en op 4 oktober 2011 werd hun zoon Max geboren. Dora is nu werkzaam als post-doc in de groep van Josef Parvizi in Stanford in de Verenigde Staten.

Dora Hermes was born on July 13, 1982 in Nijmegen, the Netherlands. In 2000 she graduated from high school, Strabrecht College in Geldrop, and started studying mathematics at the Utrecht University. After receiving her first-year certificate, she started studying psychology, also in Utrecht. In 2005 she traveled to Auckland, New Zealand to do a bachelor's research project with Prof. Dr. Michael Corballis and Dr. Jeff Hamm working on the line-motion illusion with EEG, after which she got her BSc degree. In the same year she enrolled in the Neuroscience and Cognition Master's program in Utrecht. For her first internship she studied eye movements with fMRI under the supervision of Dr. Bas Neggers at the Helmholtz Institute in Utrecht and for this project she traveled to the Max Planck Institute in Leipzig for a collaboration with Dr. Marcel Brass. For her second internship she started working on brain computer interfaces with Prof. Dr. Nick Ramsey at the University Medical Center (UMC) in Utrecht. After receiving her MSc degree in 2007, she stayed in this lab to work on the studies described in this thesis. On the 20th of March, 2011, Dora married Kai Miller and on the 4th of October, 2011, their son Max was born. Dora now works as a post-doctoral fellow within the group of Josef Parvizi at Stanford, CA, USA.